



# **IMPROVING STEEL-CLT COMPOSITE FLOOR SYSTEM**

**Achieving Circularity, Optimizing CLT Design, and  
Assessing Environmental Impact**

**T. Theodory**

---

# Delft University of Technology

---

Author:

*Tony Theodory*

Thesis research for a Master of Science in Civil Engineering at Delft University of Technology.

Sunday, September 15, 2024

## **Thesis Committee**

Dr. Florentia Kavoura	TU Delft, Chair and Daily Supervisor
Dr. Ir. G.J.P. Ravenshorst	TU Delft, Supervisor
Dr. Robin Oval	TU Delft, Supervisor
CEng MIStructE Thomas Musson	WSP, Supervisor

## PREFACE

The journey to complete this research project has been both challenging and rewarding. As my first academic contribution, this project presented new challenges and responsibilities while also encouraging the development of my problem-solving and communication skills.

Throughout this study, I have been fortunate to receive support from many remarkable individuals. I would like to extend my deepest gratitude to Dr. Florentia Kavoura for her expertise and support, which have played a key role in shaping this research. I am also sincerely thankful to Dr. Ir. G.J.P. Ravenshorst for his guidance and expertise in timber engineering, as well as to Dr. Robin Oval for his insights and unwavering support, particularly in sustainability-related matters.

I extend my heartfelt thanks to WSP for providing the necessary resources and facilities that made this study possible. I extend special thanks to CEng MIStructE Thomas Musson, my daily supervisor at WSP, whose mentorship and encouragement have been invaluable throughout this journey. Working under Thomas's guidance has been both a privilege and a blessing, as his insights greatly enriched the research process.

I am extremely grateful to my partner Nathalie, whose steadfast support has been my cornerstone not only during this thesis but throughout the entire master's program. I also want to express my heartfelt gratitude to my family and friends, whose faith in my abilities has been a continual source of motivation. Finally, and above all, I give thanks and glory to my Lord Jesus Christ, who has always strengthened me with His grace, and peace.

I hope the findings presented in this study will contribute meaningfully to the ongoing discussion surrounding sustainable construction practices. I invite you to engage with the forthcoming chapters on the improvement of Steel-CLT Composite Floor Systems and their role in advancing sustainable building solutions.

## ABSTRACT

As sustainability becomes increasingly essential in construction practices, the incorporation of concepts such as circularity and material efficiency are more required than ever. The present research investigates how these concepts can be effectively applied to Steel-Cross Laminated Timber (CLT) composite floor systems in order to promote more sustainable construction methods, specifically reducing carbon footprint. The findings are intended to benefit practicing engineers and designers, as well as lay the groundwork for future academic research and innovation in sustainable construction.

WSP developed the baseline steel-CLT composite floor system, which bonds composite materials using shear studs and grout <sup>1</sup>. However, this design restricts disassembly at the end of its lifecycle, posing challenges that limit its potential for reuse in subsequent applications. In addition to that limitation, while the system was validated via laboratory push-out tests, using a standardized CLT configuration across varying spans resulted in material inefficiencies, highlighting the need for additional optimization.

To address the aforementioned drawbacks, this study develops an "optimized design" for a Steel-CLT composite floor system that enhances both circularity and material efficiency. The optimized system, which includes demountable shear connectors, allows for easy disassembly and reuse, extending the life of its components. The study also investigates the optimal CLT configuration and lay-up to maximize material efficiency, demonstrating that adapting the CLT design to the unique characteristics of each composite floor structure (e.g., dimensions, spans, and load requirements) is crucial for optimal performance.

Finally, the baseline- and optimized designs were compared in terms of environmental impact, focusing on a Life Cycle Assessment (LCA) of embodied carbon. This evaluation highlights the environmental benefits of the optimized design, offering valuable insights into how circularity and material efficiency can significantly reduce the carbon footprint in constructions.

Overall, this research transforms the baseline steel-CLT composite floor system from a linear to a circular design, thereby highlighting the significant advantages of circular design principles within the construction industry. By advocating for the broader adoption of circular approaches, this research underscores the potential for creating a more environmentally sustainable future in building practices. In addition to achieving circularity, the study focuses on optimizing the CLT design to enhance material efficiency within the floor system. It also identifies key factors to consider when designing CLT for composite applications, ensuring that the material is used most effectively within this innovative context.

---

<sup>1</sup> Throughout the research, this system is referred to as the "baseline design."

The present paper begins with a comprehensive literature review, which provides the foundational background necessary for the research. This is followed by a detailed explanation of the design rules employed in the structural analysis. Next, the application of demountable shear connectors is discussed, highlighting their role and implications for the steel-CLT composite system. A subsequent chapter delves into the design of CLT panels, emphasizing their dual function within composite floor systems. Both the baseline and optimized floor systems are then presented, with an outline of their structural characteristics and geometric configurations, followed by a rigorous structural analysis. The study proceeds with a comparative analysis, evaluating the structural and environmental performance of both designs. This analysis resulted in conclusions that highlight the substantial role of circular design principles and material efficiency in reducing the environmental impact of construction materials and systems, as well as the crucial role that structural designers can play in advancing the decarbonization of the built environment.

# TABLE OF CONTENTS

Preface .....	II
Abstract .....	III
Table of Contents .....	V
List of Figures .....	VIII
List of Tables .....	XI
Abbreviations .....	XII
1 Introduction.....	1
1.1 Circular Design .....	2
1.2 Composite Floor systems .....	2
1.3 Problem Description and Objectives .....	4
1.4 Research Questions .....	6
1.5 Research Structure .....	6
2 Literature Review .....	8
2.1 Gamma Method for Mechanically Jointed Beams .....	8
2.1.1 Relevance to The Study .....	8
2.1.2 Relations and Equations.....	9
2.2 Pre-loaded Demountable Shear Connectors.....	12
2.2.1 Relevance to The Study .....	14
2.3 Cross-Laminated Timber Panels .....	14
2.3.1 Relevance to The Study .....	16
2.3.2 Equivalent CLT Cross-section .....	17
2.4 Effective Width of Composite Beams .....	18
2.4.1 Relevance to The Study .....	19
2.5 Spacing .....	22
2.6 Life Cycle Assessment and Embodied Carbon Calculation.....	23
2.6.1 Relevance to The Study .....	25
3 Structural Design Rules .....	28
3.1 Basis of Structural Design NEN-EN 1990.....	28
3.1.1 Consequence Class .....	28
3.1.2 Loads Combination.....	28
3.1.3 Deflection Limit .....	29
3.2 Actions according to NEN-EN 1991-1-1 .....	29

3.2.1	Combination Coefficients.....	29
3.2.2	Vertical Actions.....	30
3.3	Ultimate Limit State.....	30
3.3.1	Composite Beam Design.....	31
3.3.2	CLT Floor Design.....	32
3.4	Serviceability Limit State.....	33
3.4.1	Composite Beam Design.....	33
3.4.2	CLT Floor Design.....	34
4	Structural Properties and Application of Pre-loaded Demountable Shear Connectors.....	35
5	CLT Design Approach and Improvement.....	39
6	Structural Analysis and Comparison.....	43
6.1	Case Study.....	43
6.1.1	The Baseline Design of Steel-CLT Composite Floor System.....	45
6.1.2	The Optimized Design of Steel-CLT Composite Floor System.....	48
6.1.3	Summary of The Structural Analysis.....	50
6.2	Structural Comparison.....	52
7	Environmental Impact and Comparison.....	54
7.1	Case Study.....	54
7.1.1	Embodied Carbon Calculation for The Baseline Composite Floor System (Non-Circular Design).....	57
7.1.2	Embodied Carbon Calculation for The Optimized Composite Floor System (Circular Design).....	57
7.2	Embodied Carbon Comparison.....	60
8	Conclusion and Recommendations.....	63
8.1	Limitations.....	66
8.2	Recommendations for Future Research.....	68
	References.....	71
Appendix A	The Correction Factor for The Slip Modulus.....	75
Appendix B	The Structural Analysis.....	76
B.1	Baseline Design Structural Analysis.....	76
B.2	Optimized Design Structural Analysis.....	81
Appendix C	Cumulative Carbon Emissions Over Time and Biogenic Carbon.....	90
C.1	Baseline Design Graph.....	90

C.2	Optimized Design 50% Reused Graph .....	90
C.3	Optimized Design 70% Reused Graph .....	91
C.4	Optimized Design 90% Reused Graph .....	91
Appendix D	Python Script for Structural Analysis .....	92
D.1	Baseline Composite Floor System .....	92
D.2	Optimized Composite Floor System.....	98



## LIST OF FIGURES

Figure 1: Linear and circular economy [1].

Figure 2: Deflection and bending stress distribution of a full cross-section (A), a cross-section comprising three individual cross-sections connected via semi-rigid joints (B) and a cross-section comprising three loosely superimposed individual cross-sections (C). [12]

Figure 3: 3D picture for the baseline floor system researched by WSP.

Figure 4: Example of a composite beam with three components [12].

Figure 5: Gamma vs. Effective Bending Stiffness.

Figure 6: Embedded parts in the timber: SCT-1, SCT-2, and SCT3 [10].

Figure 7: Details of shear connections: SCT-1, SCT-2, and SCT3 [10].

Figure 8: Comparison of the three shear connectors' mean load/slip curves [10].

Figure 9: Global production of CLT in years [45].

Figure 10: Sequestered biogenic carbon (transfers/emissions) and fossil carbon (emissions) for a typical timber [13].

Figure 11: 3D visualization of a typical Steel-CLT flooring system [28]

Figure 12: CLT designer software [35].

Figure 13: Original vs homogenized cross-section [22].

Figure 14: Effective Flange Width T-beam

Figure 15: The parameters to calculate the effective width according to EC4 [31].

Figure 16: The parameters to calculate the effective width according to EC5

Figure 17: longitudinal section of composite beam.

Figure 18: Gamma vs Spacing (left); Effective bending stiffness vs Spacing (right)

Figure 19: Life cycle stages and modules [13].

Figure 20: Life cycle stages and modules for non-circular system.

Figure 21: Life cycle stages and modules for circular system.

Figure 22: Push-out test setup from [10], and friction resistance.

Figure 23: Push-out results for SCT-1 top left, SCT-2 top right, SCT-3 bottom left, and all SCT together bottom right [10].

Figure 24: Shear flow in a joint.

Figure 25: The mechanical scheme of the composite beam.

Figure 26: Joint load value in relation to the load/spacing in ULS left, in SLS right.

Figure 27: Active CLT panels in each direction (not to scale drawing).

Figure 28: neutral axis position in the composite cross-section.

Figure 29: Effective bending stiffness vs Active Cross-sectional Area of CLT (A1).

Figure 30: neutral axis position in CLT floor.

Figure 31: illustration of the active panels in each direction of the new design (not to scale drawing).

Figure 32: 3D drawing and geometry of the floor system.

Figure 33: The composite floor system designed by WSP.

Figure 34: The load-slip graph obtained from the WSP push-out test.

Figure 35: Front view of steel elements; 3D drawing right.

Figure 36: 3D drawing showing critical sections with a red dashed line.

Figure 37: Stress distribution along non-composite (top) and composite (bottom) cross-sections.

Figure 38: 3D Floor plan dimensions of the investigated story.

Figure 39: Life cycle stages and modules for non-circular system.

Figure 40: Life cycle stages and modules for circular system.

Figure 41: Cumulative carbon emissions over time for all designs.

Figure 42: Biogenic carbon graph over time for all designs.

Figure 43: A 3D representation of the load application.

Figure 44: Normal stress distribution along the composite cross-section.

Figure 45: A 3D representation of the load application on the floor.

Figure 46: A 3D representation of the load application.

Figure 47: Normal stress distribution along the composite cross-section.

Figure 48: Front view of the shear connector and the steel beam left drawing. Top view steel beam right drawing.

Figure 49: Symbols for spacing of fasteners [41].

Figure 50: Net area of the top flange in red.

Figure 51: Failure mechanisms for a steel-to-timber connection [18].

Figure 52: A 3D representation of the load application on the floor.

Figure 53: Cumulative carbon emissions over time and biogenic carbon for the baseline design.

Figure 54: Cumulative carbon emissions over time and biogenic carbon for the optimized design 50% reused.

Figure 55: Cumulative carbon emissions over time and biogenic carbon for the optimized design 70% reused.

Figure 56: Cumulative carbon emissions over time and biogenic carbon for the optimized design 90% reused.

## LIST OF TABLES

Table 1: illustrative comparison that shows how the orientation and grain direction of the CLT panels affect the composite beam.

Table 2: Materials' structural properties.

Table 3: Cross-sections' structural properties.

Table 4: Cross-sections' structural properties.

Table 5: UC for three alternatives.

Table 6: Carbon Factors.

Table 7: Structural materials volume.

Table 8: Embodied carbon calculation for non-circular system.

Table 9: Embodied carbon calculation for circular system (50% reused).

Table 10: Embodied carbon calculation for circular system (70% reused).

Table 11: Embodied carbon calculation for circular system (90% reused).

## ABBREVIATIONS

CLT	Cross laminated timber
GWP	Global Warming Potential
LCA	Life-cycle assessment
ULS	Ultimate Limit State
SLS	Serviceability Limit State

# 1 INTRODUCTION

The construction industry has a significant impact on our modern world and daily lives, however, this currently comes with a high environmental cost. The building industry, as one of the largest construction industries, has a significant impact on energy consumption, carbon emissions, and the depletion of finite raw materials. As a result of the preceding causes, there is now a clear recognition of the need for critical changes, resulting in an increased demand for sustainable practices, efficient resource utilization, and greater environmental accountability. Therefore, extensive research has been conducted in the field of civil engineering to investigate new sustainable technologies.

In response to a growing demand to reduce upfront carbon in building design, WSP, which is a global engineering consultancy, together with the University of Warwick has undertaken research and testing to develop a steel-CLT composite floor system. This system utilizes a grouted shear connection between the steel beam and CLT floor panel to optimize the strength and stiffness of the floor system. This leads to a corresponding reduction in overall steel weight and corresponding carbon emissions within EN 15804 modules A1 to A3. Building on this innovative foundation, this study aims to delve deeper into improving the circular design aspect of this floor system, as well as optimizing the design of the CLT components. The primary goal is to create structural floor system that not only meets the structural requirements but also includes demountable and reusable components, thereby promoting both system circularity and efficiency.

To achieve this objective, the study will focus on improving structural aspects critical in this composite floor system, such as the shear connector and the design of the CLT panels. First, a new shear connector from the literature will be introduced, discussed, and implemented. Following that, the design of the CLT floor will be investigated to address the function of the CLT element in the composite system. Then, the final CLT design will be developed to determine the optimal solution. The optimized floor system design will then be compared with the baseline design, which uses grout for composite action. This comparative analysis will cover both structural and environmental aspects, revealing each system's strengths and weaknesses.

The following sub-chapters will delve into fundamental aspects required to provide context to the research. Some of these include technical information, such as circularity and composite floor systems. Other sub-chapters will discuss the research description, objectives, research questions, and research structure. This will provide readers with a detailed understanding of the research context, laying the groundwork for the subsequent chapters.

## 1.1 Circular Design

Circular design is a method of designing and constructing buildings that centers on minimizing waste and reusing materials. This approach aligns with the broader concept of a circular economy, which emphasizes creating products and materials that remain in a continuous loop, extending their usability for as long as possible. Unlike the traditional linear economy, where products and materials are discarded at the end of their first life cycle, the circular economy seeks to keep them in circulation, reducing the need for new resources and minimizing environmental impact [1].

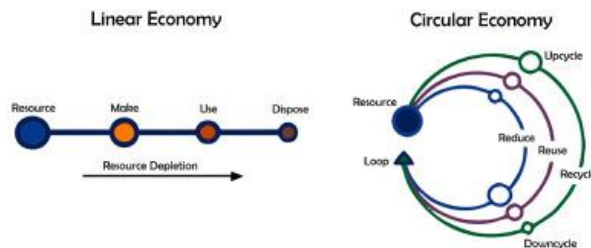


Figure 1: Linear and circular economy [1].

The circular economy represents a shift in how society thinks about the resources it uses. With a focus on extended life cycles, the circular economy promotes a society where products, components, and materials are kept at their highest usefulness and value. When applied to building design, the circular economy can create a more environmentally friendly and resource-efficient construction industry. Circular design can lead to reduced waste, lower carbon emissions, and smarter use of resources, all while making our buildings more sustainable [2].

The journey into the world of circular design comes with numerous opportunities and challenges that could reshape the construction sector. The benefits are clear, including saving resources, cutting costs, and being more eco-friendly. However, there are certain challenges, such as dealing with rules and regulations, industrial traditions, and the need for innovative technologies [3].

The research will delve into the application of circular design in construction by optimizing the baseline steel-CLT floor system from a linear design to a circular one. This approach aims to develop efficient, reusable, and practical steel-CLT composite floor systems, contributing to the goal of moving to a circular construction industry. In essence, the study seeks to advance construction practices that prioritize sustainability, environmental responsibility, and resource efficiency.

## 1.2 Composite Floor systems

A composite floor system, which combines different materials like steel and concrete or steel and timber, offers several advantages in construction. These systems aim to create stronger and more efficient flooring solutions by harnessing the unique properties of each material. The benefits of composite floor systems can include

enhanced sustainability through optimization of material use, ease of construction, and reduced unit weight [6]. Additionally, they can enhance structural properties such as stiffness and load-bearing capacity [7].

The most common composite floor system used extensively in Europe is the steel beam and concrete floor system. In this system a concrete slab, typically cast on a thin-gauge metal deck is connected to steel beams using steel dowels (headed studs or other shear connectors). Both the steel beam and the concrete slab act together to form the composite system. Another type of composite system is the timber-concrete composite (TCC) system, which combines timber (often CLT) and concrete as composite materials. This type of floor system utilizes various shear connectors to connect the floor segments, enhancing the overall strength and stiffness of the floor. Yet type of composite system is the steel-CLT composite system, which represents an innovative approach that will be the focus of this study, as detailed in the next chapter (1.3). This system offers a sustainable alternative to traditional steel-concrete systems, addressing construction needs while significantly contributing to sustainability efforts by reducing environmental impacts [8].

The design of the composite beam is a critical aspect in composite systems due to its role in defining the structural characteristics of the floor system, as the interaction between the composite components has a direct impact on the stress distribution along the cross-section. That interaction can be divided into three primary categories: no shear interaction, fully rigid interaction, and an intermediate phase known as semi-rigid interaction.

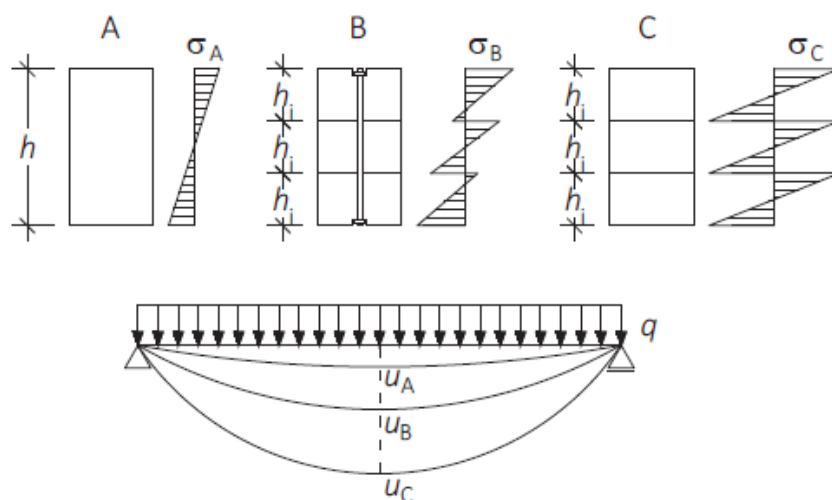


Figure 2: Deflection and bending stress distribution of a full cross-section (A), a cross-section comprising three individual cross-sections connected via semi-rigid joints (B) and a cross-section comprising three loosely superimposed individual cross-sections (C). [12]

- No Interaction:

In this category, denoted as Case C according to Figure 2 [12], the structural elements within the composite beam do not exhibit any shear interaction. Each element behaves



independently, leading to negligible composite action. This is the theoretical situation of a floor slab bearing directly on a beam without any connection between the two.

- Fully Rigid Interaction:

In this category, denoted as Case A in Figure 2, fully rigid interaction occurs. The structural elements within the composite beam act as one. With fully rigid joints, often achieved through glued connections, they exhibit a cohesive behavior acting as a single, rigid unit. The Euler-Bernoulli beam theory applies to the overall cross-section, and the bending stress distribution and deflection follow specific patterns. For example, assuming constant moduli of elasticity and dimensions of the beams, the bending stress ( $\sigma$ ) in the outer fiber follows the relationship  $\sigma_A \leq \sigma_B \leq \sigma_C = 3 \sigma_A$ , and the deflection ( $u$ ) adheres to the relationship  $u_A \leq u_B \leq u_C = 9 u_A$ .

- Semi-Rigid Interaction:

Source [12] emphasizes that in the semi-rigid interaction phase (Case B in Figure 2), where shear connectors are employed, stress distribution along the beam's cross-section is improved. This enhancement leads to increased load capacity and decreased deflections. The type and stiffness of shear connectors, represented by the slip modulus ( $k$ ), become pivotal factors influencing the rigidity of the system. The load-bearing capacity and stiffness of mechanically jointed beams, like Case B, lie between those with no joints (Case C) and those with fully rigid (glued) joints (Case A).

In the subsequent Gamma Method chapter, the slip modulus ( $k$ ) and its' role in determining the effective bending stiffness of the mechanically jointed cross-sections are elaborated in detail.

In summary, composite floor systems are an established approach to creating stronger, stiffer, and more material efficient structural floor systems in modern construction. By combining different materials and utilizing shear connectors, these systems provide a toolbox of options for the practicing engineer to realize highly efficient solutions which offer numerous benefits.

## 1.3 Problem Description and Objectives

WSP is committed to innovating structural solutions that meet modern sustainability criteria. This commitment focuses on decarbonization of structural designs. CLT, known for its low carbon and bio-based properties, plays a key role in this decarbonization effort. Therefore, WSP has prioritized the development of a composite steel-CLT floor system to replace traditional concrete floors in composite construction with CLT. In this study, this system is referred to as the "baseline design/floor system." This novel system being researched and tested by WSP and the University of Warwick, uses steel headed shear studs welded to the top flange of steel beams and located in grouted pockets in the CLT floor panels to form a sufficient composite connection, as shown in Figure 3.

While the use of grout is highly effective in realizing a stiff connection, a grouted connection reduces the potential for demountability of the floor system at the end of the buildings useful. Thus, it can be said that the use of grout does not align with the principles of circular design. In which materials should be reclaimed and reused in the market once no longer needed in the original, or current building.

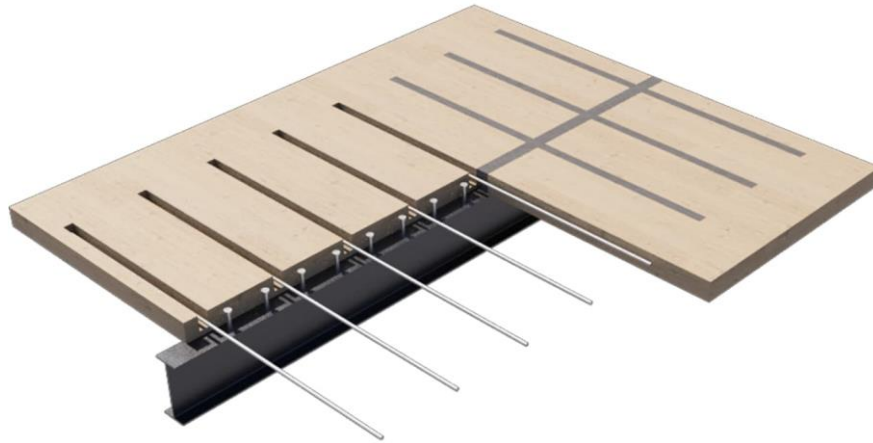


*Figure 3: 3D picture for the baseline floor system researched by WSP.*

One of the primary objectives of this study is to enhance the circularity of the baseline steel-CLT composite floor system by investigating new shear connectors that better align with circularity criteria. This improvement aims to bridge the gap between the innovative floor system and the fundamental goals of circular design.

The baseline system was designed and tested to assess the structural behavior of the composite beam and the shear connector. As a result, the CLT configuration had to remain consistent across different spans due to its critical role in forming the grout pockets and determining the stiffness of the composite beam. The presence of a variable cross-section along the beam's longitudinal direction further complicates the analytical determination of its behavior, making accurate improvement of the CLT design more challenging.

The second major objective is to refine the CLT design configuration within composite floor structures. This aspect of the research will address the challenges related to CLT design in a composite context, aiming to identify the optimal configuration that enhances the material efficiency of the floor system.

By the conclusion of this study, an optimized floor system will be developed. This system is designed to be circular, ensuring it not only performs effectively in its initial application but also can be disassembled and reused, thereby supporting multiple life cycles. Additionally, the optimized system will feature a revised CLT configuration that provides adequate structural performance while minimizing floor thickness.

## 1.4 Research Questions

This chapter explains the key research questions required to achieve the primary goal of improving the design of the steel-CLT floor system, with a focus on circularity and optimizing the CLT panels. In addition to these primary inquiries, several sub-questions have been meticulously crafted to break down the main problem into smaller portions. These sub-questions contribute not only to a thorough understanding of the primary research question, but also contribute to the organization of the research methodology, and approach.

### **Primary Research Question:**

Can the circular design of steel-CLT floor systems be realized, and what are the structural benefits and drawbacks of this innovative solution?

How can a CLT configuration be designed to function optimally as an integral component of the composite beam and floor system?

What are the advantages and disadvantages of the optimized floor system versus the baseline floor system?

### **Sub-questions:**

- How can mechanical fasteners, specifically shear connectors, be designed to optimize the structural performance of steel-CLT composite beams while maintaining principles of circular design and sustainability?
- Is the attainment of truly circular steel-CLT composite floors a feasible objective with the existing body of knowledge and technological capabilities?
- In what ways can the steel-CLT composite floor systems be standardized to ensure efficient implementation while adhering to circular design principles?
- What parameters are integral to the design equation, and how can these parameters be effectively managed to achieve the optimal design?

## 1.5 Research Structure

As mentioned previously, the primary goals of this research are to develop a circular design for steel-CLT composite floors and to enhance the design of the CLT panels. The research methodology unfolds systematically, beginning with the baseline floor system design developed by WSP, which incorporates grout as a bonding material. This design provides the basic framework for geometry and initial parameters on which the subsequent studies are undertaken.

However, the study begins with a comprehensive literature review, establishing a solid technical foundation by presenting the state of art and current assumptions derived from existing research. Following this, the application of the new demountable shear

connectors will be discussed, highlighting their impact on composite action and structural performance of the composite floor system. The next section focuses on the CLT panels and their dual function within composite floor structures, adding complexity to their design. This part of the study includes the derivation of a detailed design approach, culminating in the determination of the optimal CLT panels configuration to be used in the final optimized design.

During the study, the Gamma method, an analytical approach to perform structural analysis for composite beams, will be used to obtain structural results for the various design studies. This method was chosen because it provides clarity when defining parameters, leading to greater understanding of individual parameter impacts on the structural behavior. The Gamma method will be discussed in detail in Chapter 2.1.

After determining the optimized design for the steel-CLT composite floor system. The final phase begins with a comparison of the newly developed floor system to the baseline one. This comparison, which focuses on structural and environmental aspects, reveals each system's respective strengths and weaknesses, providing valuable insights into design choices and requirements. The outcomes of this comparison will be thoroughly validated, verified, and discussed.

The research concludes with a discussion that covers the insights gained throughout the study. The findings are compiled into a comprehensive conclusion that provides valuable insights into the design of steel-CLT composite floors as well as recommendations for future research.

## 2 LITERATURE REVIEW

This chapter serves as a comprehensive guide, delving into various subjects to reveal important scientific insights. The goal is to establish a foundational understanding that will improve the reader's overall understanding of the topic. The focus here is on elucidating key subjects relevant to this study using information from existing literature.

Each subject will be thoroughly explained, followed by an additional subchapter that establishes the link between the subject matter and the current study. This structured approach enables the reader to systematically establish a solid scientific foundation on every subject before delving into its relevance to the study.

The significance of this chapter stems from its role as an information repository, containing all of the essential knowledge that will be used in subsequent chapters to achieve the objectives outlined in the previous chapter. After completing this chapter, the reader will have the necessary knowledge to navigate and comprehend the following sections with ease.

### 2.1 Gamma Method for Mechanically Jointed Beams

The Gamma Method is a proven analysis tool in structural engineering, providing a manual calculation method for simple mechanically jointed beams. This method, outlined in Annex B of EC 5 [18], allows for efficient structural analysis of beams and columns with up to three single components. Möhler, who developed the Gamma method used elasticity relations based on Euler-Bernoulli beam theory within the cross-section to determine the bending stiffness and stress distribution across the composite cross-section. The relations and equations are explained in subchapter 2.1.2.

The Gamma Method is applicable solely to simply supported beams subjected to uniformly distributed loads and centrally loaded columns. It's valid only when a maximum of three individual components are non-abutted over the member length, and continuous fasteners with constant stiffness along the member length are utilized. Additionally, it assumes negligible shear deformations of the beam, making it suitable in scenarios involving large spans [12]. In those cases, bending deformations are significantly higher than shear deformations, so shear deformations are disregarded.

#### 2.1.1 Relevance to The Study

Adopting an analytical approach for structural analysis offers several key advantages. One of the primary benefits is the clear definition of parameters, which allows for their individual impacts to be thoroughly investigated and understood. This clarity facilitates a more precise exploration of how each parameter influences the composite beam's behavior. Additionally, the ability to perform numerous structural analyses in a short period of time is a significant advantage. This efficiency is particularly beneficial for conducting parametric studies, where multiple parameters can be systematically varied

to assess their effects on the composite beam's performance. These advantages make the analytical approach especially valuable in this study, which aims to optimize several parameters.

However, the gamma method's relative versatility extends across different materials, making it a widely applied method in composite beam design. It is included in various regulatory documents, such as EC5 for timber, where it's used for composite timber applications. Additionally, it's integrated into EC5 Structural design of timber-concrete composite structures for designing composite timber-concrete beams [20]. Numerous research articles [19][21] validate the accuracy of this method in reflecting the serviceability and ultimate response of timber-concrete composite beams in the linear elastic phase.

This study focuses on long-span composite beams comprising steel and CLT structural materials. The literature review indicates promising accuracy of the gamma approach compared to full-scale test results [22]. The comparison between structural analysis results derived from different numerical models and those determined using the gamma method underscores its reliability.

The preceding discussion highlights the gamma method's effectiveness and adaptability, seamlessly integrating into the design processes of various composite structural materials. Leveraging its benefits and previous investigations, this study employs the gamma method as an analytical approach for structural analysis in the subsequent chapters.

### 2.1.2 Relations and Equations

The derivation procedure for the following relations is detailed in Annex 5 of the Timber Engineering book [12]. The system of differential equations originates from elasticity relations, based on beam theory, and is applied to force and moment equilibrium under specific boundary conditions. This process results in a system of equations, which, when solved, yield the displacement equations necessary for determining the coefficient  $\gamma$ :

$$\gamma_i = \frac{1}{1+p} \quad (2.1)$$

$$p = \frac{\pi^2 * E_i * A_i * s_i}{k_i * l^2} \quad (2.2)$$

Where:

$E_i$  Modulus of elasticity.

$A_i$  Cross-sectional area.

$s_i$  Fastener spacing in joint between individual components.

$k_i$  Slip modulus of fasteners.

$l$  Member length.

This coefficient  $\gamma$  is a critical parameter that acts as a reduction factor for the bending stiffness, stresses, and shear forces, representing the semi-rigidity in the composite cross-section. The value of  $\gamma$  depends on the rigidity of the shear connectors linking the different materials (composite components) in the cross-section, ranging from 0 to 1. A  $\gamma$  value of 0 indicates no shear interaction between the individual composite components, while  $\gamma = 1$  signifies full interaction, also known as maximum shear interaction.

In the effective bending stiffness equation for composite beams, the coefficient  $\gamma$  reduces the Steiner terms ( $E_i * A_i * a_i^2$ ) of the bending stiffness:

$$(EI)_{ef} = \sum_{i=1}^3 (E_i * I_i + \gamma_i * E_i * A_i * a_i^2) \quad (2.3)$$

Where:

$(EI)_{ef}$  Effective bending stiffness.

$I_i$  Second moment of area.

$\gamma_i$  Gamma coefficient for  $i = 1$  and  $i = 3$ . For  $i = 2$  which is the composite component that passes through the neutral axis of the composite cross-section  $\gamma_2 = 1$  (see Figure 4).

$a_i$  Distances between the center of gravity of the individual components to the neutral axis.

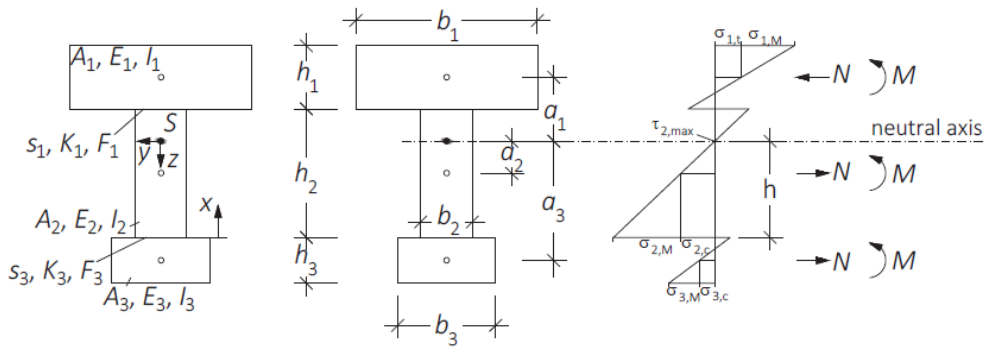


Figure 4: Example of a composite beam with three components [12].

The following graph illustrates the relationship between bending stiffness and the coefficient  $\gamma$ . As the  $\gamma$  value increases, the bending stiffness also increases, primarily due to the enhanced contribution of the Steiner term. This graph was generated using data from the baseline design, treating  $\gamma$  as a variable that incrementally increases in a looped process, with the effective bending stiffness recorded at each step.

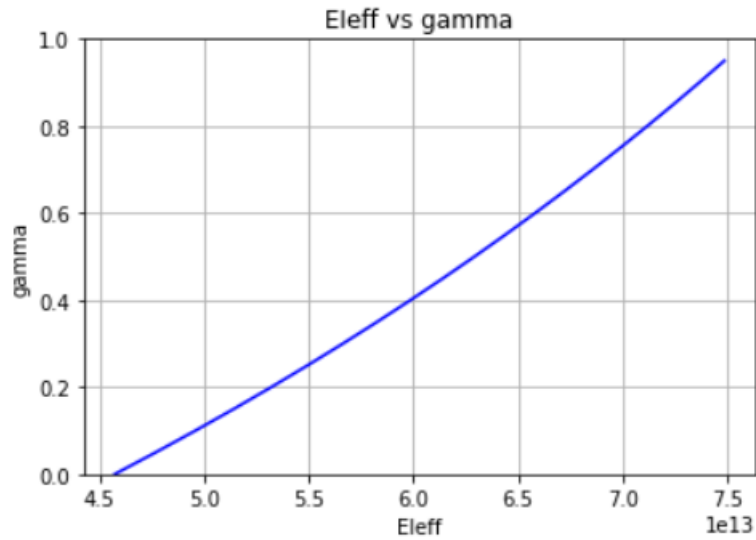


Figure 5: Gamma vs. Effective Bending Stiffness.

The normal stress distribution equations are derived from moment equilibrium across the composite cross-section, following the same assumptions. The derivation process is also explained in Annex 5 of the Timber Engineering book [12]. The stress equations are as follows:

$$\sigma_{i,t(c)} = \frac{\gamma_i * E_i * a_i}{(EI)_{ef}} * M \quad (2.4)$$

$$\sigma_{i,m} = \frac{0,5 * E_i * h_i}{(EI)_{ef}} * M \quad (2.5)$$

Where:

$\sigma_{i,t(c)}$  The normal stress in the center of gravity of the individual components.

$\sigma_{i,m}$  The normal stress in the outer fibers of the individual components.

$M$  External moment.

$h_i$  Depth of individual component.

Refer to Figure 4 for the stress distribution along the composite cross-section.

Using a similar approach, the shear stress relations are determined, leading to the derivation of the shear flow equation. The load on the fasteners is then calculated as the product of the shear flow and the spacing between the fasteners:

$$t_{ef} = \frac{V * \gamma_1 * E_1 * A_1 * a_1}{(EI)_{ef}} \quad (2.6)$$

$$F_i = t_{ef} * s \quad (2.7)$$

Where:

$t_{ef}$  Shear flow.



- $V$  Shear force.
- $F_i$  Fastener load.
- $s$  Spacing.

## 2.2 Pre-loaded Demountable Shear Connectors

Shear connectors are essential in composite beams because they resist the slip and the longitudinal shear at the interface of the composite components, allowing for the desirable composite behavior. Composite steel-concrete structures use a variety of shear connectors, including headed steel studs, perfobond ribs, t-rib connectors, oscillating perfobond strips, waveform strips, t-connectors, channel connectors, and non-welded connectors [36]. The significance of these connectors lies in their ability to improve the structural integrity and load-bearing capacity of composite beams by rigidly or semi-rigidly combining the steel beam and floor concrete components. On the other hand, traditional shear connections face sustainability challenges, such as being non-deconstructible or non-recyclable, leading to energy-intensive and environmentally damaging deconstruction processes and limited opportunities for component reuse [36]. For instance, when traditional shear connections are removed, they often end up in landfills, contributing to waste and environmental pollution. As a result, there is an increased need for demountable and recoverable shear connectors, such as pre-loaded bolted connectors in composite beams to address these sustainability concerns and encourage environmentally friendly construction approaches [36]. In the following paragraph, pre-loaded bolted shear connectors are introduced, which provide the advantage of demountability and reusability, aligning with the principles of sustainability and circularity.

The stiffness of the shear connector, represented by the slip modulus ( $k$ ), is a critical factor in determining the rigidity of composite beams and the stress distribution through the composite cross-section under load application. This slip modulus is directly related to the reduction factor  $\gamma$ , indicating its significant influence on the structural mechanics of composite systems. Determining the slip modulus typically involves undertaking push-out tests or following prescriptive design criteria outlined in the relevant Eurocode and that has been validated using comparable experimental methodologies.

Overall, shear connectors are essential in composite beam design, as they play a crucial role in realizing the required composite structural behavior. The type of shear connector, whether demountable or not, has a direct impact on the circularity of the composite floor system, highlighting the importance of the shear connector in realizing sustainable design solutions.

This study will focus on the three Pre-loaded Demountable Shear Connectors introduced at the World Conference on Timber Engineering 2023. These connectors align with circular design principles by allowing for deconstruction and potential reuse.

This report assigns the three shear connectors the nomenclature SCT-1, SCT-2, and SCT-3. These connectors, described in a paper [10], were tested in the laboratory using the standardized push-out test methodology. All three variants include an embedded steel tube that fits into a drilled hole in the timber floor panel. Each type of connector differs in the attached steel elements to the bottom side: SCT-1 employs a round steel ring, SCT-2 integrates a round steel ring with a spiked timber connector, and SCT-3 incorporates a rectangular steel plate with openings and four inclined screws (see Figure 6).

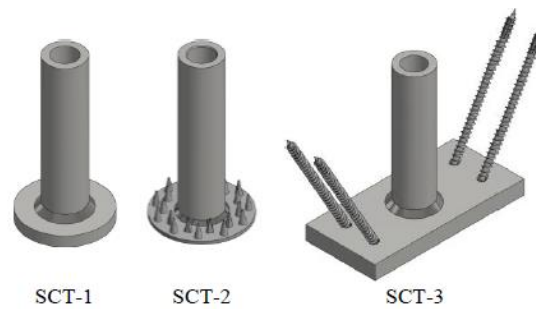


Figure 6: Embedded parts in the timber: SCT-1, SCT-2, and SCT3 [10].

On the top side of the steel tube, a rounded steel ring is positioned before securing pre-loaded steel bolts through the timber part and the top flange of the steel section, effectively connecting both cross-sections. The pre-loaded bolts necessitate the upper steel ring to protect the timber from being crushed due to the pre-loading. Figure 7 shows the details of the geometry after assembly.

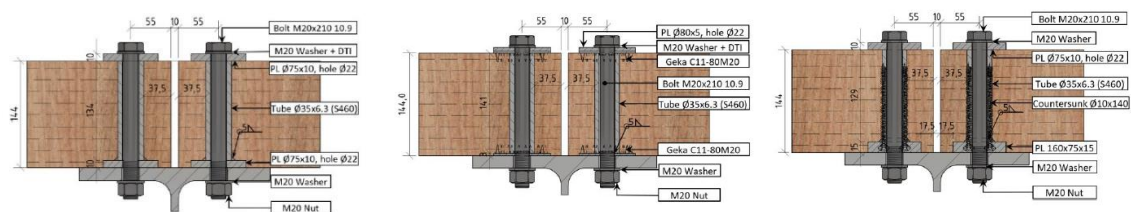


Figure 7: Details of shear connections: SCT-1, SCT-2, and SCT3 [10].

The results of the push-out test carried out by [10] are shown in Figure 8, where the load/slip graph displays similar behavior for all three connections. The initial stage, which is characterized by relatively high stiffness, is the result of preloading the bolts to 70% of their ultimate strength. This preloading introduces friction between the steel tube and bolt. This force resists the shear force between the timber panel and the steel beam, resulting in the observed initial no slip and corresponding high stiffness; more information on this subject is discussed in Chapter 4. Following the initial stage, an initial slip occurs at a shear load ranging from 30 to 45 kN, depending on the SCT type. When that slip occurs, the steel bolt shifts inside the tube until it comes into contact with both the beam's flange and the inner steel tube. Following contact, stiffness increases similarly to traditional steel-timber bolt connections.

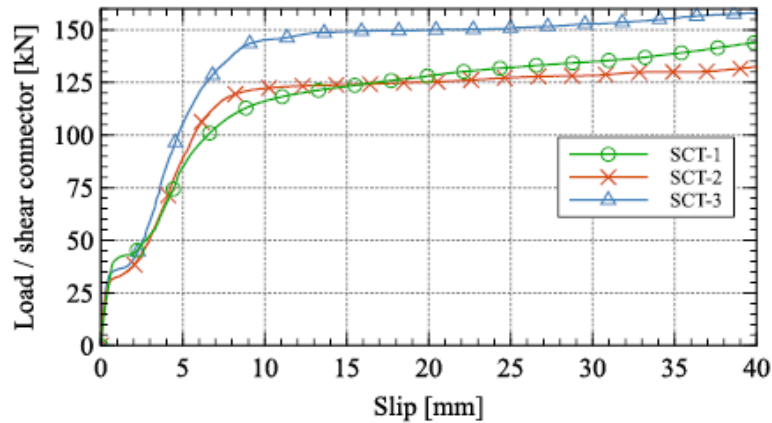


Figure 8: Comparison of the three shear connectors' mean load/slip curves [10].

Therefore, these shear connectors offer a significant advantage in terms of initial stiffness compared to traditional bolt shear connectors, thanks to bolt pre-loading. This enhanced stiffness is particularly beneficial for design scenarios where the loads acting on the shear connector do not exceed the initial phase boundary condition. Furthermore, the push-out test results included in the paper are presented for one shear connector. However, it's important to note that these connections are used in pairs (see Figure 6), effectively doubling the provided stiffness. This means that the initial stiffness provided by a pair of connectors is comparable to traditional steel shear studs, as demonstrated later in Chapter 4. In addition to these advantages, these connectors are designed following circular principles, allowing for demountability and reusability, a feature not found in traditional shear studs.

### 2.2.1 Relevance to The Study

The previously described shear connectors are promising for integration into the steel-CLT composite beams proposed in this study. However, applying them to this study presents challenges, particularly in determining the slip modulus, because existing push-out test data is based on experiments with LVL timber, which has material properties and characteristics different from CLT. A correction factor has been determined and used to address this mismatch so that the initial slip modulus found in the push-out test can apply to steel-CLT composites. This procedure involves calibrating the slip modulus value from the available push-out test data with the slip modulus calculated using EC5, which allows the reliance on the EC5 to determine the differences between the LVL and CLT and determining the correction factor. Chapter 4 provides a more detailed explanation of the Structural Properties and Application of Pre-loaded Demountable Shear Connectors.

## 2.3 Cross-Laminated Timber Panels

Cross-laminated timber (CLT) is a highly engineered wood product that provides structural engineers with a versatile structural material with good strength to weight ratio for use in different structural purposes [23]. CLT is made up of several layers of

timber lamella that are normally positioned perpendicular to one another and joined together under pressure using adhesive. This crosswise lamination process enhances the timber material's structural characteristics, including improved strength and stiffness. Furthermore, this crosswise arrangement of timber layers allows CLT structures to efficiently transfer loads in both parallel and perpendicular directions, improving the material's isotropic behavior. This feature enables engineers to take advantage of CLT's strength in a variety of configurations and orientations, allowing the designer to optimize structural performance [23].

CLT's structural characteristics make it ideal for a wide range of load-bearing applications, including floors, beams, walls, and columns. Furthermore, the material's lightweight nature makes it easier to transport and assemble [23].

Due to the above advantages the use of CLT in the construction industry is rapidly increasing [45]. Espinoza, O., Trujillo, V. R., Mallo, M. F. L., and Buehlmann, U. identified in their paper [45] that from 1995 to 2015, CLT production increased from less than 50,000 m<sup>3</sup> per year to over 1,000,000 m<sup>3</sup> per year by 2015. CLT is quickly becoming the market leading mass timber panel system in Europe.

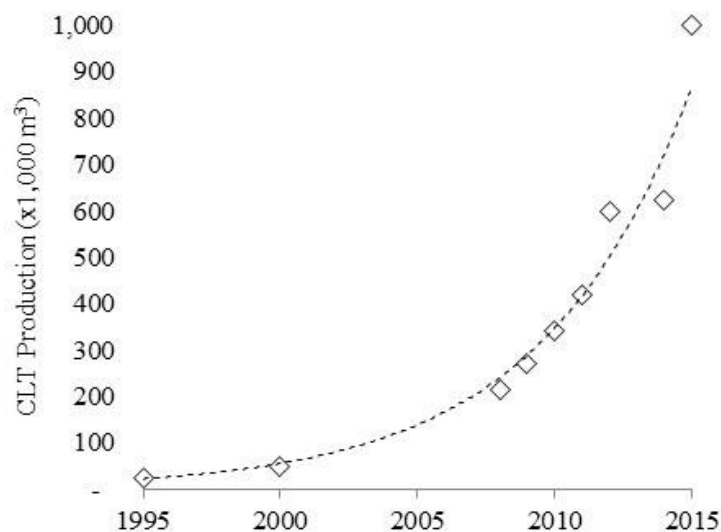


Figure 9: Global production of CLT in years [45].

Biogenic carbon refers to the carbon sequestered within timber, which reduces atmospheric CO<sub>2</sub> levels and contributes to climate change mitigation. In lifecycle assessments, the carbon stored in timber is factored in, making it a more sustainable option than materials like concrete or steel. However, when timber decomposes or burns at the end of its life, the stored carbon is released back into the atmosphere. Proper management, such as adopting circular design principles, can extend the duration of carbon storage by prolonging the material's lifecycle, thereby enhancing timber's environmental benefits [13].

Figure 10 illustrates the calculation of carbon emissions for timber structures, where biogenic carbon is distinguished from fossil carbon. During the production and

construction phases (Modules A1-A5), biogenic carbon is transferred into the structure, while fossil carbon is emitted. At the end of the structure's life, the biogenic carbon is released back into the atmosphere. However, in the case of a circular design, the structure is reused at the end of its life, extending its lifecycle and keeping the carbon stored for a longer period [13]. Further discussion on this topic is provided in Chapter 2.6.

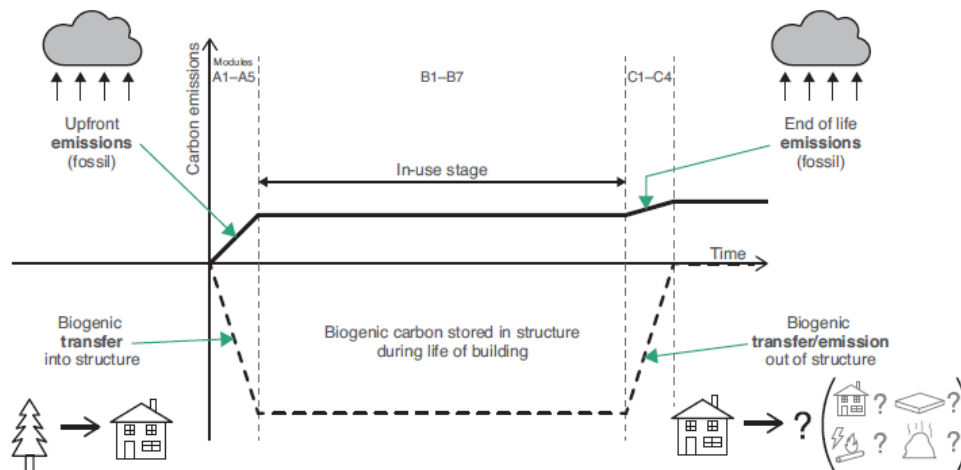


Figure 10: Sequestered biogenic carbon (transfers/emissions) and fossil carbon (emissions) for a typical timber [13].

### 2.3.1 Relevance to The Study

This study employs CLT panels for the structural floor, forming a composite material on top of the I-shaped steel beams. This choice is motivated by CLT's remarkable adaptability, allowing panels to be oriented in various directions to optimize floor system design, and the fact that CLT is the most commonly used and available mass timber floor panel system in the Dutch market. A CLT structure will have a strong out-of-plane direction and a weaker out-of-plane direction at 90 degrees to the strong direction because of its orthotropic features, which indicate that a panel's strength varies depending on the angle between stress and fiber direction [23]. As a result, the CLT floors have several panels that are purposefully oriented differently to improve strength and stiffness in particular orientations.

One of the main advantages of designing CLT floors lies in the ability to customize their strength and stiffness in two directions. By positioning certain CLT panels perpendicular to others, the structural behavior of the CLT floor can be significantly influenced. This provides the designer with an almost unlimited choice in panel configuration to suit their specific situation. However, designing a CLT floor as a composite structure introduces complexity. In contrast to designing a non-composite floor that spans between beams, where the strong axis of the floor is usually oriented in the y-direction (as shown in Figure 11 in black), designing a composite system involves additional factors because, in addition to meeting structural requirements for the floor spanning

between the beams, the CLT floor directly affects the strength and stiffness of the composite beam.

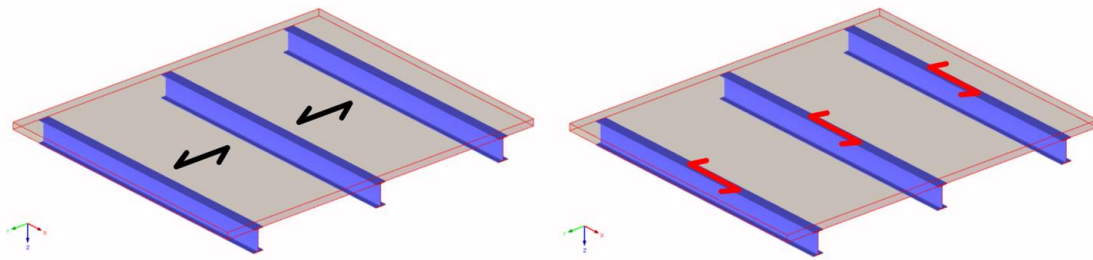


Figure 11: 3D visualization of a typical Steel-CLT flooring system [28].

For instance, the bending stiffness of the composite beam is directly related to the stiffness of all the components in the composite system, including the CLT panels that work in the longitudinal direction of the beam, represented as the x-direction in Figure 11 (shown in red). Consequently, optimizing the orientation of CLT panels becomes a complex parameter. This study conducts a parametric analysis to define the relationship between the CLT panel setup and the composite beam's load-bearing capacity to determine the optimal design of the CLT floors within the composite system. This topic is further discussed in Chapter 5.

### 2.3.2 Equivalent CLT Cross-section

Examining a cross-section of a typical CLT panel indicates that it is made up of multiple layers that are glued together to form a composite structure itself. At this point it is assumed that the modulus of elasticity perpendicular to the grain,  $E_{90}$ , is negligible ( $E_{90} = 0$ ), implying that layers oriented perpendicular to the grain make no structural contribution [23]. This is the common assumption taken in current codified CLT design. Furthermore, it is assumed that the modulus of elasticity parallel to the grain is equal to the mean value of the panel's modulus of elasticity, denoted as  $E_0$ . Again, this is the common assumption taken in the current standards. Figure 12 depicts a CLT panel with a bending moment (25 kNm) applied around the neutral axis to show the stress distribution across the cross-section height when considering these assumptions.

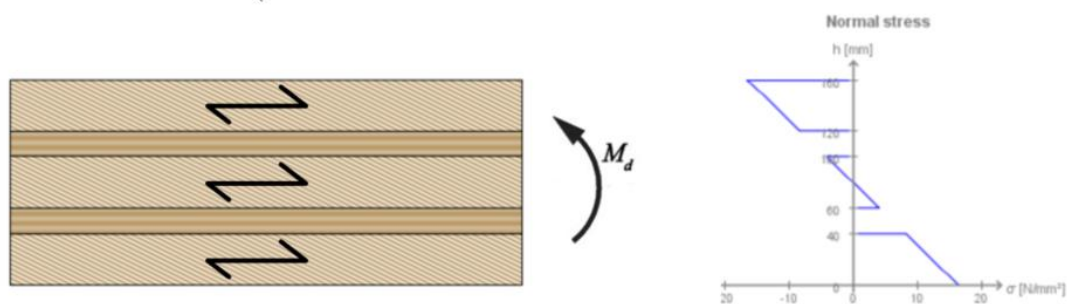


Figure 12: CLT designer software [35].

This approach becomes more complicated when designing composite beams with both CLT and steel, as in this study. To address this complexity, a method has been developed by [22] to homogenize the CLT floor panel. In this method, an equivalent homogeneous cross-section replaces the CLT cross-section (see Figure 13), ensuring that the resulting and original cross-sections are equivalent in certain structural properties [22].

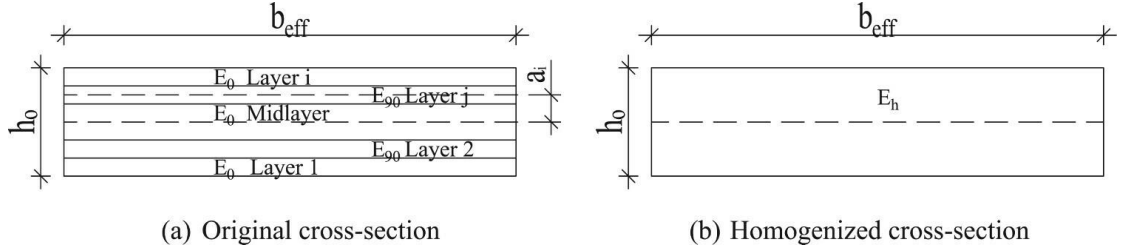


Figure 13: Original vs homogenized cross-section [22].

Furthermore, a singular value for the elastic modulus,  $E$ , of the homogenized CLT panel is derived. Notably, the dimensions of the CLT panel remain constant throughout the homogenization process [22]. This method is known as the EA-equivalent method, and the elastic modulus is calculated using the following equation:

$$E_h * A_h = (EA)_{eff} \quad (2.8)$$

$$A_h = h_0 * b_{eff} \quad (2.9)$$

$$(EA)_{eff} = \sum_{i=1}^n E_i * A_i \quad (2.10)$$

$$E_{eff} = \sum_{i=1}^n \frac{E_i * A_i}{A_{tot}} \quad (2.11)$$

Where:

$E_h$ : the elastic modulus of the homogenized CLT cross-section.

$A_h$ : the area of the homogenized CLT cross-section.

$h_0$ : the height of the CLT slab.

$b_{eff}$ : the effective width of the CLT slab.

$E_i$ : the elastic modulus of each layer depends on the orientation of the layer.

$A_i$ : the area of each layer.

## 2.4 Effective Width of Composite Beams

The effective width of the top flange of a beam working compositely with the floor slab, specifically the effective flange width ( $b_e$ ) for T-beams, is crucial for design considerations as it denotes the part of the beam actively countering compression forces in the cross-section. Understanding this effective flange width is paramount, influencing force distribution within the beam and impacting overall strength and



stiffness. Engineers, by accounting for this width, can properly design T-beams to endure anticipated loads and perform optimally in their intended applications [29].

The flange collaborates with the beam to resist longitudinal compression forces [29], ensuring the entire flange effectively counters compression forces in the cross-section. It plays a pivotal role in distributing compression forces along the beam evenly, enhancing load-bearing capabilities [29].

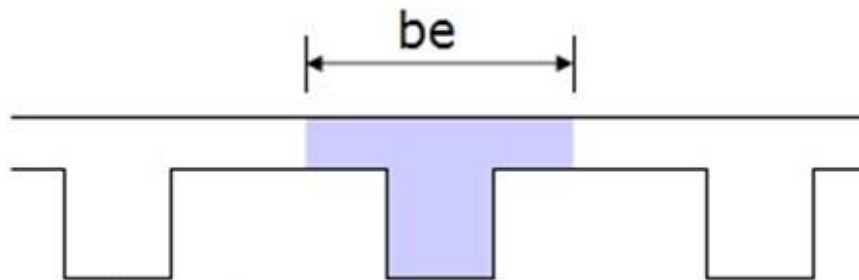


Figure 14: Effective Flange Width T-beam [29].

#### 2.4.1 Relevance to The Study

While research on the effective width in timber structures is limited compared to composite steel and concrete structures [30], a relevant study [30] explored the effective width of timber composite beams under positive bending. Utilizing structural analysis on various numerical models, the study validated results with experimental tests, presenting a formula for determining the effective width. Unfortunately, the formula, which is suitable for spans ranging from 6 to 10 meters [30], is not applicable to the broader span objectives of this study. Specifically, the composite floor system under investigation has a span of 12 meters, extending beyond the formula's valid range.

In this study, however, a conservative approach will be used to determine the effective width of the composite steel-CLT beam by applying design formulas from Eurocode 4 and Eurocode 5. Eurocode 4 provides guidelines for composite steel and concrete structures, while Eurocode 5 addresses ribbed plates composed of ribs and CLT plates. Both methods will be applied, and the lower effective width value will be selected for structural analysis.

The Eurocode 4 design formula for determining the effective width of a composite beam is expressed as:

$$b_{ef,EC4} = b_0 + \sum b_{ei} \quad (2.12)$$



Where:

$b_{ef,EC4}$  The effective width according to EC4.

$b_0$  the distance between the centers of the outstand shear connectors.

$b_{ei}$  the value of the effective width of the concrete flange on each side of the web, computed as  $L_e/8$  but not exceeding geometric width  $b$ .

The length  $L_e$  is the approximate distance between points of zero bending moment, conservatively equating to the span  $l$  in this study as the composite beams are simply supported on the edges. Therefore, for the composite Steel-CLT beam holds the following:

$$b_0 = 0$$

$$b_{ei} = l/8$$

$$b_{ef,EC2} = l/4$$

According to Eurocode 5 [18], the effective width of a composite beam consisting of CLT plates and ribs is determined as follows:

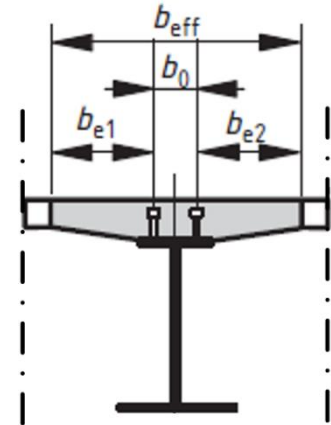


Figure 15: The parameters to calculate the effective width according to EC4 [31].

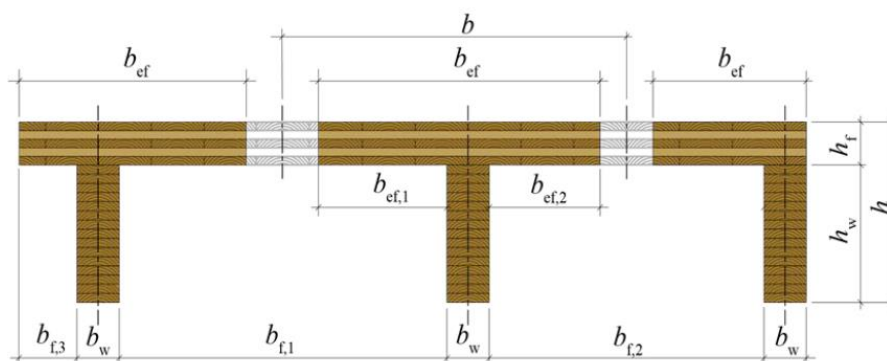


Figure 16: The parameters to calculate the effective width according to EC5 [38].

$$b_{ef,EC5} = b_{rib} + \sum b_{ef,i} \quad (2.13)$$

$$b_{ef,i} = b_i \left( 0.5 - 0.35 \left( \frac{b_i}{l} \right)^{0.9} \left( \frac{(EA)_i}{(GA)_{xy}} \right)^{0.45} \right) \quad (2.14)$$

Where:

$b_{ef,EC5}$  The effective width according to EC5.

$b_{rib}$  The width of the rib.

$b_{ef,i}$  The effective width at either side of the rib.

$b_i$  The clear distance between two ribs.

$l$  The span.

$(EA)_i$  The in-plane stiffness of the layers with grain parallel to x-direction per meter width.

$(GA)_{xy}$  The shear stiffness of the gross cross-section per meter width.

As a result, the effective width of the composite beam will be:

$$b_{ef} = \min(b_{ef,EC4}, b_{ef,EC5}) \quad (2.15)$$

By following this method, the study ensures a conservative and accurate determination of the effective width, incorporating both structural codes' considerations.

## 2.5 Spacing

The spacing ( $s$ ) between shear connectors is a critical factor influencing the behavior of composite beams, particularly in the interaction between the steel beam and the CLT floor system. This relationship is quantitatively expressed in the gamma method through the gamma factor ( $\gamma$ ), a key parameter that governs the degree of interaction within the composite beam. The equation for the gamma factor highlights the significance of spacing, showing how it directly impacts the  $\gamma$  value, and thereby the level of interaction between the steel and CLT components:

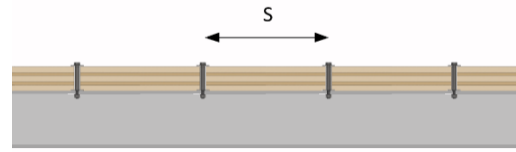


Figure 17: longitudinal section of composite beam.

$$\gamma = \frac{1}{1 + \frac{\pi^2 * E * A * s}{k * l^2}} \quad (2.16)$$

A detailed explanation of this equation and its implications can be found in Chapter 2.1.2.

However, the subsequent Figure 18 illustrate the relationship between spacing and both the gamma factor and bending stiffness. These results are based on the baseline composite beam design, which is described in Chapter 6.1.1. Upon examining the data for spacings of 200 and 800 millimeters, the gamma factor is found to be 0.9 and 0.69, respectively, corresponding to effective bending stiffness values of  $0.99 * 10^{14}$  N/mm<sup>2</sup> and  $0.91 * 10^{14}$  N/mm<sup>2</sup>. This shows an 8% reduction in bending stiffness from a spacing increase from 200 to 800 millimeters, demonstrating the sensitivity of composite beams to the spacing and the resultant importance of this parameter.

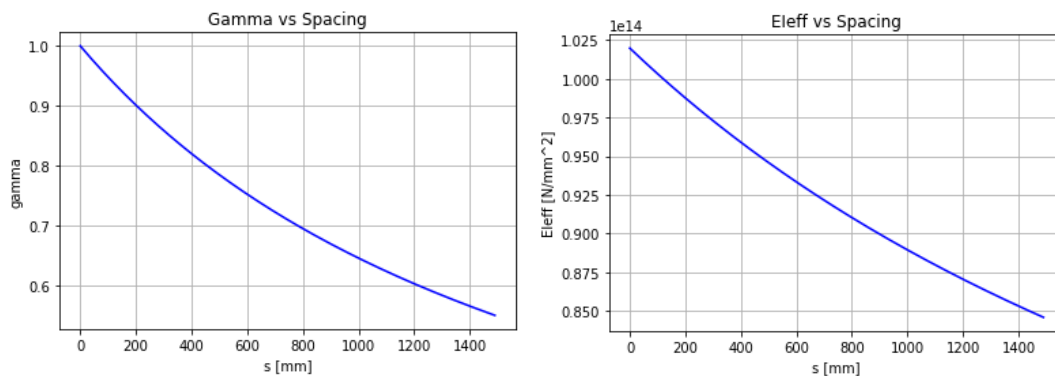


Figure 18: Gamma vs Spacing (left); Effective bending stiffness vs Spacing (right)

Furthermore, spacing also influences the horizontal shear force acting on the shear connector, as explained in Chapter 4. That Chapter will delve deeper into this influence, offering insights into how spacing is handled within the scope of this study.

## 2.6 Life Cycle Assessment and Embodied Carbon Calculation

The life cycle assessment (LCA) is a vital method for evaluating the environmental impacts at all stages of a product's life, from raw material extraction through production, use, disposal or reuse. This comprehensive approach assesses how each phase contributes to overall environmental burdens [42]. LCA examines the environmental footprint of a product or service by measuring impacts such as energy consumption during manufacturing, fuel usage in transportation, and ecological effects at the end of life. This enables meaningful comparisons between different products, materials, and processes, guiding more sustainable choices [43]. This study will specifically focus on the Global Warming Potential (GWP) impact by utilizing the embodied carbon impact category.

Embodied Carbon calculation serves as a comprehensive method for evaluating the GWP of a building [15]. This assessment considers all stages, from raw material extraction to manufacturing, construction, use, and eventual disposal or recycling [13]. By accounting for these stages, LCA provides a holistic perspective on the environmental impact of a construction project, offering insights into areas where carbon emissions can be minimized.

Embodied carbon refers to the total carbon equivalent associated with the production, transportation, and assembly of building materials throughout their life cycle [13]. It represents the total greenhouse gas emissions and global warming impact embedded in the very structure of buildings and provides an indication of the global carbon footprint of construction projects.

The calculation of embodied carbon is driven by the imperative to understand and mitigate the impact construction activities have on global warming. As the construction industry is a significant contributor to global carbon emissions, quantifying embodied carbon is a proactive step towards sustainable practices [13][15]. It enables stakeholders to make informed decisions regarding material selection, construction methods, and overall project design.

The Intergovernmental Panel on Climate Change (IPCC) is clear that to prevent significant harm to societies, man-made carbon emissions into the atmosphere must be rapidly reduced significantly. Reducing the embodied (upfront) carbon in our buildings is essential. However, reducing embodied carbon is consistent with broader sustainability objectives, such as reducing environmental impact, conserving resources, and fostering resilience. Sustainable construction practices emphasize using materials with lower embodied carbon and adopting innovative technologies and design strategies to enhance overall efficiency [14].

In the realm of structural materials, the choices between steel, concrete, and timber have significant implications for embodied carbon and overall environmental impact.

Concrete, primarily influenced by the amount of Portland Cement (PC), can be optimized for lower embodied carbon by substituting PC with supplementary cementing materials like Ground Granulated Blast Furnace Slag (GGBS) or Pulverized Fuel Ash (PFA). However, the production of these alternatives is tied to carbon-intensive industries, posing challenges for future supplies. Lowering concrete strength grades can reduce embodied carbon, but the impact on reinforced concrete sections depends on the associated demand for steel reinforcement. Steel's carbon factor varies based on recycled content and production method, with electric arc furnace (EAF) steel having a lower carbon factor than basic oxygen furnace (BOF) steel. The choice of steel products and production technique further influences carbon factors. Timber, with its unique biogenic carbon characteristics, sequesters carbon during growth, which can be climatically beneficial. However, the end-of-life fate of biogenic carbon, whether transferred out of the structure, burnt, or sent to landfill, must be considered. Reporting of biogenic carbon in timber assessments depends on certification from sustainably managed forests, with considerations for different life cycle stages. Each material choice involves a delicate balance between strength, durability, and environmental impact, highlighting the importance of informed decision-making in construction and design [13].

While using low carbon structural materials can lead to reduced embodied carbon, the designers have much more impact on carbon content through the optimization of the design and using fewer materials more efficiently. This approach is much more effective in minimizing embodied carbon in the short term. On the other hand, designing for circularity involves ensuring that structural materials retain their highest structural state at the end of their life cycle, allowing for their reuse. With this approach, carbon reduction occurs over the long term with each reuse of the material.

However, embodied carbon as a key design metric has a great framework to determine the carbon dioxide equivalent emissions along all life cycle stages. It therefore provides a framework for assessing both upfront embodied carbon and the impacts of circularity in building design. Figure 19 shows those 4 stages and the additional module beyond system boundary:

1. **Product Stage (Cradle to Gate):** This phase, which includes Modules A1 through A3, accounts for the carbon footprint measured in kgCO<sub>2</sub>e during the extraction, processing, manufacturing, and transportation of materials until the product is ready to leave the factory [13]. Notably, the recycled content of a product influences carbon emissions at this stage, regardless of its end-of-life recycling status, which is addressed in Module D.
2. **Construction Process Stage:** Modules A4 and A5 address the kgCO<sub>2</sub>e emissions associated with material transport to the construction site, energy consumption during on-site activities (such as site huts and machinery use), and carbon emissions associated with the production, transportation, and end-of-life processing of materials wasted on-site [13].

3. **Use Stage:** Modules B1 to B7 include the kgCO<sub>2</sub>e emissions caused by the building's use, maintenance, repair, replacement, refurbishment, and operational energy and water consumption [13]. Module B4, which focuses on replacement, is especially important when discussing embodied carbon during the use stage.
  4. **End of Life Stage:** Modules C1 to C4 account for the kgCO<sub>2</sub>e emissions during decommissioning, stripping out, demolition, deconstruction, transportation of materials away from the site, waste processing, and disposal of materials [13].
- **Beyond Life Cycle Impacts (Module D):** This additional module provides a more comprehensive view of environmental impacts beyond the project's life cycle. It calculates the net kgCO<sub>2</sub>e benefits or loads associated with recycling materials (for example, using scrap steel in steelmaking for future projects), energy recovery from materials (for example, energy generated by burning of timber products), and full reuse of materials/products in comparison to standard practices or products they would replace [13].

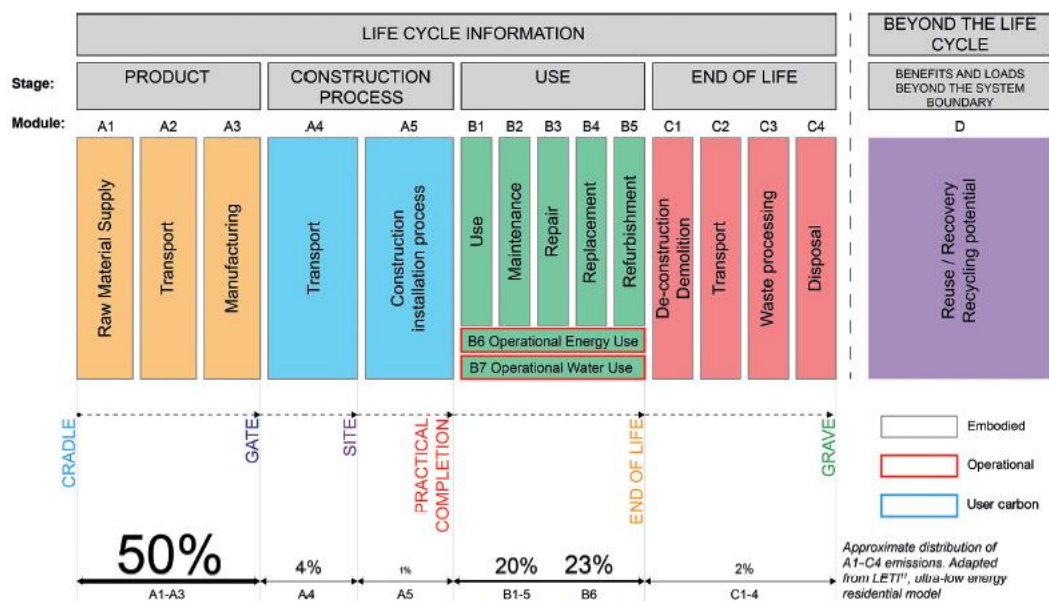


Figure 19: Life cycle stages and modules [13].

## 2.6.1 Relevance to The Study

In the final phase of this study, a comparison will be made between the optimized floor system (circular system) and the baseline floor system (linear system). This comparison focuses on both environmental and structural aspects, using the embodied carbon calculation as the primary metric to demonstrate the differences in environmental impact between the two floor systems. According to the Institution of Structural Engineers [13], "Calculating embodied carbon in the same rigorous way across all designs will allow meaningful comparisons to be made between structural schemes, developing our understanding of embodied carbon as well as how we can most effectively reach net zero carbon."

However, calculating embodied carbon for circular systems presents unique challenges due to its multi-cycling perspective, which introduces uncertainties and complexity in module D [32]. Researchers like Emilie, Michael, and Mona have highlighted these complexities, leading many studies to exclude Module D to avoid such complications [32]. This study will investigate the whole life carbon (A-C), so Module D is excluded from the embodied carbon calculation for simplicity.

Figure 19 illustrates that the production stage (A1-A3) accounts for roughly 50% of all environmental impacts in the life cycle [13]. Therefore, optimizing structural materials during this stage can significantly reduce environmental impact [32].

This study will focus exclusively on the first and second life cycles in the embodied carbon calculation comparison. This approach is taken to avoid uncertainty about future impacts and the potential shifting of environmental burdens to future generations [34]. As noted by [34], the long lifespan of buildings introduces significant difficulty in accurately determining future scenarios, which can impact the LCA of the embodied carbon.

Since both flooring systems perform the same function, the operational stage (B1-B7) will remain consistent and thus be excluded from the calculation. Figure 20 depicts the life cycle stages used in this study to calculate embodied carbon for the baseline floor system for two life cycles.

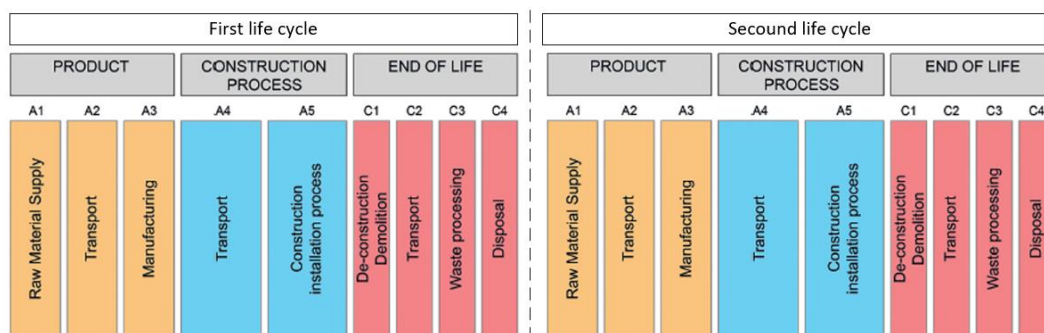


Figure 20: Life cycle stages and modules for non-circular system.

Figure 21 depicts the life cycle stages used in this study to calculate embodied carbon for the optimized floor system for two life cycles, characterized by the connection between C2 in the first life cycle and A4 in the second life cycle, representing circularity through materials reusability. It is reasonably assumed that not all materials from the first life cycle could be reused. Therefore, the reusable percentage will skip the product stage (A1-A3) in the second life cycle, which cannot be the case for the necessary new materials required to complete the structure (unavoidable new materials). These materials cause carbon emissions in the product stage at the beginning of the second life cycle.

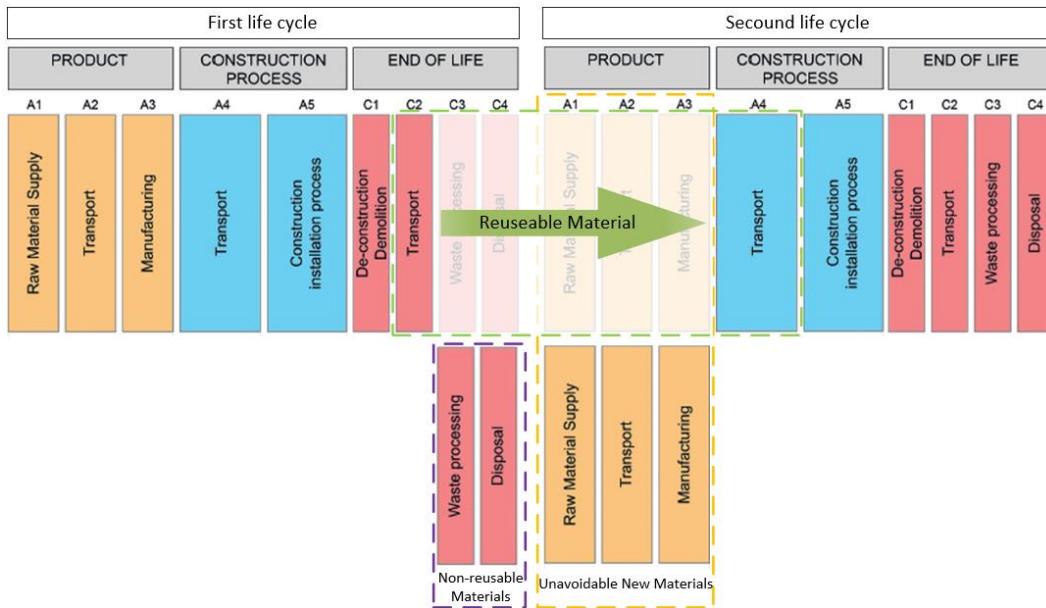


Figure 21: Life cycle stages and modules for circular system.

Through a comparative carbon calculation, this study intends to highlight the environmental benefits achieved by enhancing the circularity and material efficiency of the steel-CLT composite floor system. This analysis will provide a clear understanding of the positive environmental impact resulting from these improvements. The detailed comparison will be presented in Chapter 7.



### 3 STRUCTURAL DESIGN RULES

This chapter presents the design load application and the corresponding design checks. These steps ensure that the design meets Eurocode requirements. The checks are incorporated into a Python script that performs structural analysis using the gamma method, followed by all structural checks for the ultimate limit state (ULS) and serviceability limit state (SLS).

Structural analysis will be conducted on both the baseline design and the optimized design achieved in this study. However, the shear connector in the baseline design will not be re-checked because it has already been tested in a push-out test. Instead, the focus will be on the optimized composite floor system using the pre-loaded shear connector adopted in this study. This is necessary because this study applies those shear connectors in a different setup than the original experiment described in the literature.

The design checks clearly distinguish between the ULS and SLS states and differentiate between the composite beam and the CLT floor, which confront different loads and design criteria. This ensures a comprehensive evaluation of each component's performance under relevant conditions.

#### 3.1 Basis of Structural Design NEN-EN 1990

The structural design process under Eurocode EN-1990, Basis of Structural Design, involves several key factors, including consequence class, load combinations for ULS and serviceability limit state SLS, and deformation limits for SLS. These factors ensure the reliability and safety of the structural system [39].

##### 3.1.1 Consequence Class

To examine the most conservative design scenarios and ensure the applicability of these floor systems for various uses, this study employs Consequence Class 3 (CC3). CC3 accounts for major consequences such as significant loss of life, severe economic impacts, social consequences, or environmental damage. The corresponding load factor is  $K_{FI} = 1.1$  [39].

##### 3.1.2 Loads Combination

For the ultimate limit state, two load combination formulas are used:

Formula 6.10a:

$$K_{FI} * \gamma_{G,j} * G_{k,j} + K_{FI} * \gamma_{Q,1} * \psi_{0,1} * Q_{k,1} + \sum_{j \geq 1} (K_{FI} * \gamma_{Q,i} * \psi_{0,i} * Q_{k,i}) \quad (3.1)$$

Formula 6.10b:

$$\xi_j * K_{FI} * \gamma_{G,j} * G_{k,j} + K_{FI} * \gamma_{Q,1} * Q_{k,1} + \sum_{j \geq 1} (K_{FI} * \gamma_{Q,i} * \psi_{0,i} * Q_{k,i}) \quad (3.2)$$

Where:

- $K_{FI}$  Factor applicable to actions for reliability differentiation.
- $\gamma_{G,j}$  Partial factor for permanent actions.
- $G_{k,j}$  Permanent actions.
- $\gamma_{Q,1}$  Partial factor for leading variable action.
- $Q_{k,1}$  Leading variable action.
- $\psi_{0,1}$  Coefficient for combination value.
- $\xi_j$  Reduction coefficient (=0,89).
- $\psi_{0,i}$  Coefficient for combination value.
- $Q_{k,i}$  Other variable actions.

For the serviceability limit state characteristic, the following formula is applied:

$$G_{k,j} + Q_{k,1} + \sum_{j \geq 1} (\psi_{0,i} * Q_{k,i}) \quad (3.3)$$

Where:

- $G_{k,j}$  Permanent actions.
- $Q_{k,1}$  Leading variable action.
- $\psi_{0,i}$  Coefficient for combination value.
- $Q_{k,i}$  Other variable actions.

### 3.1.3 Deflection Limit

Since the research is investigating floor systems, the vertical deflection for the floor system must meet the deflection requirement. According to the national annex chapter A1.4.3 in the characteristic serviceability limit state, the recommended maximum allowed vertical deflection of the horizontal structure can be determined as follows:

$$w \leq w_{max} = \frac{L}{250} \quad (3.4)$$

$w$  Deflection of beam/floor.

$w_{max}$  Maximum allowed deflection.

## 3.2 Actions according to NEN-EN 1991-1-1

This norm regulates the actions on structures and will be used to determine the combination coefficients and the vertical actions acting on the floor system [40].

### 3.2.1 Combination Coefficients

The relevant combination coefficients are as follows [40]:

- Partial factor for permanent actions  $\gamma_{G,j} = 1.35$
- Partial factor for leading variable action  $\gamma_{Q,1} = 1.5$
- Reduction coefficient  $\xi_j = 0.89$
- Factor for combination value of a variable action ( $\psi_0$ ) for category A (domestic, residential areas):  $\psi_0 = 0.4$

### 3.2.2 Vertical Actions

To accurately calculate the vertical actions acting on the floor system, detailed inputs regarding the geometry and weight of the structural materials are essential. The permanent dead load, a critical factor in these calculations, is determined for each design variation separately in the relevant chapters.

#### 3.2.2.1 Permanent dead load

The permanent dead load represents the weight of the structure itself and any applied finishes, ceilings, and services. This load varies between the baseline design and the optimized design due to changes in beam and CLT panels geometry. Therefore, it is crucial to reference the specific chapters where these calculations are detailed:

- Baseline Design: The permanent dead load for the baseline floor system is calculated in Appendix B.1.
- Optimized Design: The permanent dead load for the optimized floor system is calculated in Appendix B.2.

#### 3.2.2.2 Imposed loads

Imposed loads refer to additional loads applied to the floors. For this study, the floor system is evaluated as a residential area structure (category A) with the following distributed loads:

**For the CLT floor:**

$$Q_{k,1} = 2.0 \text{ kN/m}^2$$

**For the composite beam:**

$$q_{k,1} = 2 * b = 6.0 \text{ kN/m}$$

$b$  is the distance between the composite beams, see Chapter 6.1 for more details on the geometry of the structure.

## 3.3 Ultimate Limit State

The Ultimate Limit State (ULS) checks ensure that the structure has an acceptable probability of having sufficient strength and stiffness to bear the highest loads and forces without collapse or irreversible damage. To accurately perform these checks, design rules from multiple Eurocodes are used.

### 3.3.1 Composite Beam Design

The structural analysis using the gamma method provides the stress distribution along the composite cross-section. To ensure safety in accordance with Eurocodes, the stress distribution is controlled at the maximum position at the mid span.

#### 3.3.1.1 Load Combinations

The load combinations for ULS acting on the composite beam as a distributed line load involves the following load cases:

From Formula 6.10a:

$$\text{LC1:} \quad q_{design,beam} = K_{FI} * \gamma_{G,j} * g_{k,j} \quad (3.5)$$

$$\text{LC2:} \quad q_{design,beam} = K_{FI} * \gamma_{G,j} * g_{k,j} + K_{FI} * \gamma_{Q,1} * \psi_{0,1} * q_{k,1} \quad (3.6)$$

From Formula 6.10b:

$$\text{LC3:} \quad q_{design,beam} = \xi_j * K_{FI} * \gamma_{G,j} * g_{k,j} \quad (3.7)$$

$$\text{LC4:} \quad q_{design,beam} = \xi_j * K_{FI} * \gamma_{G,j} * g_{k,j} + K_{FI} * \gamma_{Q,1} * q_{k,1} \quad (3.8)$$

From these load combinations, the critical distributed line load acting on the composite beam can be identified.

#### 3.3.1.2 Steel Design

The steel design focuses on cross-section checks for the steel components, excluding local buckling and lateral torsional buckling. This exclusion is due to the steel beam in the composite system being subjected primarily to moment forces, causing compression only in the top flange and part of the web. The buckling of these components can be neglected because the shear connectors provide restraint, and the design remains within the elastic phase. Therefore, the following normal stress check is used according to NEN-EN 1993 [41]:

$$\sigma_{Ed} \leq \frac{f_y}{\gamma_{M0}} \quad (3.9)$$

$\sigma_{Ed}$  Design value of stress

$f_y$  Yield strength

$\gamma_{M0}$  Partial factor for resistance of cross-sections

#### 3.3.1.3 Timber Design

The cross-section checks for the timber components under bending stress according to NEN-EN 1995 are as follows [23]:

$$\sigma_{m,y,d} \leq f_{m,d} = k_{sys} * k_{mod} * \frac{f_{m,k}}{\gamma_M} \quad (3.10)$$

Where:

$\sigma_{m,y,d}$	Design bending stress about the principal y-axis
$f_{m,d}$	Design bending strength about the principal y-axis.
$k_{sys}$	System strength factor.
$k_{mod}$	Modification factor for duration of load and moisture content.
$f_{m,k}$	Characteristic bending strength.
$\gamma_M$	Partial factor for material properties

### 3.3.1.4 Shear Connector Design

The optimized design incorporates pre-loaded shear connectors. Given the differences in the configuration of these connectors compared to the original experiment described in the literature [10], it is essential to verify their safety and applicability.

The design of the shear connectors is validated using steel design rules and the Johansen model for timber checks. Since pre-loaded shear connectors are unique to the optimized design, these checks are detailed in the ULS results of Appendix B.2.

In contrast, baseline design employs headed shear studs and grout as shear connectors. These connectors have been tested in push-out experiments. The data from these tests is used in the design, thus requiring no further investigation.

### 3.3.2 CLT Floor Design

The normal stress distribution in the CLT floor is evaluated at the midspan position to ensure safety according to the relevant Eurocodes.

#### 3.3.2.1 Load Combinations

The load combinations for ULS acting on the CLT floor as a distributed surface load involve the following load cases:

From Formula 6.10a:

$$\text{LC1:} \quad Q_{design, floor} = K_{FI} * \gamma_{G,j} * G_{k,j} \quad (3.11)$$

$$\text{LC2:} \quad Q_{design, floor} = K_{FI} * \gamma_{G,j} * G_{k,j} + K_{FI} * \gamma_{Q,1} * \psi_{0,1} * Q_{k,1} \quad (3.12)$$

From Formula 6.10b:

$$\text{LC3:} \quad Q_{design, floor} = \xi_j * K_{FI} * \gamma_{G,j} * G_{k,j} \quad (3.13)$$

$$\text{LC4:} \quad Q_{design, floor} = \xi_j * K_{FI} * \gamma_{G,j} * G_{k,j} + K_{FI} * \gamma_{Q,1} * Q_{k,1} \quad (3.14)$$

From these load combinations, the critical distributed surface load acting on the CLT floor can be identified.

#### 3.3.2.2 Timber Design

The cross-section checks for the timber components under bending stress according to NEN-EN 1995 are as follows [18][23]:

$$\sigma_{m,y,d} \leq f_{m,d} = k_{sys} * k_{mod} * \frac{f_{m,k}}{\gamma_M} \quad (3.15)$$

$$\sigma_{m,y,d} = \frac{M_{y,d}}{W_{x,net}} \quad (3.16)$$

Where:

$M_{y,d}$  The moment design value about the y-axis.

$W_{x,net}$  The panel's net moment of resistance.

## 3.4 Serviceability Limit State

The Serviceability Limit State (SLS) checks ensure that the structure meets stiffness requirements as per the Eurocode criteria. To perform these displacement checks accurately the design rules from several Eurocodes have been applied. The deflection limit for both the composite beam and the floor is set as introduced in Chapter 3.1.3.

### 3.4.1 Composite Beam Design

#### 3.4.1.1 Load Combinations

The load combinations for SLS acting on the composite beam as a distributed line load involves the following load cases:

$$\text{LC1:} \quad q_{design,beam} = g_{k,j} \quad (3.17)$$

$$\text{LC2:} \quad q_{design,beam} = g_{k,j} + q_{k,1} \quad (3.18)$$

From these load combinations, the critical distributed line load acting on the composite beam can be identified.

#### 3.4.1.2 Creep and Stiffness Reduction

To calculate deformations in the SLS for structures consisting of components with different time dependencies, the mean value for the final modulus of elasticity of the CLT component ( $E_{mean,fin}$ ) and the slip modulus ( $k_{ser,fin}$ ) are determined using the following expressions [18][23]:

$$E_{fin} = \frac{E_{eff}}{1 + k_{def}} \quad (3.19)$$

$$k_{ser,fin} = \frac{k_{test}}{1 + k_{def}} \quad (3.20)$$

Where:

$E_{eff}$  The effective modulus of elasticity.

$k_{test}$  The slip modulus was determined from the push-out test.

$k_{def}$  The modification factor for creep deformation related to the service class. For this study, which focuses on floor systems for buildings, the structure is assumed to be in service class 1, meaning  $k_{def} = 0.6$ .

## 3.4.2 CLT Floor Design

### 3.4.2.1 Load Combinations

The load combinations for SLS acting on the CLT floor as a distributed surface load involves the following load cases:

$$\text{LC1:} \quad Q_{design, floor} = G_{k,j} \quad (3.21)$$

$$\text{LC2:} \quad Q_{design, floor} = G_{k,j} + Q_{k,1} \quad (3.22)$$

From these load combinations, the critical distributed surface load acting on the CLT floor can be identified.

### 3.4.2.2 Creep and Stiffness Reduction

The approach for calculating creep and stiffness reduction for the CLT floor follows the same methodology as mentioned previously in Chapter 3.4.1.2.

## 4 STRUCTURAL PROPERTIES AND APPLICATION OF PRE-LOADED DEMOUNTABLE SHEAR CONNECTORS

This chapter continues the discussion in chapter 2.2, elaborating the structural properties of the identified shear connectors. Here, the focus shifts to further details concerning slip modulus determination and its application in a steel-CLT scenario.

As previously highlighted, the push-out tests conducted on these connectors revealed a high initial stiffness, denoted as  $k_{\text{initial}}$ , attributed to the pre-loading of the steel bolts, reaching 70% of their ultimate tensile strength [10].

This pre-loading generates friction force ( $F_{\text{friction}}$ ) between the steel tube and bolt, providing resistance to lateral forces applied during testing ( $F_{\text{test}}$ ). Figure 22 visually represents the forces at play during the initial phase of the push-out test. However, regardless of the stiffness of the composite materials, the initial slip will occur when  $F_{\text{test}}$  exceeds  $F_{\text{friction}}$ , indicating that the friction caused by pre-loading is insufficient to prevent the bolt from slipping inside the tube. Thus, it is assumed that the initial slip occurs at a specific load  $F_{\text{test}}$  and is solely related to the pre-loading of the steel bolts and the friction coefficient between those elements, with no influence from the properties of the composite materials.

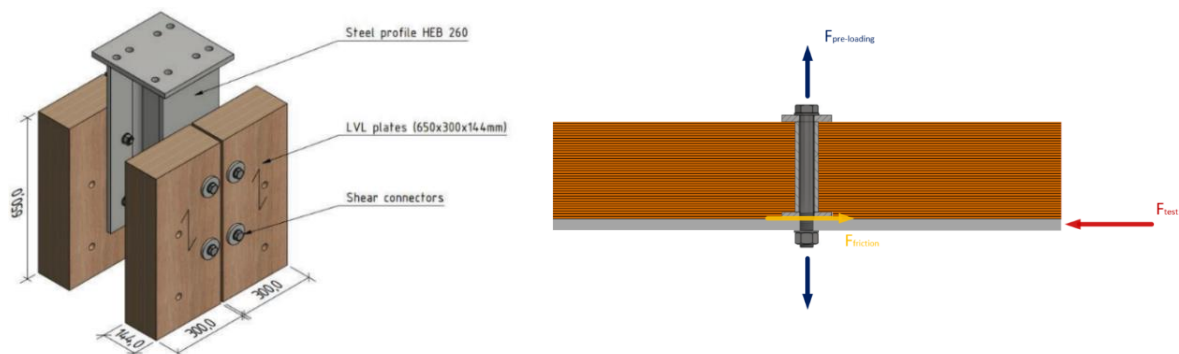


Figure 22: Push-out test setup from [10], and friction resistance.

It is crucial to note that the initial stiffness  $k_{\text{initial}}$ , stemming from friction between steel elements, may remain inconsistent across different timber types in composite beams utilizing these pre-loaded bolts. Therefore, utilizing the stiffness obtained from the push-out experiment performed on steel-LVL composition in the steel-CLT composition is not a proven assumption, and this kind of assumption requires validation through experiments or numerical analysis of various types of composition. However, since that is not the focus of this study, a correction factor will be determined using the available data from the push-out test and the slip modulus design equation from EC5. This correction factor will be multiplied with  $k_{\text{initial}}$  to ensure a conservative adoption for  $k_{\text{initial}}$ , in steel-CLT compositions.



Thus, the  $k_{initial}$  value of a single shear connector has to be determined first. This number is obtained from the load-slip graph of the push-out test at  $F_{test} \leq 30$  kN, and it is identical for the three types of connectors (see Figure 23). Therefore:

$$k_{initial,LVL} = k_{initial,SCT-1} = k_{initial,SCT-2} = k_{initial,SCT-3} = \frac{Load}{Slip} = \frac{160 * 1000}{1.8} \\ = 88888.89 \approx 89000 \frac{N}{mm} \text{ (per shear connector)}$$

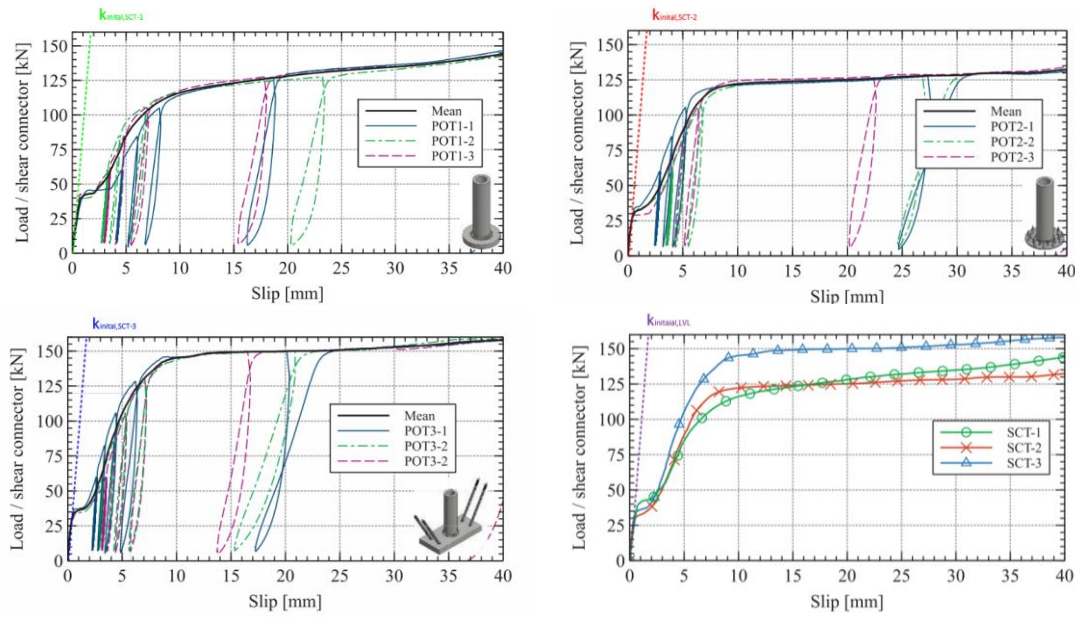


Figure 23: Push-out results for SCT-1 top left, SCT-2 top right, SCT-3 bottom left, and all SCT together bottom right [10].

This  $k_{initial}$  is observed in all three shear connectors when the load per shear connector ( $F_{test}$ ) is below 30 kN. Hence, controlling the shear loads on the joint between composite materials ensures utilization of the high stiffness of the shear connectors at the initial stage, with  $F_{test}$  not exceeding 30 kN per shear connector. Since all three shear connectors exhibit identical behavior in the initial phase of the push-out test, they are all deemed applicable for this study. Consequently, SCT-1 has been selected as the shear connector for this study.

The method for determining the correction factor is detailed in Appendix A The Correction Factor for The Slip Modulus. Through this approach, the correction factor is established as  $r = 0.75$ . Consequently, the slip modulus for a single shear connector in a steel-CLT composite connection is calculated as  $k_{initial,CLT} = k_{initial,LVL} * r = 66750$  N/mm (per shear connector).

As previously stated, this  $k_{initial,CLT}$  value can be used only if the  $F_{test}$  does not exceed 30 kN per shear connector. However,  $F_{test}$  translates to  $F_{joint}$  in composite beams, which occurs from the slip between the composite materials. Understanding the structural analysis using the gamma method is necessary to understand how  $F_{joint}$  can be managed and the factors influencing its magnitude (see Chapter 2.1.2 for a more detailed explanation). In that chapter, the equation for determining the load on the joint is expressed as the shear flow multiplied by the spacing between the shear connectors:

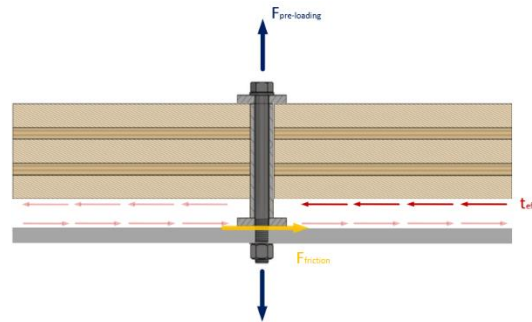


Figure 24: Shear flow in a joint.

$$F_{joint} = t_{ef} * s \quad (4.1)$$

Where:

$t_{ef}$ : Shear flow [N/mm].

$s$ : Spacing [mm].

This equation highlights that controlling the load on a row of shear connectors is achievable by adjusting the spacing parameter, ensuring that  $F_{joint}$  remains within the 30 kN boundary. To demonstrate this concept, a parametric study was conducted on a simply supported composite beam subjected to an equally distributed line load  $q$  [kN/m]. This composite beam has the exact geometry and characteristics of the optimized design outlined in Chapter 6.1.2 that features pre-loaded demountable shear connectors. Here, the stiffness  $k_{initial,CLT}$  is employed as the slip modulus in the analysis, multiplied by two due to the application of connectors in pairs. Hence:  $k_{initial,CLT,2} = 2 * k_{initial,CLT} = 133500 \text{ N/mm}$ .

Considering the application of shear connectors in pairs, the shear force boundary in this scenario is 60 kN per row of connectors. Figure 25 illustrates the mechanical scheme, providing a visual representation of the setup.

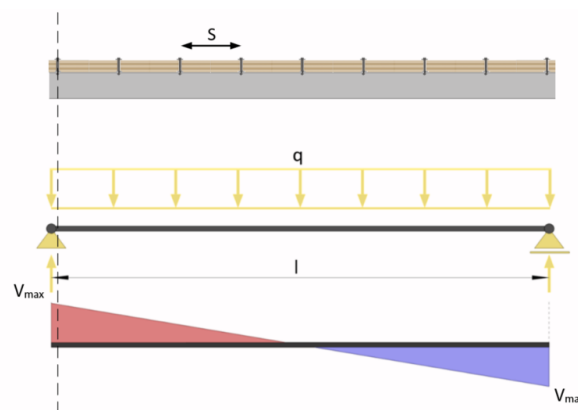


Figure 25: The mechanical scheme of the composite beam.

Figure 26 illustrates the relationship between the distributed load  $q$  and the spacing in both the ULS and the SLS. The left graph represents ULS, while the right graph represents SLS. The blue curve delineates the boundary where the joint force  $F_{\text{joint}}$  equals 30 kN, assisting in determining the maximum  $q$  that does not exceed the maximum joint force acting on one shear connector. The maximum design load for ULS ( $q_{\text{design,beam,ULS}}$ ) is indicated by the horizontal dashed red line, while for SLS ( $q_{\text{design,beam,SLS}}$ ) it is represented by the horizontal dashed green line. These design load values are determined in Chapter 6.1.2.

By utilizing these graphs, the required spacing between the shear connectors can be determined for both ULS and SLS, allowing for the effective application of the high slip modulus value  $k_{\text{inital,CLT,2}}$  in the composite beam design. To ensure this, the spacing value should remain less than the contact point between the blue curve and the red or green dashed line, facilitating the use of  $k_{\text{inital,CLT,2}}$ .

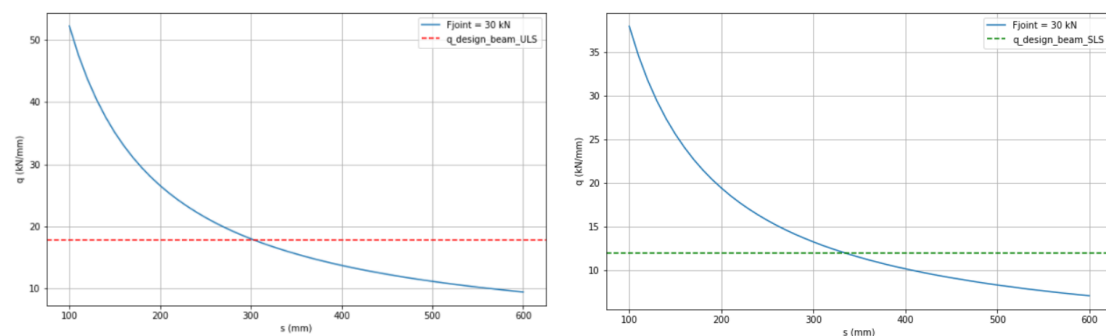


Figure 26: Joint load value in relation to the load/spacing in ULS left, in SLS right.

The reason for having separate graphs for ULS and SLS is due to the different behaviors of the composite beam in each state. In SLS, the elastic modulus of the timber and the slip modulus must be reduced to account for the impact of creep. This results in different responses for the composite beam in ULS and SLS, necessitating individual graphs for each state. Therefore, the spacing value  $s$  should be lower than  $s_{\text{max}}$ :

$$s < s_{\text{max}}$$

$$s_{\text{max}} = \min[s_{\text{ULS}}, s_{\text{SLS}}] = \min[300 \text{ mm}, 320 \text{ mm}]$$

$s_{\text{ULS}}$  and  $s_{\text{SLS}}$  are determined from the graph.

As a result, the spacing value for the final design is set to:  $s = 280 \text{ mm}$ .

The application of the high slip modulus value ( $k_{\text{inital,CLT,2}}$ ) in the optimized composite floor system is a significant step forward in implementing pre-loaded demountable shear connectors into practical use. This approach not only enhances the system's structural performance, but it also brings these connectors closer to achieving their full potential, establishing them as strong alternatives to standard shear connectors in composite floor systems.

## 5 CLT DESIGN APPROACH AND IMPROVEMENT

Chapter 2.3 explained the significance of panel and grain direction in CLT design. This chapter delves into the importance of CLT panels' design within composite systems, highlighting their dual structural functions and addressing the design challenges involved. The optimized design of the CLT floor for this study will be presented at the end of this chapter.

In a composite system, the CLT floor serves not only as a floor structure but also as a crucial component of the composite beam. Therefore, the CLT must possess specific structural properties in both directions to fulfill its dual functions effectively. Figure 27 illustrates the two sections relevant to the baseline composite floor system, highlighting the panels active in each direction.

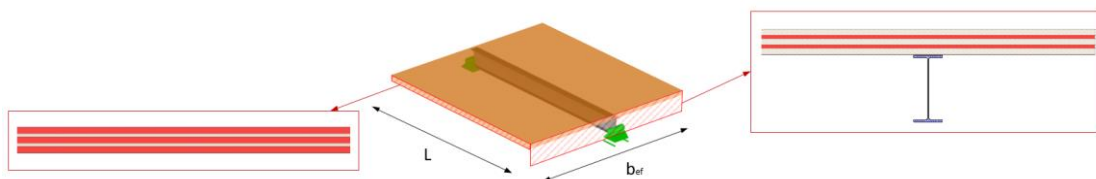


Figure 27: Active CLT panels in each direction (not to scale drawing).

### Composite Function

The CLT panels, with their grains aligned parallel to the span direction of the composite beam, serve as active components in the composite action of the beam. These panels play a crucial role in enhancing the overall stiffness of the composite beam and contribute to bearing a portion of the stress. In the baseline design, the second and fourth layers, each 20 mm thick, function as the active panels.

### Floor Structure Function

As part of the floor structure, the CLT panels with grains oriented perpendicular to the span of the composite beam are the active layers. These panels provide the necessary support for the floor function, ensuring load distribution across the floor surface. In the baseline design, the first, third, and fifth layers, each 40 mm thick, perform this function, contributing to the overall strength and stability of the floor system.

### Important Design Aspects for Composite Function

Since steel is much stiffer than timber, the neutral axis is located within the steel profile, placing the timber far from this axis. This positioning means the CLT contributes to the composite beam's second moment of area mainly through the Steiner theorem. The equation for the effective bending stiffness of the composite beam using the gamma method, with the Steiner term for the CLT highlighted, is:

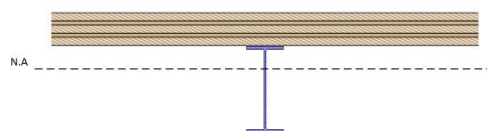


Figure 28: neutral axis position in the composite cross-section.

$$(EI)_{ef} = \sum_{i=1}^3 (E_i * I_i + \gamma_i * E_i * A_i * a_i^2) = (EI)_{ef,steel} + (EI)_{ef,timber} \quad (6.1)$$

$$(EI)_{ef} = (EI)_1 + (E_{eff,2} * I_2 + \gamma_2 * E_{eff,2} * A_2 * a_2^2) \quad (6.2)$$

The effective elastic modulus is calculated as follows (refer to Chapter 2.3.2 for details):

$$E_{eff} = \sum_{i=1}^n \frac{E_i * A_i}{A_{tot}} = \frac{E_{timber} * A_{2,active}}{A_2} \quad (6.3)$$

Applying 6.3 in 6.1 gives:

$$(EI)_{ef} = (EI)_1 + \left( \frac{E_{timber} * A_{2,active}}{A_2} * I_2 + \gamma_2 * \frac{E_{timber} * A_{2,active}}{A_2} * A_2 * a_2^2 \right) \quad (6.4)$$

$$(EI)_{ef} = (EI)_1 + \left( \frac{E_{timber} * A_{2,active}}{A_2} * I_2 + \gamma_2 * E_{timber} * A_{2,active} * a_2^2 \right) \quad (6.5)$$

This equation highlights the significance of the active area of the CLT, denoted as  $A_{2,active}$  which is calculated as  $A_{2,active} = h_{active\_panels} * b_{effective}$ . Increasing  $A_{2,active}$  by raising the number of active panels (i.e., increasing  $h_{active\_panels}$ ) results in enhanced effective stiffness, despite potentially reducing the interaction factor  $\gamma_2$ .

To better understand this complex relationship between  $A_{2,active}$  and  $(EI)_{ef}$ , a parametric study was conducted using baseline design data from Chapter 6.1.1. This study explored how variations in  $h_{active\_panels}$  impact the effective bending stiffness,  $(EI)_{ef}$ , with results illustrated in the graph below. The graph was generated by applying  $h_{active\_panels}$  as a variable in a loop function, incrementally increasing it from 0 to 200 mm and calculating  $(EI)_{ef}$  at each step through the Gamma method analysis.

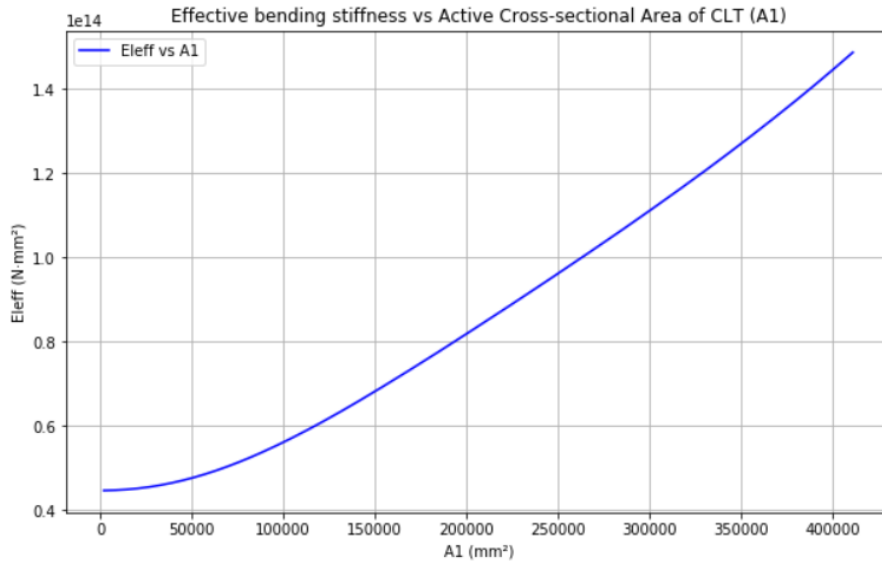


Figure 29: Effective bending stiffness vs Active Cross-sectional Area of CLT (A1).

These results demonstrate that maximizing the active CLT area is crucial for designing efficient composite beams. By strategically increasing  $h_{active\_panels}$  engineers can

significantly improve the stiffness of the composite system, enhancing overall structural performance.

### Important Design Aspects for Floor Structure Function

The symmetrical design of the CLT cross-section ensures that the neutral axis passes through its center. To optimize the floor structure, the outer panels, which have the greatest impact on the second moment of area ( $I_y$ ), should be active. Thus, the position of active panels in the floor structure is critical; the further these panels are from the neutral axis, the more effective they are.



Figure 30: neutral axis position in CLT floor.

### Illustrative Example of CLT Design Improvement

This example uses the baseline floor system as input, modifying only the CLT configuration without changing the CLT height ( $h_{CLT}$ ). The thickness of the CLT panels used in this example is not standard production size, and it serves only to demonstrate the benefits of altering the CLT configuration, as shown in the structural analysis results in the table below:

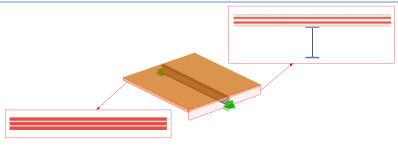
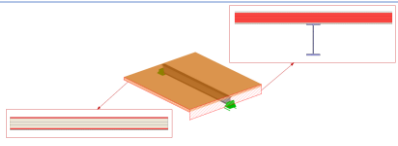
	Baseline Design	Example CLT design
<b>CLT</b>	40/20/40/20/40	6/50/48/50/6
<b>Orientation, red panels are the active ones</b>		
<b>ULS Critical Check</b>		
<b>Composite beam</b>	UC = 0.6	UC = 0.6
<b>CLT floor</b>	UC = 0.2	UC = 0.8
<b>SLS Critical Check</b>		
<b>Composite beam</b>	<u>UC = 0.9</u>	<u>UC = 0.7</u>
<b>CLT floor</b>	UC = 0.2	UC = 0.7

Table 1: illustrative comparison that shows how the orientation and grain direction of the CLT panels affect the composite beam.

This example demonstrates that by optimizing the CLT panel configuration alone—without modifying other parameters—there was a 20% improvement in the SLS capacity, which is critical for floor performance. Specifically, the example design exhibited 20% less deflection compared to the baseline design. These results validate the effectiveness of the discussed design strategies for improving CLT performance within composite systems.

### Optimized CLT Design for This Study

The optimized CLT design considers market availability and cost-effectiveness, selecting standard panel thicknesses. For fire safety, the design includes three active

layers as floor structure components: the two outer layers and the middle layer. This configuration ensures robustness, allowing the floor to maintain load-bearing capacity even if one outer layer fails due to fire.

Final CLT Design:

- CLT configuration: 10/40/20/40/10
- CLT height ( $h_{CLT}$ ): 120 mm
- Orientation (red panels are active in each direction):

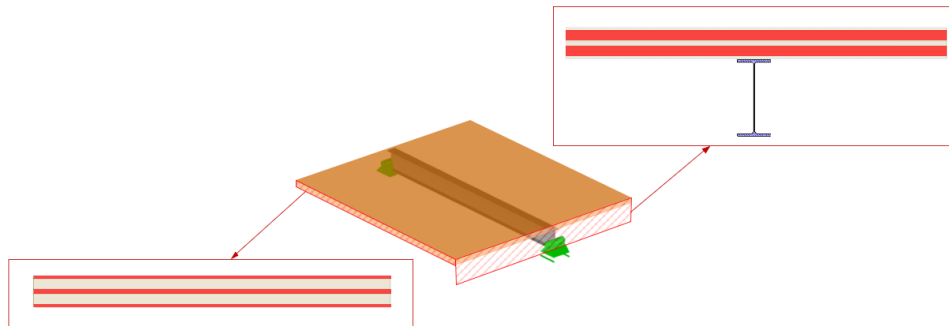


Figure 31: illustration of the active panels in each direction of the new design (not to scale drawing).

This optimized CLT floor design, featuring revised panel thicknesses and a reduced total CLT height, provides efficient structural performance while using 40 mm less material than the baseline design. Therefore, the improved configuration maintains structural integrity while increasing material efficiency.

The following chapter will present both the baseline and optimized designs, along with their respective structural analysis results. A comparative analysis will demonstrate the improvements achieved in the CLT design, highlighting the benefits of the optimizations in terms of performance and material savings.

## 6 STRUCTURAL ANALYSIS AND COMPARISON

This chapter provides a comprehensive structural analysis and comparison of the baseline and optimized composite floor system designs through a case study. The primary objective is to assess and compare the structural performance of both systems, offering a detailed understanding of the impact of the optimizations. As part of this case study, both floor systems are evaluated under identical functional requirements and boundary conditions to ensure a fair and objective comparison. This consistent methodology allows for an unbiased evaluation of how the optimizations have influenced structural performance. The results from this analysis are critical for the subsequent comparative evaluation and will offer valuable insights into the structural improvements achieved in this study.

### 6.1 Case Study

In this case study, both the baseline and optimized designs of steel-CLT composite floor systems are presented, along with their structural characteristics, which are used for the structural analysis. The detailed calculations and checks involved in the structural analysis are provided in Appendix B.

To ensure an accurate and consistent comparison, both designs incorporate the same geometric parameters, derived from the baseline design's application in the United Kingdom:

- Span of the composite beams,  $L = 12$  m.
- Distance between the composite beams,  $b = 3$  m.

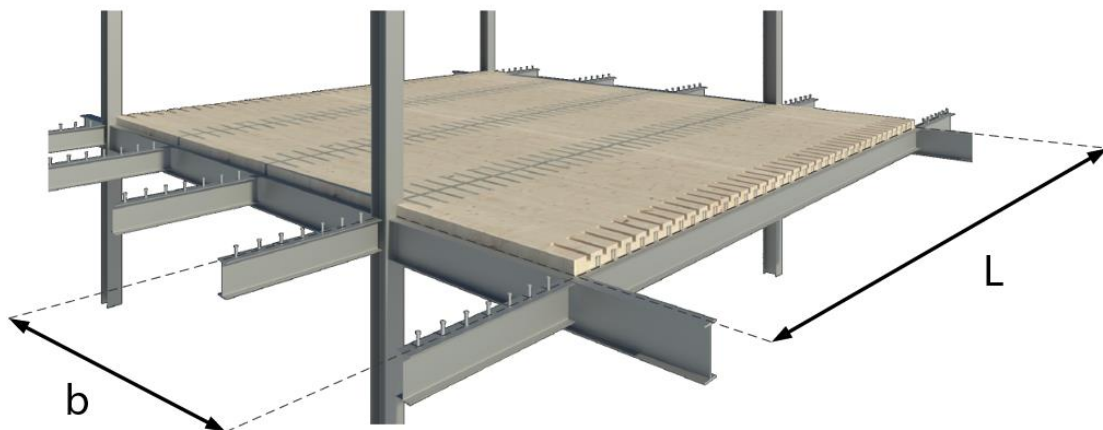


Figure 32: 3D drawing and geometry of the floor system.

The following table shows the structural properties of all materials used in both the baseline design and the optimized design of this research:

Characteristic	Value [unit]
----------------	--------------



<b>Steel 355</b>	
<b>Specific weight (<math>\gamma</math>)</b>	78.5 [kN/ m <sup>3</sup> ] 7850 [kg/ m <sup>3</sup> ]
<b>Modulus of elasticity (<math>E_s</math>)</b>	210000 [N/mm <sup>2</sup> ]
<b>Shear Modulus (<math>G</math>)</b>	80769.2 [N/mm <sup>2</sup> ]
<b>Yield strength (<math>f_y</math>)</b>	355 [N/mm <sup>2</sup> ]
<b>Ultimate strength (<math>f_u</math>)</b>	490 [N/mm <sup>2</sup> ]
<b>Timber C24</b>	
<b>Specific weight (<math>\gamma</math>)</b>	4.2 [kN/ m <sup>3</sup> ] 420 [kg/ m <sup>3</sup> ]
<b>Density-char (<math>\rho_k</math>)</b>	350 [kg/ m <sup>3</sup> ]
<b>Modulus of elasticity parallel (<math>E_{0,mean}</math>)</b>	11000 [N/mm <sup>2</sup> ]
<b>Modulus of elasticity perpendicular (<math>E_{90,mean}</math>)</b>	370 [N/mm <sup>2</sup> ]
<b>Shear Modulus (<math>G_{mean}</math>)</b>	690 [N/mm <sup>2</sup> ]
<b>Partial safety factor (<math>\gamma_M</math>)</b>	1.3
<b>Characteristic strength for bending (<math>f_{m,k}</math>)</b>	24 [N/mm <sup>2</sup> ]
<b>Characteristic strength for tension (<math>f_{t,0,k}</math>)</b>	14.5 [N/mm <sup>2</sup> ]
<b>Characteristic strength for tension perpendicular (<math>f_{t,90,k}</math>)</b>	0.4 [N/mm <sup>2</sup> ]
<b>Characteristic strength for compression (<math>f_{c,0,k}</math>)</b>	21 [N/mm <sup>2</sup> ]
<b>Characteristic strength for compression perpendicular (<math>f_{c,90,k}</math>)</b>	2.5 [N/mm <sup>2</sup> ]
<b>Characteristic strength for shear-torsion (<math>f_{v,k}</math>)</b>	4 [N/mm <sup>2</sup> ]
<b>Mean value of density (<math>\rho_{mean}</math>)</b>	420 [kg/m <sup>3</sup> ]
<b>Concrete C30/37</b>	
<b>Specific weight (<math>\gamma</math>)</b>	25 [kN/ m <sup>3</sup> ] 2500 [kg/ m <sup>3</sup> ]
<b>Modulus of elasticity (<math>E_c</math>)</b>	33000 [N/mm <sup>2</sup> ]
<b>Shear Modulus (<math>G_{mean}</math>)</b>	13750 [N/mm <sup>2</sup> ]
<b>Characteristic cylinder compressive strength (<math>f_{ck}</math>)</b>	30 [N/mm <sup>2</sup> ]
<b>Steel Bar S460</b>	
<b>Specific weight (<math>\gamma</math>)</b>	78.5 [kN/ m <sup>3</sup> ] 7850 [kg/ m <sup>3</sup> ]
<b>Modulus of elasticity (<math>E_s</math>)</b>	210000 [N/mm <sup>2</sup> ]
<b>Shear Modulus (<math>G</math>)</b>	80769.2 [N/mm <sup>2</sup> ]
<b>Yield strength (<math>f_y</math>)</b>	460 [N/mm <sup>2</sup> ]
<b>Ultimate strength (<math>f_u</math>)</b>	540 [N/mm <sup>2</sup> ]

Table 2: Materials' structural properties.

## 6.1.1 The Baseline Design of Steel-CLT Composite Floor System

### 6.1.1.1 Structural Properties

The baseline design for this research is WSP's Steel-CLT composite floor system, which is improved to meet the study's objectives. This chapter gives an overview of the structural characteristics of that baseline design.

The design was first developed and validated in the United Kingdom and is being researched by WSP and the University of Warwick. Standard rolled steel beams, CLT slabs, shear studs, grout, and transverse reinforcement form the floor system; these are the essential structural elements of the composite system described in this chapter.

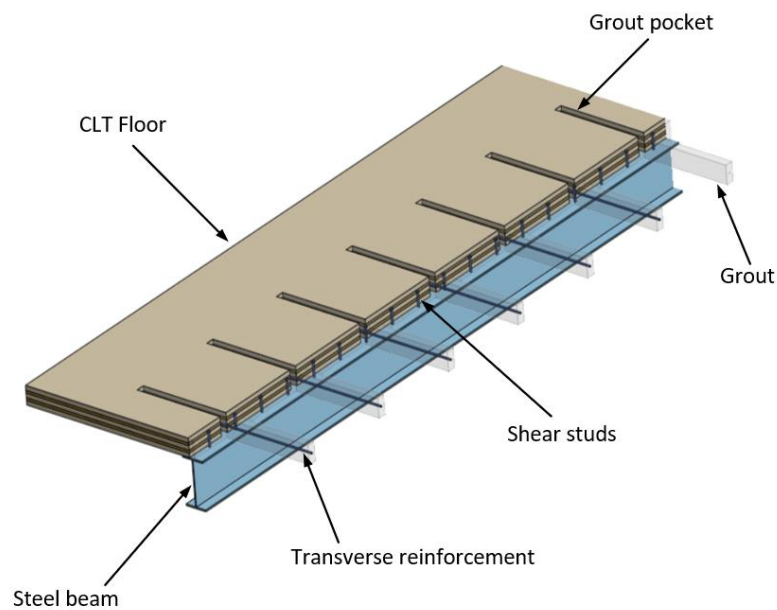
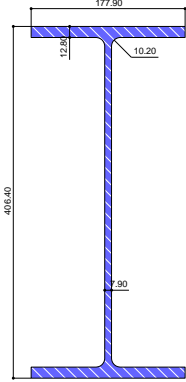



Figure 33: The composite floor system designed by WSP.

#### 6.1.1.1.1 The Cross-Sections Properties

The table below displays the geometry and structural properties of the cross-sections used in the baseline design. This I-profile is from the standard catalogue of UK steel profiles.

Property	Value [unit]	Cross-section view
<b>I-profile: UB 406x178x60</b>		
<b>Height (h)</b>	406.4 [mm]	
<b>Width (b)</b>	177.9 [mm]	
<b>Web thickness (t<sub>w</sub>)</b>	7.9 [mm]	
<b>Flange thickness (t<sub>f</sub>)</b>	12.8 [mm]	
<b>Root fillet radius</b>	10.2 [mm]	
<b>Cross-section area (A)</b>	7652 [mm <sup>2</sup> ]	
<b>Second moment of area (I<sub>y</sub>)</b>	2.16 * 10 <sup>8</sup> [mm <sup>4</sup> ]	

<b>Second moment of area (<math>I_z</math>)</b>	1.20 * 10 <sup>7</sup> [mm <sup>4</sup> ]	
<b>Weight (<math>g_{Steel}</math>)</b>	0.6 [kN/m]	
<b>CLT: 40/20/40/20/40</b>		
<b>Height (<math>h_{CLT}</math>)</b>	160 [mm]	
<b>Layer one thickness (<math>t_1</math>)</b>	40 [mm]	
<b>Layer two thickness (<math>t_2</math>)</b>	20 [mm]	
<b>Layer three thickness (<math>t_3</math>)</b>	40 [mm]	
<b>Layer four thickness (<math>t_4</math>)</b>	20 [mm]	
<b>Layer five thickness (<math>t_5</math>)</b>	40 [mm]	
<b>Weight (<math>G_{CLT}</math>)</b>	0.672 [kN/ m <sup>2</sup> ]	
<b>Second moment of area (<math>I_y</math>) per meter width</b>	3.04 * 10 <sup>8</sup> [mm <sup>4</sup> ]	
<b>Effective width:</b> <b>The following approach is explained in chapter 2.4.</b> <b>According to Eurocode 4:</b> $b_{ef,EC4} = \frac{L}{4} = 3000 \text{ mm}$ <b>According to Eurocode 5:</b> $b_{ef,EC5} = b_{rib} + \sum b_{ef,i}$ $b_{ef,i} = b_i \left( 0.5 - 0.35 \left( \frac{b_i}{l} \right)^{0.9} \left( \frac{(EA)_i}{(GA)_{xy}} \right)^{0.45} \right) = 938 \text{ mm}$ $b_{rib} = b_{steel \text{ beam}} = 178 \text{ mm}$ $b_i = 3000 \text{ mm}$ $L = 12000 \text{ mm}$ $(EA)_i = 11000 * 2 * 20 = 440000 \text{ N/mm}$ $(GA)_{xy} = 690 * 160 = 110400 \text{ N/mm}$ $b_{ef,EC5} = 178 + 2 * 938 = 2054 \text{ mm}$ <b>Final value of effective width is:</b> $b_{ef} = \min(b_{ef,EC4}, b_{ef,EC5}) = 2054 \text{ mm}$		
<b>Orientation:</b> The CLT floor's strong axis is positioned perpendicular to the direction of the composite beam. Therefore, the composite beam only has two 20 mm layers operating in it. The grain of those layers are parallel to the span direction of the beam.		

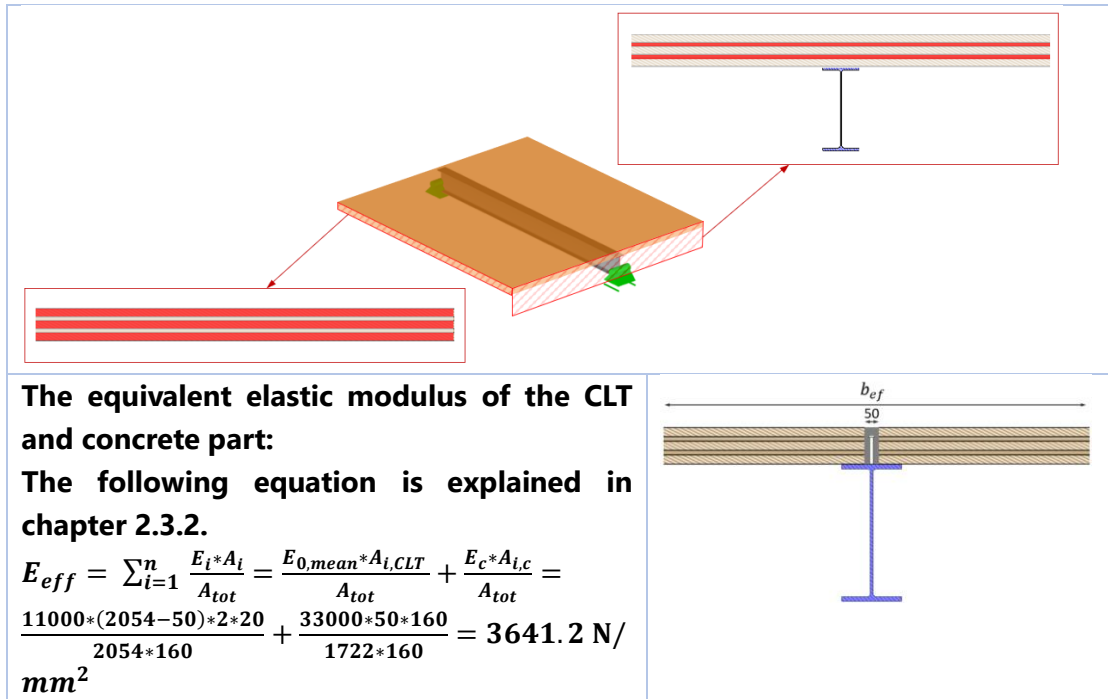


Table 3: Cross-sections' structural properties.

For simplicity, a constant cross-section along the composite beam has been assumed, which means that the steel transversal bars are not considered into the structural analysis.

#### 6.1.1.1.2 The Shear Connector Properties

WSP developed a composite floor system that utilizes steel and CLT as the primary materials. The central challenge in this design was to identify an effective shear connector capable of ensuring proper composite interaction between the steel and CLT. To address this, a specific shear connector was designed and rigorously tested to validate its effectiveness. This connector consists of shear studs welded to the top flange of the steel I-beam, with CLT panels positioned above the beam. The arrangement of the CLT panels creates pockets, which are subsequently filled with grout. This grout acts as the bonding agent between the steel and CLT, facilitating composite action. Additionally, supplementary pockets are introduced in the perpendicular direction, reinforced with steel bars, to enhance the shear-load transfer between the grout and the CLT slab.

However, WSP determined the following load-slip behavior from the push-out tests that are undertaken at the University of Warwick, and the stiffness of the shear connector is calculated to be  $k_{sc} = 149.6 \text{ kN/mm}$  up to  $P_{Rk} = 93 \text{ kN/stud}$ .

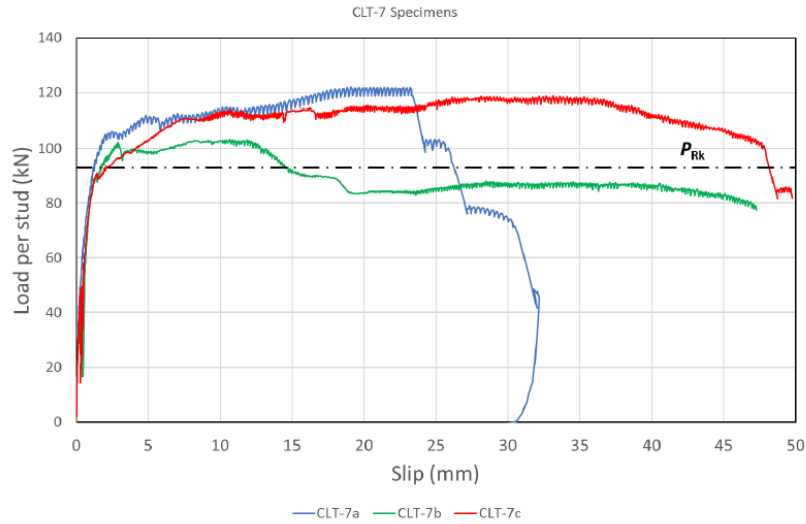


Figure 34: The load-slip graph obtained from the WSP push-out test.

### 6.1.2 The Optimized Design of Steel-CLT Composite Floor System

This chapter describes the final design of the steel-CLT composite floor system developed during this research. This optimized design improves on the baseline design by achieving the study's circularity and CLT efficiency objectives. To this end, new shear connectors have been introduced to achieve circularity, and a novel CLT design has been developed to optimize the dual function of the CLT panels, thereby improving CLT efficiency. Aside from these improvements, the geometry of the structure and the material properties remain unchanged, allowing for a logical and fair comparison of the two designs in the following chapters.

The geometry of the optimized design maintains the same span and beam width as the baseline design presented at the beginning of the case study, with one notable exception: the spacing of the shear connectors. This spacing value, previously determined in Chapter 4, was calculated based on the critical load acting on the composite beam in both the ULS and the SLS. The resulting optimal spacing value for the shear connectors is  $s = 280 \text{ mm}$ .

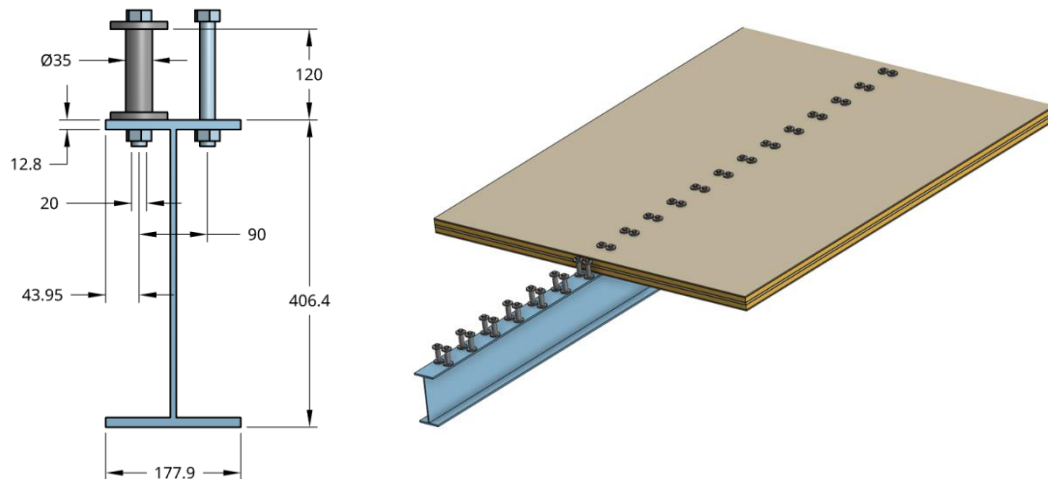


Figure 35: Front view of steel elements; 3D drawing right.

### 6.1.2.1 Structural Properties

#### 6.1.2.1.1 The Cross-Sections Properties

Table 2 at the beginning of the case study declares the structural characteristics of all materials utilized in the baseline and optimized designs of this study.

The table below displays the geometry and structural properties of the cross-sections used in the optimized design only. This I-profile, which was used in the baseline design, comes from the standard UK steel profile collection.

Property	Value [unit]	Cross-section view
<b>I-profile: UB 406x178x60</b>		
<b>Height (h)</b>	406.4 [mm]	
<b>Width (b)</b>	177.9 [mm]	
<b>Web thickness (t<sub>w</sub>)</b>	7.9 [mm]	
<b>Flange thickness (t<sub>f</sub>)</b>	12.8 [mm]	
<b>Root fillet radius</b>	10.2 [mm]	
<b>Cross-section area (A)</b>	7652 [mm <sup>2</sup> ]	
<b>Second moment of area (I<sub>y</sub>)</b>	2.16 * 10 <sup>8</sup> [mm <sup>4</sup> ]	
<b>Second moment of area (I<sub>z</sub>)</b>	1.20 * 10 <sup>7</sup> [mm <sup>4</sup> ]	
<b>Weight (g<sub>Steel</sub>)</b>	0.6 [kN/m]	
<b>CLT: 10/40/20/40/10</b>		
<b>Hight (h<sub>CLT</sub>)</b>	120 [mm]	
<b>Layer one thickness (t<sub>1</sub>)</b>	10 [mm]	
<b>Layer two thickness (t<sub>2</sub>)</b>	40 [mm]	
<b>Layer three thickness (t<sub>3</sub>)</b>	20 [mm]	
<b>Layer four thickness (t<sub>4</sub>)</b>	40 [mm]	
<b>Layer five thickness (t<sub>5</sub>)</b>	10 [mm]	
<b>Weight (G<sub>CLT</sub>)</b>	0.5 [kN/ m <sup>2</sup> ]	
<b>Second moment of area (I<sub>y</sub>) per meter width</b>	6.1 * 10 <sup>7</sup> [mm <sup>4</sup> ]	
<b>Effective width:</b>		
<b>The following approach is explained in chapter 2.4.</b>		
<b>According to Eurocode 4:</b>		
$b_{ef,EC4} = \frac{L}{4} = 3000 \text{ mm}$		
<b>According to Eurocode 5:</b>		
$b_{ef,EC5} = b_{rib} + \sum b_{ef,i}$		
$b_{ef,i} = b_i \left( 0.5 - 0.35 \left( \frac{b_i}{l} \right)^{0.9} \left( \frac{(EA)_i}{(GA)_{xy}} \right)^{0.45} \right) = 626.5 \text{ mm}$		
$b_{rib} = b_{steel \ beam} = 178 \text{ mm}$		
$b_i = 3000 \text{ mm}$		
$L = 12000 \text{ mm}$		

$$(EA)_i = 11000 * 2 * 40 = 880000 \text{ N/mm}$$

$$(GA)_{xy} = 690 * 120 = 82800 \text{ N/mm}$$

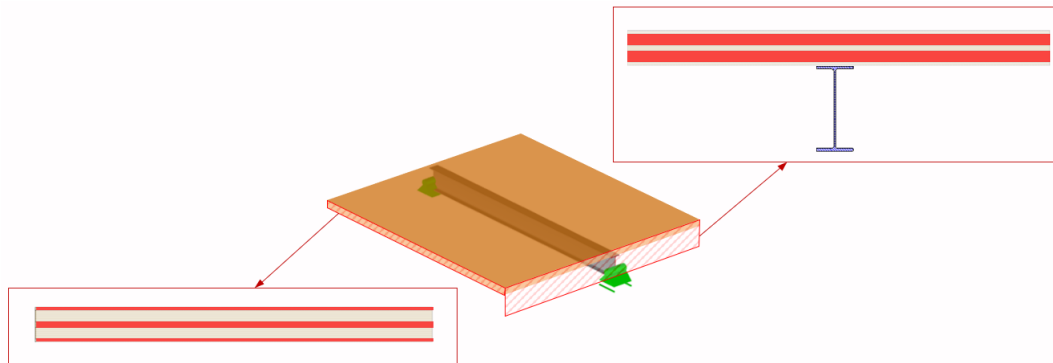
$$b_{ef,EC5} = 178 + 2 * 626.5 = 1431 \text{ mm}$$

**Final value of effective width is:**

$$b_{ef} = \min(b_{ef,EC4}, b_{ef,EC5}) = 1431 \text{ mm}$$

**Orientation:**

The composite beam has two 40 mm layers operating in it. The grain of those layers are parallel to the span direction of the beam.



**The equivalent elastic modulus of the CLT and concrete part:**

**The following equation is explained in chapter 2.3.2.**

$$E_{eff} = \sum_{i=1}^n \frac{E_i * A_i}{A_{tot}} = \frac{E_{0,mean} * A_{i,CLT}}{A_{tot}} = \frac{11000 * 1431 * 2 * 40}{1431 * 120} = 7333.3 \text{ N/mm}^2$$

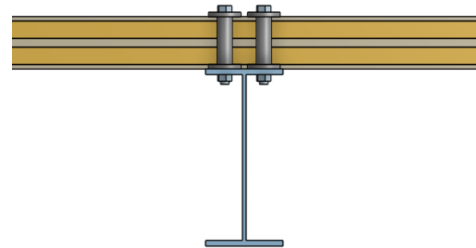


Table 4: Cross-sections' structural properties.

#### 6.1.2.1.2 The Shear Connector Properties

The pre-loaded shear connector is employed in this design. The properties of this connector are detailed in Chapter 4.

#### 6.1.3 Summary of The Structural Analysis

A detailed structural analysis has been conducted for both designs, as outlined in Appendix B. This analysis utilized the inputs, loads, boundary conditions, and design rules discussed previously. The focus was placed on two critical cross-sections that were assumed to be the most structurally significant and thus required evaluation in accordance with the relevant Eurocode standards. The first critical section is located at the midspan of the composite beam, while the second is at the midspan of the CLT panels between the composite beams.

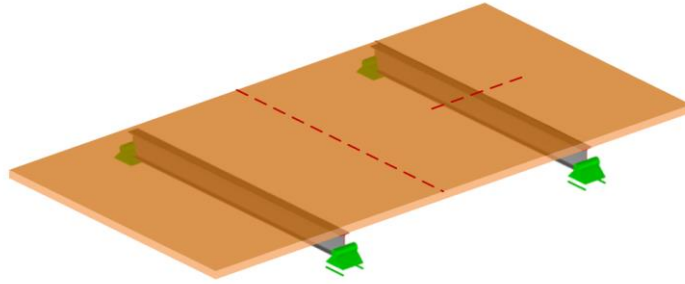


Figure 36: 3D drawing showing critical sections with a red dashed line.

At these critical sections, the normal stress distribution along the cross-sections was assessed under ULS conditions, and the displacement of the structure was evaluated for SLS compliance. The same analytical approach was applied consistently to both designs to ensure a fair comparison.

To determine the bending stiffness and normal stress distribution of the composite beam, the Gamma method was employed, while standard structural mechanics principles were used to analyze the floor structure. Python scripts were developed to automate the structural analysis, with the specific code for each design provided in Appendix D.

The results of the structural analysis are presented in the next chapter as Unity Check (UC) values, which serve as a comparative measure of the performance of both designs in terms of structural adequacy. These UC values facilitate a clear comparison of the two designs' strengths and weaknesses under both ULS and SLS conditions.



## 6.2 Structural Comparison

After completing the structural analysis in Appendix B.1 for the baseline design, the implementation of new shear connectors and the optimized CLT design were carried out to achieve the optimized design and perform the structural analysis in Appendix B.2.

This chapter presents a structural comparison between the baseline design and the optimized one. The comparison is based on results obtained from the structural analysis of both floor systems, which includes previously discussed geometry, loads, and checks.

Additionally, a third floor system is included in the comparison. This system consists of the same steel beam and CLT floor from the optimized design but without interaction between these materials, resulting in a non-composite system. The purpose of adding the non-composite option is to highlight the added value from the composition of structural materials and to evaluate if the gain in capacity justifies the additional complexity of composite systems compared to non-composite ones.

This comparison considers both ULS and SLS results for all three systems. The volume of structural materials used in each floor system, an important aspect for evaluating material efficiency, can be found in Chapter 7.1, Table 7.

The table below presents the comparison between the three floor systems:

State/Design			Baseline Design	Optimized Design	Optimized Design Non-Composite
			Unity Check		
ULS	Composite beam	Steel	0.6	0.6	0.8
		Timber	0.3	0.5	0.3
	CLT floor		0.2	0.7	0.7
SLS	Composite beam		0.9	0.9	1.5
	CLT floor		0.2	0.8	0.8

Table 5: UC for three alternatives.

The results from the baseline design and the optimized design show that the composite beam in both designs behaves similarly, despite the optimized design using a CLT floor with a height 40 mm less than the baseline design. This difference explains the increase in UC values for the CLT floor in the optimized design. The optimized design demonstrates similar structural behavior to the baseline one, as both designs have the same critical UC values. However, the optimized design uses 1.093 m<sup>3</sup> less timber per composite floor system and 0.012 m<sup>3</sup> more steel than the baseline design, and it eliminates the use of concrete (values from Table 7).

The following chapter discusses the environmental impact, where the difference in material volume is more crucial. From a structural perspective, the optimized design performs as well as the baseline design but with fewer materials, making it more efficient.

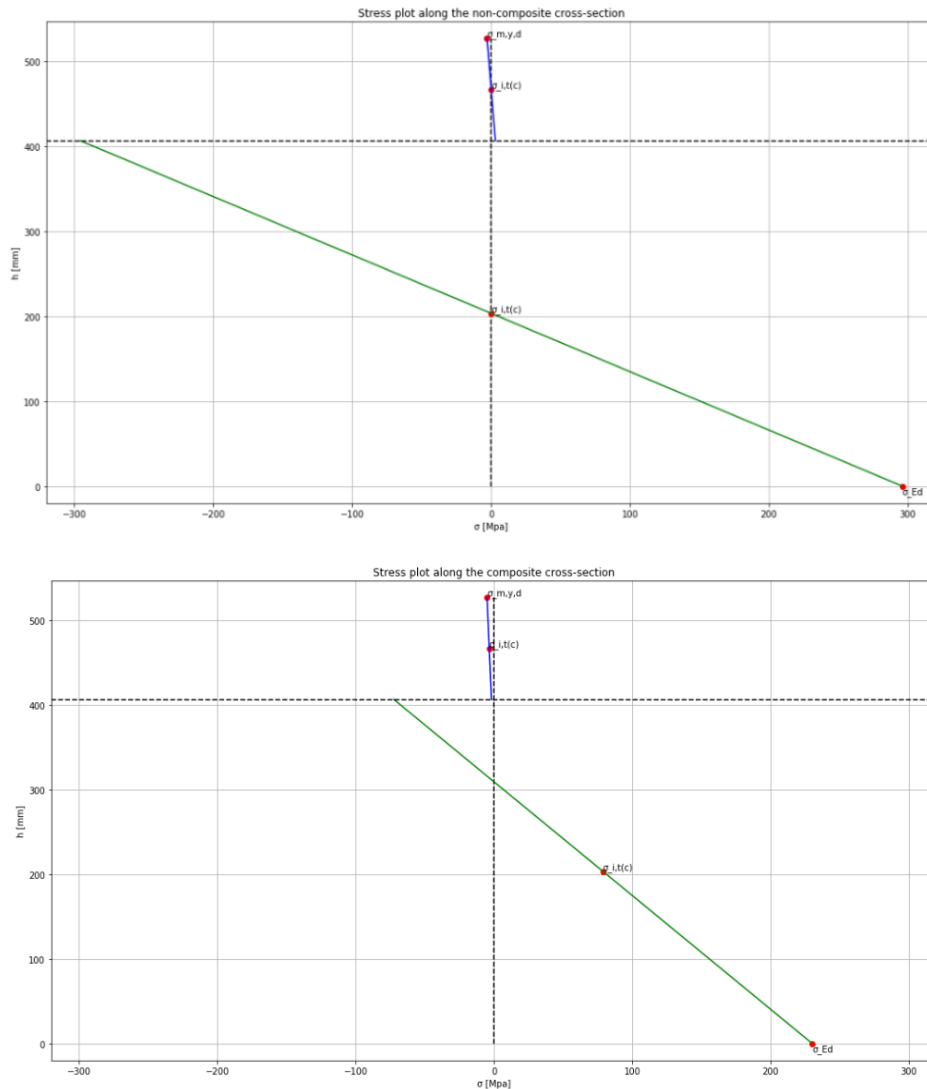


Figure 37: Stress distribution along non-composite (top) and composite (bottom) cross-sections.

Figure 37 illustrates the stress distribution along non-composite (top) and composite (bottom) cross-sections. The non-composite beam highlights the benefits of composite systems by showing better stress distribution along the composite system's cross-section in ULS. Since both designs are sufficient in ULS, this aspect might not have significant importance in the comparison and can even be considered a plus point for the non-composite system.

In SLS, however, the bending stiffness in the composite system ( $7.82 \cdot 10^{13} \text{ Nmm}^2$ ) is much higher than in the non-composite system ( $4.56 \cdot 10^{13} \text{ Nmm}^2$ ). This is demonstrated in the deflection check, where the composite beam has 60% more capacity than the non-composite beam. This substantial increase in the stiffness of the composite floor

system is a crucial gain in capacity and one of the main benefits of composite systems in general.

The structural comparison highlights that the optimized design not only achieves comparable structural performance to the baseline one but also enhances material efficiency by eliminating concrete and reducing timber usage. Moreover, the significant increase in stiffness underscores the advantages of composite floor systems over non-composite alternatives.

## 7 ENVIRONMENTAL IMPACT AND COMPARISON

This chapter compares the environmental impact of the baseline floor system (non-circular design) and the optimized composite floor system (circular design) using embodied carbon calculations. To perform these calculations practically, a case study of a real project by WSP is used, with certain assumptions made to facilitate the process without compromising the comparison's neutrality.

The methodology for calculating the embodied carbon for each design is explained in Chapter 2.6, detailing the included life cycle stages tailored separately for the circular and non-circular designs.

### 7.1 Case Study

The case study focuses on a 20-story residential building in Amsterdam, constructed with steel columns and beams, and composite floors and core for stability. For simplicity, the embodied carbon calculation is limited to one story of the building, excluding the core, primary beams, and columns. Thus, the calculation includes only the composite floor structure.

Two scenarios are considered for the embodied carbon calculation. The first scenario examines the baseline composite floor system design, while the second scenario examines the optimized floor system design. The optimized design is not expected to be 100% reusable in its second life cycle due to potential damage during deconstruction or reconstruction, variations in floor plan geometry, structural condition, and the effects of timber creep. Therefore, the reuse of the floor system in the second life cycle is evaluated under three different reuse percentages: 50%, 70%, and 90%.

The embodied carbon calculation is performed for one story, starting with a 50-year first life cycle. It then extends to a second life cycle, assuming a new project 100 km away from the original location. For the baseline design (non-circular), all structural materials must complete stage C (end of life), and a new floor system is created for the second life cycle. For the optimized design (circular), stage C2 in the first life cycle connects to A4 in the second life cycle, highlighting the benefits of material reusability.

The floor plan dimensions for the investigated story are shown in Figure 38. The 3D floor plan indicates that 24 floor units are used to construct one story, with each unit having a 12-meter span and 3-meter width. Both designs use the same number of units as the floor systems share the same geometry.

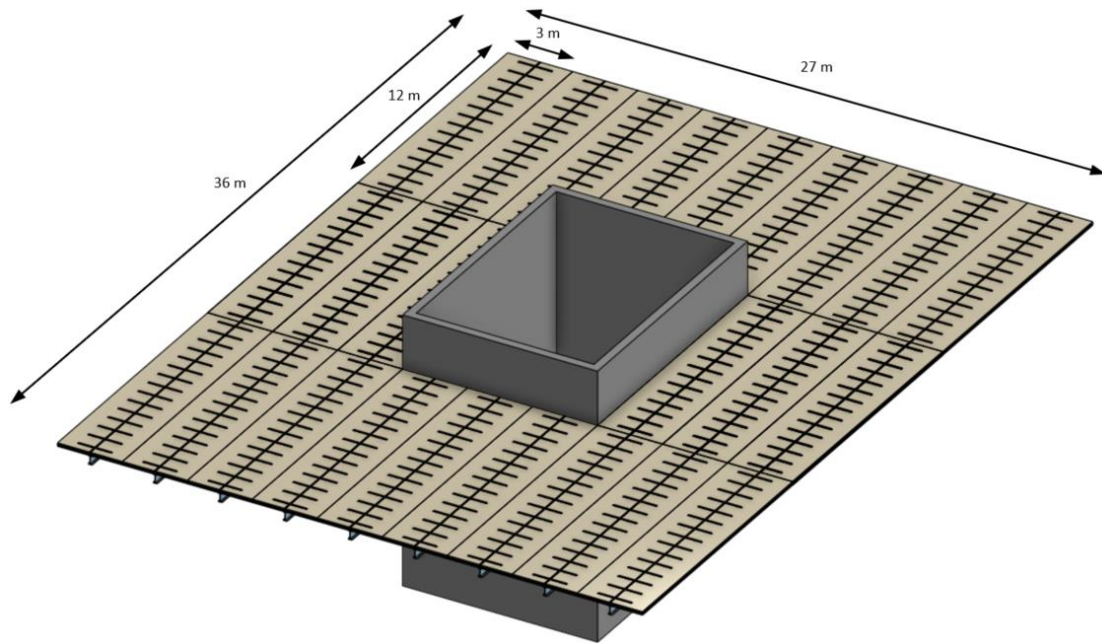


Figure 38: 3D Floor plan dimensions of the investigated story.

The input carbon factors, sourced from [44], are shown in the table below and explained subsequently:

Used Material/Carbon Factor [kgCO <sub>2</sub> e/kg]	A1-A3	A4	A5w	C2-C4	Biogenic carbon
<b>Concrete</b> In situ concrete, Global Average (excludes China).	0.191	0.005	0.053	0.018	-
<b>Steel*</b> Structural sections, global rolled open sections.	1.550	0.183	0.010	0.018	-
<b>Timber</b> Timber manufactured structural timber, global CLT 100% FSC/PEFC	0.437	0.161	0.010	1.667	-1.64
(*): Steel elements for various applications are grouped together in one category for convenience.					

Table 6: Carbon Factors.

#### Additional Calculation Factors:

- **A4 (Transportation):**
  - Concrete: Locally manufactured; 50 km by road  
 $A4 = 50 \text{ km} * 0.10749 \text{ gCO}_2\text{e/kg/km/1,000} = 0.005 \text{ kgCO}_2\text{e/kg.}$
  - Steel: Globally manufactured; 200 km by road; 10000 km by sea  
 $A4 = 200 \text{ km} * 0.10749 \text{ gCO}_2\text{e/kg/km/1,000} + 10000 \text{ km} * 0.01614 \text{ gCO}_2\text{e/kg/km/1,000} = 0.183 \text{ kgCO}_2\text{e/kg.}$
  - Timber: European manufactured; 1500 km by road  
 $A4 = 1500 \text{ km} * 0.10749 \text{ gCO}_2\text{e/kg/km/1,000} = 0.161 \text{ kgCO}_2\text{e/kg.}$
- **A5a (Site Activities):** Neglected as conservatively considered to be similar for both options and for any second life cycle.
- **C1 (Deconstruction/Demolition):** Due to the absence of information from the contractor, this value has been assumed to be the same for deconstruction or demolition [13];  $3.4 \text{ kgCO}_2\text{e/m}^2 * \text{area of the story}$ ;  $C1 = 3.4 * 36 \text{ m} * 27 \text{ m} = 3305 \text{ kgCO}_2\text{e} = 3.3 \text{ tCO}_2\text{e.}$
- **C2 (Transportation to reuse/recycling/landfill):** 100 km;  $C2 = 100 \text{ km} * 0.10749 \text{ gCO}_2\text{e/kg/km/1,000} = 0.011 \text{ kgCO}_2\text{e/kg.}$
- **C3-C4:**
  - Steel/Concrete:  $0.013 \text{ kgCO}_2\text{e/kg.}$
  - Timber:  $1.66 \text{ kgCO}_2\text{e/kg}$  (Wood for Good EPD EoL scenario).

The materials volume for each floor system per one unit is as follows:

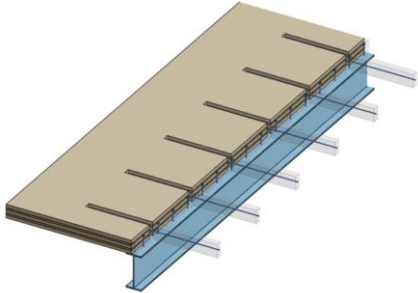
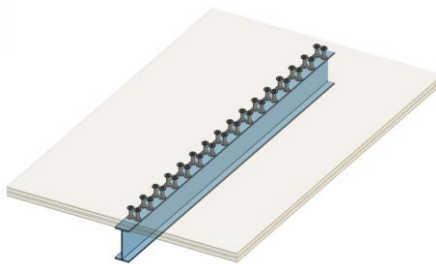
Volume [m <sup>3</sup> ]	Baseline Design		Optimized Design	
	<b>Concrete</b>	Grout pockets	0.348	-
<b>Steel</b>	Beam + shear studs + bars	0.094	Beam + shear connectors	0.106
<b>Timber</b>	Floor	5.412	Floor	4.319
<b>3D one unit section</b>				

Table 7: Structural materials volume.

### 7.1.1 Embodied Carbon Calculation for The Baseline Composite Floor System (Non-Circular Design)

The life cycle stages and modules for the non-circular system are detailed in Chapter 2.6.1. Material weights are specified in Table 2, and carbon factors are sourced in previous Chapter (7.1). The embodied carbon is calculated using the following LCA for one story of the case study building.

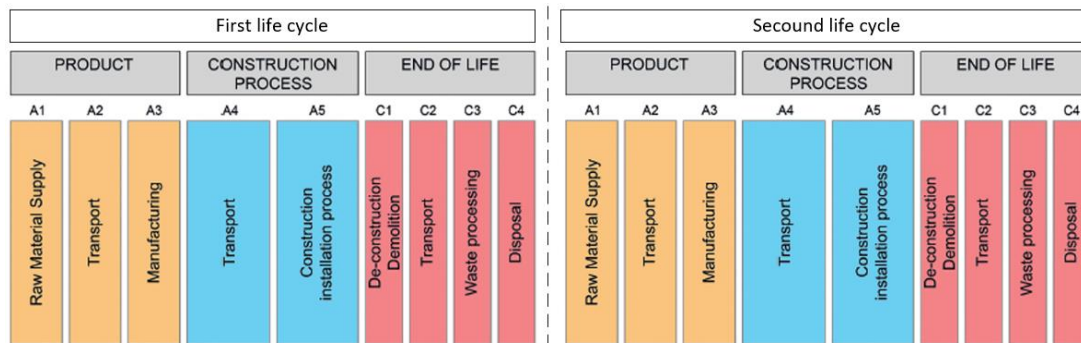


Figure 39: Life cycle stages and modules for non-circular system.

The calculations are as follows:

Calculation	Volum e [m <sup>3</sup> ]	Mass [kg]	A1-A5 [kgCO <sub>2</sub> e ]	C1-C4 [kgCO <sub>2</sub> e]	Biogenic carbon [kgCO <sub>2</sub> e]
<b>Concrete</b>	8.352	20880	5199	376	-
<b>Steel</b>	2.256	17712	30872	319	-
<b>Timber</b>	129.888	54552	33168	90938	-89465
<b>Total first life cycle (LC1)</b>	-	-	69239	(∑ C2-C4) + C1 = 91633	-89465
<b>Total second life cycle (LC2)</b>	-	-	69239	91633	-89465
<b>Whole life carbon for two life cycles</b>	LC1 + LC2 = 2 * LC1 = 142874 = 143 tCO <sub>2</sub> e				

Table 8: Embodied carbon calculation for non-circular system.

Appendix B includes an illustrative graph of cumulative carbon emissions over time and biogenic carbon for the baseline design.

### 7.1.2 Embodied Carbon Calculation for The Optimized Composite Floor System (Circular Design)

The life cycle stages and modules for the circular system are discussed in Chapter 2.6.1. Material weights are specified in Table 2, and carbon factors are sourced in previous

Chapter (7.1). The embodied carbon is calculated using the following LCA for one story of the case study building.

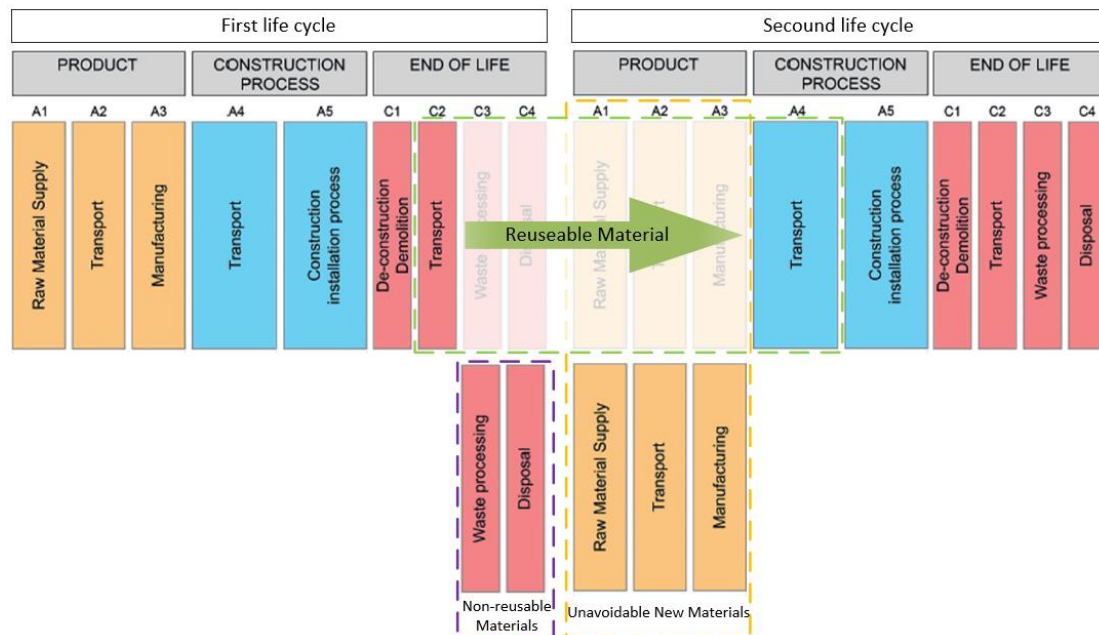


Figure 40: Life cycle stages and modules for circular system.

The embodied carbon calculation is performed for three cases, with different reusability percentages (50%, 70%, and 90%) after the end of life in the first life cycle.

### Case 1: 50% Reusability in the Second Life Cycle

First Life Cycle (LC1)					
Calculation	Volume [m <sup>3</sup> ]	Mass [kg]	A1-A5 [kgCO <sub>2</sub> e]	C1-C4 for non-reusable materials 50% [kgCO <sub>2</sub> e]	Biogenic carbon for non-reusable materials 50% [kgCO <sub>2</sub> e]
Steel	2.544	19970	34808	359 * 0.5	-
Timber	103.656	43535	26469	72573 * 0.5	-71397 * 0.5
<b>Total for LC1</b>	-	-	61277	( $\sum$ C2-C4) + C1 = 39771	-35698
Second Life Cycle (LC2)					
Calculation	Transport reusable materials 50% From C2 to A4 [kgCO <sub>2</sub> e]	A1-A5 new materials 50% [kgCO <sub>2</sub> e]	A5w for reusable materials 50% [kgCO <sub>2</sub> e]	C1-C4 LC2 [kgCO <sub>2</sub> e]	Biogenic carbon end LC2
<b>Total for LC2</b>	698 * 0.5	61277 * 0.5	635 * 0.5	359 + 72573	-71397



<b>Whole life carbon for two life cycles</b>	$LC1 + LC2 =$ $(61277 + 39771 - 35698) + (349 + 30638 + 317 + 72932 - 71397) =$ $98.2 \text{ tCO}_2\text{e}$
--	--

Table 9: Embodied carbon calculation for circular system (50% reused).

Appendix B includes an illustrative graph of cumulative carbon emissions over time and biogenic carbon for the optimized design 50% reused.

### Case 2: 70% Reusability in the Second Life Cycle

First Life Cycle (LC1)					
Calculation	Volume [m <sup>3</sup> ]	Mass [kg]	A1-A5 [kgCO <sub>2</sub> e]	C1-C4 for non-reusable materials 30% [kgCO <sub>2</sub> e]	Biogenic carbon for non-reusable materials 30% [kgCO <sub>2</sub> e]
Steel	2.544	19970	34808	359 * 0.3	-
Timber	103.656	43535	26469	72573 * 0.3	-71397 * 0.3
<b>Total for LC1</b>	-	-	61277	( $\sum C2-C4$ ) + C1 * 0.3 = 25185	-21419
Second Life Cycle (LC2)					
Calculation	Transport reusable materials 70% From C2 to A4 [kgCO <sub>2</sub> e]	A1-A5 new materials 30% [kgCO <sub>2</sub> e]	A5w for reusable materials 70% [kgCO <sub>2</sub> e]	C1-C4 LC2 [kgCO <sub>2</sub> e]	Biogenic carbon end LC2
<b>Total for LC2</b>	698 * 0.7	61277 * 0.3	635 * 0.7	359 + 72573	-71397
<b>Whole life carbon for two life cycles</b>	$LC1 + LC2 =$ $(61277 + 25185 - 21419) + (489 + 18383 + 444 + 72932 - 71397) =$ $85.9 \text{ tCO}_2\text{e}$				

Table 10: Embodied carbon calculation for circular system (70% reused).

Appendix B includes an illustrative graph of cumulative carbon emissions over time and biogenic carbon for the optimized design 70% reused.

### Case 2: 90% Reusability in the Second Life Cycle

First Life Cycle (LC1)					
Calculation	Volume [m <sup>3</sup> ]	Mass [kg]	A1-A5 [kgCO <sub>2</sub> e]	C1-C4 for non-reusable materials 10% [kgCO <sub>2</sub> e]	Biogenic carbon for non-reusable materials 10% [kgCO <sub>2</sub> e]



<b>Steel</b>	2.544	19970	34808	359 * 0.1	-
<b>Timber</b>	103.656	43535	26469	72573 * 0.1	-71397 * 0.1
<b>Total for LC1</b>	-	-	61277	( $\sum$ C2-C4) + C1 = 10598	-7140
<b>Second Life Cycle (LC2)</b>					
<b>Calculation</b>	<b>Transport reusable materials 90% From C2 to A4 [kgCO<sub>2</sub>e]</b>	<b>A1-A5 new materials 10% [kgCO<sub>2</sub>e]</b>	<b>A5w for reusable materials 90% [kgCO<sub>2</sub>e]</b>	<b>C1-C4 LC2 [kgCO<sub>2</sub>e]</b>	<b>Biogenic carbon end LC2</b>
<b>Total for LC2</b>	698 * 0.9	61277 * 0.1	635 * 0.9	359 + 72573	-71397
<b>Whole life carbon for two life cycles</b>	LC1 + LC2 = (61277 + 10598 - 7140) + (628 + 6128 + 571 + 72932 - 71397) = 73.6 tCO <sub>2</sub> e				

Table 11: Embodied carbon calculation for circular system (90% reused).

Appendix B includes an illustrative graph of cumulative carbon emissions over time and biogenic carbon for the optimized design 90% reused.

## 7.2 Embodied Carbon Comparison

This section presents a comparison of embodied carbon emissions across two life cycles for both the baseline (non-circular) and optimized (circular) designs. The results are depicted in a graph that illustrates the cumulative carbon emissions over time for each design, clearly highlighting the impact at each stage of the life cycle.

In the first life cycle, specifically after Module A, the optimized design shows a significant reduction in embodied carbon, with all three cases reporting a value of 61.3 tCO<sub>2</sub>e. This is lower than the baseline design's value of 69.2 tCO<sub>2</sub>e. The reduction primarily results from improvements in material efficiency applied to the CLT panels in the optimized design. The optimized design uses 26.2 m<sup>3</sup> less timber than the baseline design. Although the optimized design incorporates slightly more steel—0.3 m<sup>3</sup> compared to the baseline, which also uses grout—the impact of this additional steel on the overall embodied carbon is minimal. The substantial savings from reduced CLT usage and the elimination of grout dominate the carbon calculation.

At the beginning of the second life cycle, the differences between the optimized cases become more pronounced due to variations in material reusability. The gap between the optimized designs and the baseline design widens significantly as the reusability of materials is factored in.

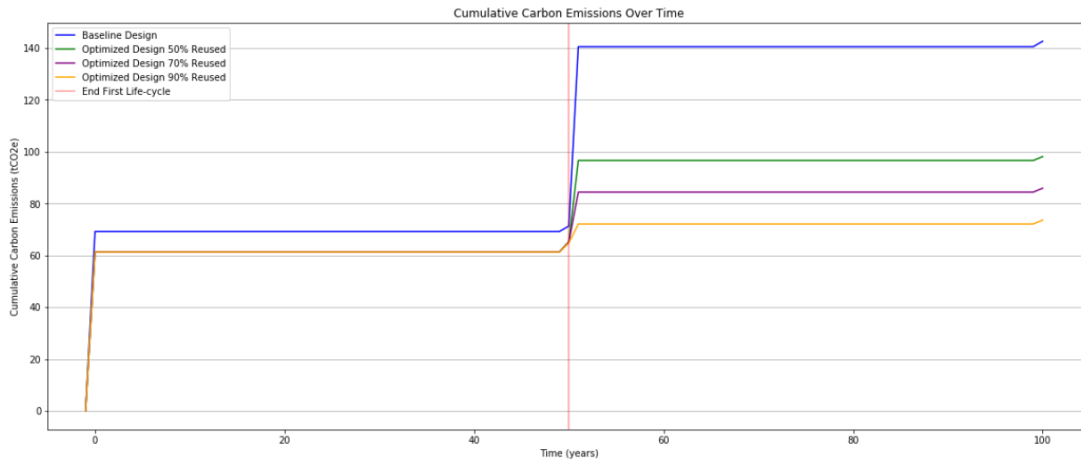


Figure 41: Cumulative carbon emissions over time for all designs.

Designing for reusability, and evaluating three scenarios—where 50%, 70%, and 90% of the materials at the end of the first life cycle are reused in the second life cycle—leads to substantial reductions in whole life embodied carbon. Specifically, the reductions are 32.5%, 41.5%, and 50.6%, respectively, compared to the baseline (non-circular) design.

The biogenic carbon graph below demonstrates yet another advantage of material reusability. Despite differences in reusability percentages between the three cases, most of the captured carbon in the timber remains stored within the structure for twice as long. In contrast, the baseline design results in the release of all captured carbon into the atmosphere at the end of each life cycle.

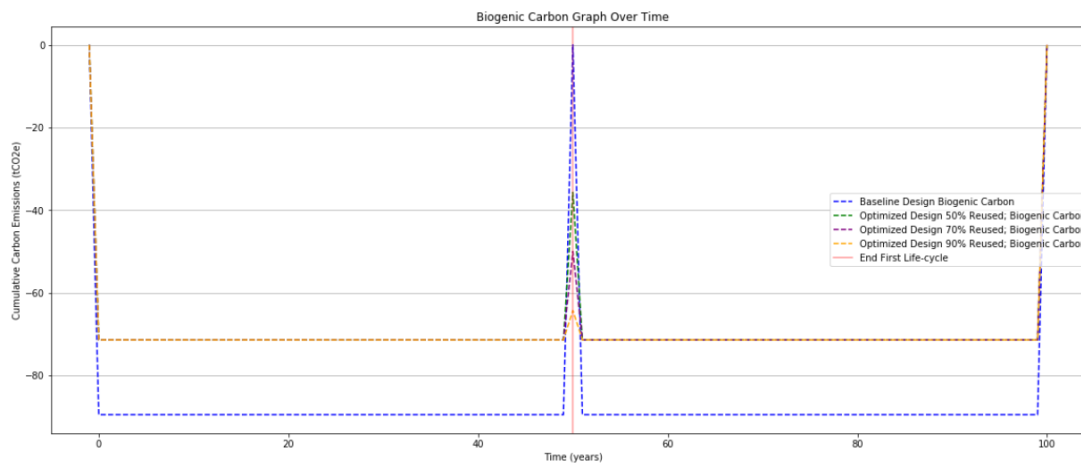


Figure 42: Biogenic carbon graph over time for all designs.

The significant reductions in carbon emissions demonstrated in this comparison underscore the environmental advantages of material efficiency and circular design principles. Material efficiency plays a crucial role in lowering carbon emissions in the first life cycle (Modulus A), offering short-term environmental benefits. Moreover, circular design principles, particularly reusability, highlight the potential for substantial environmental gains. Even partial reuse of materials can significantly reduce the carbon footprint of construction projects and advance sustainable development goals.

Additionally, circular design extends the duration of carbon sequestration within timber structures, delaying the release of captured carbon until the end of the material's life. This reinforces the long-term environmental benefits of incorporating circular design into construction practices.

## 8 CONCLUSION AND RECOMMENDATIONS

This study aimed to improve the Steel-CLT composite floor system, focusing on achieving circularity, optimizing CLT design within composite concepts, and assessing the environmental impact of improvements. Based on these objectives, the primary research questions were formed and are answered below. Additionally, the limitations encountered during the study are acknowledged and discussed. Lastly, given the significant potential and challenges of the Steel-CLT composite floor system, multiple recommendations for future research have been identified to further develop our understanding and facilitate the practical application of this system.

### Answers to Research Questions:

- **Can the circular design of steel-CLT floor systems be realized, and what are the structural benefits and drawbacks of this innovative solution?**

Yes, based on the technical analysis conducted, the steel-CLT composite floor system can indeed be designed as a circular system, allowing for recovery and reuse at the end of each life cycle. This study achieved circularity by replacing the baseline grouted shear connectors with demountable steel bolt connectors. Recent research focuses on developing pre-loaded demountable shear connectors, and this study adopts these connectors due to their unique characteristics. In addition to their demountability, these connectors offer high stiffness (slip modulus) that is comparable to traditional shear studs used in steel-concrete composite structures. As a result, incorporating these shear connectors transforms the steel-CLT composite floor system from a linear design to a circular one, with minimal reduction in stiffness, ensuring the system's structural performance is maintained.

The adaptation of these connectors was thoroughly explained in Chapter 4. The push-out test results performed on LVL, sourced from the literature, were applied in this study, with a correction factor introduced to determine the slip modulus for the shear connectors in CLT applications. This resulted in a value of  $k_{initial,CLT} = 66.7 \text{ kN/mm}$  (per shear connector).

In terms of structural performance under ultimate and serviceability limit states, there are no significant structural advantages in adopting the circular design, as both the baseline and optimized systems meet current standards. However, the primary drawback lies in the increased complexity and potential construction costs, driven by the higher number of shear connectors and the need to preload each one. Additional challenges, such as ensuring proper tolerances, maintaining temporary stability during CLT panel installation, and managing overhead work to secure the connectors, must be addressed to develop a practical, market-ready circular solution.

- **How can a CLT configuration be designed to function optimally as an integral component of the composite beam and floor system?**

In a composite system, CLT panels play two critical roles. First, they act as an integral part of the composite beam, significantly enhancing its stiffness and sharing the stress applied to the composite beams. Second, they function as a floor system, requiring sufficient strength and stiffness to span between beams effectively. This study addresses these dual functions and conducts an in-depth investigation in Chapter 5, focusing on key considerations for designing CLT panels in composite systems.

By exploring various configurations of CLT floors that meet the functional requirements of the steel-CLT composite floor system, the study demonstrates that the material efficiency of the CLT in the baseline design can be improved. One of the key strategies identified is maximizing the active area of CLT ( $A_{2,active}$ ) in the composite beam while ensuring that the top and bottom panels maintain sufficient capacity to function as part of the floor structure in the perpendicular direction. These panels must have a sufficiently high second moment of area ( $I_y$ ) to ensure the necessary structural performance in this orientation. For a more detailed explanation of these concepts and design strategies, refer to Chapter 5.

As a result of this investigation, the study identifies an optimal CLT design configuration. However, CLT panels are not currently manufactured in this configuration due to the relatively low usage of steel-CLT composite floor systems. Thus, the final design was adapted to account for market availability and practical considerations, resulting in a CLT panel with a height of  $h_{CLT} = 120$  mm, which is 25% less than the height used in the baseline design.

The structural analysis conducted on the optimized design in Appendix B.2 shows that the changes made to improve material efficiency did not compromise the structural performance. In fact, the optimized design demonstrated a 30% increase in CLT floor structure unity check under ULS conditions compared to the baseline design, while still maintaining a unity check value below one, indicating that it meets the necessary safety requirements. In addition, the SLS analysis revealed a 60% increase in unity check for the optimized design of CLT floor structure, but it remained within acceptable limits, confirming that the floor structure continues to perform effectively. These results validate the improvements made to the CLT configuration, achieving one of the research's main objectives of improving the design and efficiency of CLT in steel-CLT composite systems.

- **What are the advantages and disadvantages of the optimized floor system versus the baseline floor system?**

This study addressed this question by conducting two key comparisons: a structural comparison and an environmental impact assessment.

**The structural comparison** (Chapter 6.2) demonstrates the superiority of the optimized design in several areas. Introducing a new demountable shear connector was crucial for transitioning the design from a linear to a circular model. Despite

the new connector having a slip modulus 10% lower than that of the baseline design, this reduction in stiffness was compensated by optimizing other parameters, such as the spacing between shear connectors. As a result, both the baseline and optimized floor systems performed structurally sound, with the optimized design successfully achieving the goal of circularity without compromising structural integrity.

Moreover, the structural comparison highlighted the optimized design's higher material efficiency. By eliminating concrete and reducing timber usage, the optimized design maintained structural adequacy while achieving a 20% reduction in timber use. This underscores the importance of developing design approaches for CLT panels in composite systems. The design approach used in this study resulted in more efficient material use, achieving, as previously stated, one of the research's main objectives of improving CLT design and efficiency. Chapter 5 provides further details on the CLT design approach and design used in this study.

Additionally, when comparing the optimized composite floor system to a non-composite system using the same cross-sections, materials, and boundary conditions, the composite system was found to be 60% stiffer. This demonstrates the significant capacity gain that composite floor systems offer over non-composite alternatives, highlighting the advantages of composite design in enhancing structural performance.

The second comparison (Chapter 7.2) focused on **the environmental impact** of each design, specifically through a life cycle assessment for embodied carbon. This analysis revealed that the optimized design resulted in lower carbon emissions across multiple stages. In the first life cycle, at the end of Module A, the optimized design produced 11% fewer emissions than the baseline. This reduction was mainly due to decreased timber usage and the elimination of grout in the optimized design.

The benefits of circularity became even more apparent when considering a second life cycle. Depending on material reuse assumptions—ranging from 50% to 90% reuse—the optimized design reduced embodied carbon by 32.5% to 50.6% compared to the baseline. This substantial reduction illustrates the environmental advantages of adopting circular design principles even though the case study included only two life cycles. The results highlight that significant reductions in carbon emissions can be achieved in the building industry through more efficient material use and the adoption of circular design practices.

The disadvantage lies in the unknown variables that might affect the future reusability of the optimized floor system. This uncertainty was addressed by investigating different reuse scenarios, with material reusability percentages of 50%, 70%, and 90%.

Few sub-research questions were presented alongside the primary research questions; those questions were addressed during the study, and they served the purpose of splitting the core questions into smaller questions to aid in the discovery of the best approach for the study. Therefore, there is no need to go into more detail about those sub-questions.

### **The Analytical Approach and Parametric Studies:**

The Gamma method was employed throughout this study to perform structural analyses on the composite beams, highlighting the effectiveness of analytical approaches when investigating complex structures like composite beams. This method not only provided accurate results for structural analysis but also proved invaluable in exploring the intricate relationships between key parameters within the system.

In this study, the Gamma method was used to conduct parametric studies by varying specific parameters within a defined range and boundary conditions. This allowed for a detailed assessment of how changes in one parameter influenced specific outputs—an essential aspect when working with complex composite structures. The parametric studies enabled a deeper understanding of how seemingly minor changes in variables can significantly impact the structural performance of composite beams.

The following parametric studies were conducted:

1. The relationship between the Gamma coefficient and effective bending stiffness (see Figure 5).
2. The relationship between the spacing of shear connectors and the Gamma coefficient, and consequently its impact on effective bending stiffness (see Figure 18).
3. The relationship between the shear force acting on the joint between two composite elements and the spacing of shear connectors (see Figure 26).
4. The relationship between the active cross-sectional area of CLT and the effective bending stiffness (see Figure 29).

These studies demonstrate the profound role that parametric analysis plays in understanding complex structural behaviors. By using the Gamma method, this research was able to develop a more nuanced understanding of the interdependence between key design factors, paving the way for more efficient and effective composite beam designs.

## **8.1 Limitations**

Several limitations have been acknowledged in the study and require further investigation in future research.

- **Application of Demountable Pre-Loaded Shear Connectors:**

The application of demountable pre-loaded shear connectors in Steel-CLT composite floor system presents an innovative approach, but it requires thorough experimental testing and validation. In Chapter 5, several assumptions were made to estimate the initial stiffness of these connectors in the Steel-CLT system. While these assumptions were based on theoretical models and literature, they require experimental verification to ensure their accuracy, especially in real-world applications.

Experimental validation is also critical for verifying the assumptions made during the ULS analysis. One of the key assumptions was the dismissal of the potential for plastic hinge formation in the steel components under shear loads below 30 kN. Although supported by push-out test results, this assumption could not be fully validated through the Johansen model, which does not incorporate pre-loading effects in its design equations.

In conclusion, the current limitations in assessing the structural performance of those demountable pre-loaded shear connectors underscore the need for further experimental testing. Only through such validation can the assumptions made in this study be fully confirmed, ensuring the reliable application of these connectors in Steel-CLT composite floor system.

- **Determination of Life Cycles Number:**

Although this study provides important insights into the environmental impact of Steel-CLT composite floor systems, it is necessary to recognize the limitation in estimating the total number of life cycles the system can perform. As a result, the LCA was restricted to the first and second life cycles to minimize uncertainties related to potential future impacts. This conservative approach ensures reliability in the current analysis but leaves room for further exploration.

Future research should investigate the long-term structural performance of Steel-CLT composite systems across multiple life cycles to better understand their maximum lifespan. This would enable a more comprehensive LCA on embodied carbon, revealing the full extent of the difference in carbon footprint between linear and circular designs. By extending the analysis over several life cycles, the study could further demonstrate the significant environmental benefits of circular design principles, reinforcing their potential as a long-term solution for reducing the carbon footprint of construction projects.

- **Vibration Considerations:**

Vibration analysis was excluded from the scope of this study, meaning the design checks did not take vibrational loads into account. However, vibrations can be a critical factor in the performance of timber floor systems, and their impact on Steel-CLT composite floor systems should not be overlooked.



Given the importance of vibrational response, especially in lightweight floor systems, further research should focus on conducting a detailed vibration analysis of Steel-CLT systems. This would involve modeling the entire floor system and applying appropriate damping values.

## 8.2 Recommendations for Future Research

In addition to addressing the limitations mentioned above, several other recommendations for future research can help further develop this composite floor system.

- **Effective Width of Composite Steel-CLT Beams:**

Investigate the relationship between steel and CLT as composite elements to determine the effective width of the composite beam more accurately. This study used the smallest value from the two approaches described in Eurocode 4 and Eurocode 5. A more precise investigation is needed to accurately estimate this critical parameter, which significantly influences the structural characteristics of the composite beam.

- **Tolerance of Bolt Holes:**

Investigate the tolerances of bolt holes used to bind composite components and construct shear connectors. This aspect is crucial, especially during construction, where the deflection of the steel beam before placing the CLT floor may prevent proper alignment of bolt holes. Enlarging the holes to solve this issue could impact the stiffness of the shear connector, thus affecting the composite interaction. Therefore, determining the appropriate tolerances is vital for the design developed in this study.

- **Prefabrication and Transportation:**

One of the main objectives of this study was to achieve a circular floor system. Prefabricating this floor system for transportation and placement on primary beams at the building site would be a significant advantage. A detailed study is needed to address the challenges of prefabrication and transportation. Prefabrication could improve the quality of shear connectors since they would be constructed and preloaded in a controlled environment. Additionally, it would simplify and speed up the construction and deconstruction processes, facilitating reuse and enhancing the system's overall efficiency.

- **Cost Analysis:**

While this study primarily focuses on the structural and environmental aspects of the steel-CLT composite floor systems, conducting a cost analysis would add significant value to the evaluation, given the crucial role of financial considerations in determining the feasibility of these designs for real-world market application.

Although the optimized, circular design offers a lower carbon footprint compared to the baseline design, as demonstrated in the environmental comparison, this reduction in carbon emissions may come at a higher financial cost, which could be revealed through a detailed cost analysis.

Although the circular design offers clear environmental benefits, these come with associated costs that may impact its market adoption. The financial burden of reusing materials could outweigh the benefits, particularly due to the additional expenses involved in the complex deconstruction process and transportation at the end of each life cycle. A thorough cost analysis would reveal whether the savings in material reuse and carbon reduction are sufficient to offset these added expenses, providing a comprehensive understanding of the feasibility of implementing the optimized design in practical, market-driven applications.

- **Recommendations for Parametric Studies:**

- **Optimal Shear Connector Distribution Pattern**

This study primarily looked at the impact of shear connector spacing on shear load distribution while maintaining the longitudinal distribution pattern constant. Given that shear flow is typically a linear function, peaking at the supports and decreasing towards the mid-span, optimizing the distribution pattern could enhance the efficiency of shear connector usage in a composite beam. To achieve this, a parametric study is recommended to identify the optimal spacing distribution pattern for shear connectors. Employing the Gamma method for structural analysis and calculating the effective spacing ( $s_{ef}$ ) using Equation 9.17 from Eurocode 5 [18] will provide a more customized distribution pattern. This approach has the potential to reduce the number of required shear connectors, thereby improving efficiency and cost-effectiveness

- **Steel Section Geometry**

A parametric study should be conducted to explore the effects of varying the steel cross-section on the composite beam's performance. Although the steel profile was treated as a constant parameter in this study, examining alternative profiles could yield significant improvements. For instance, evaluating the potential of using IFB beams instead of traditional I-sections could be beneficial. IFB beams, with their wider bottom flanges, might enhance the strength and stiffness of the composite beam. By adding more steel to the outer bottom flange, the neutral axis of the composite beam would shift downward. This shift can positively impact effective stiffness, as concentrating materials at the top and bottom of the cross-section is likely to increase effective bending stiffness. Thus, exploring various steel section geometries could lead to more efficient composite beam designs.

In conclusion, this study has successfully advanced the steel-CLT composite floor system by achieving circularity and optimizing the CLT configuration design. The structural and environmental comparisons demonstrate the significant benefits of these improvements. Future research should build upon these findings to further develop and refine steel-CLT composite floor systems, aiming to advance sustainable building practices.

## REFERENCES

- [1] Akhimien, N. G., Latif, E., & Hou, S. S. (2021). Application of circular economy principles in buildings: A systematic review. *Journal of Building Engineering*, 38, 102041. <https://doi.org/10.1016/j.jobe.2020.102041>
- [2] Ghobadi, M., & Sepasgozar, S. M. E. (2023). Circular economy strategies in modern timber construction as a potential response to climate change. *Journal of Building Engineering*, 77, 107229. <https://doi.org/10.1016/j.jobe.2023.107229>
- [3] Kanters, J. (2020). Circular Building Design: An analysis of barriers and drivers for a circular building sector. *Buildings*, 10(4), 77. <https://doi.org/10.3390/buildings10040077>
- [4] Munaro, M. R., Freitas, M. D. C. D., Tavares, S. F., & Bragança, L. (2021). Circular Business Models: current state and framework to achieve sustainable buildings. *Journal of the Construction Division and Management*, 147(12). [https://doi.org/10.1061/\(asce\)co.1943-7862.0002184](https://doi.org/10.1061/(asce)co.1943-7862.0002184)
- [5] Sariatli, F. (2017). Linear Economy versus Circular Economy: A Comparative and Analyzer Study for Optimization of Economy for Sustainability. *Visegrad Journal on Bioeconomy and Sustainable Development*, 6(1), 31–34. <https://doi.org/10.1515/vjbsd-2017-0005>
- [6] Potuzak, M. T., Sener, K. C., & Roueche, D. B. (2023). Numerical Studies on the Flexural Behavior of Steel-Timber Composite Floor Systems. *ASCE*. <https://doi.org/10.1061/9780784484777.029>
- [7] Shahnewaz, M., Jackson, R., & Tannert, T. (2023). Reinforced cross-laminated timber-concrete composite floor systems. *Engineering Structures*, 291, 116395. <https://doi.org/10.1016/j.engstruct.2023.116395>
- [8] Pimentel, R., Simões, R. F., & Da Silva, L. S. (2022). Demountable Steel-CLT composite floors for Net-Zero Carbon buildings: State of the art and design principles. *Ce/Papers*, 5(2), 184–195. <https://doi.org/10.1002/cepa.1713>
- [9] New composite floor construction. (n.d.). Retrieved from <https://ieeexplore.ieee.org/document/9735119>
- [10] Romero, A., Yang, J., Hanus, F., Degée, H., & Odenbreit, C. (2023). PUSH-OUT TESTS ON CONNECTIONS FOR DEMOUNTABLE AND REUSABLE STEEL-TIMBER COMPOSITE BEAM AND FLOORING SYSTEMS. *ResearchGate*. <https://doi.org/10.52202/069179-0464>
- [11] Johnson, R. P. (2018). *Composite structures of steel and concrete: Beams, Slabs, Columns and Frames for Buildings*. John Wiley & Sons.
- [12] Blass, H. J., & Sandhaas, C. (2017). *Timber Engineering - Principles for design*. KIT Scientific Publishing.

- [13] Gibbons, O. P. (2022). How to calculate embodied Carbon.
- [14] Ding, G. (2018). Embodied carbon in construction, maintenance and demolition in buildings. In Springer eBooks (pp. 217–245). [https://doi.org/10.1007/978-3-319-72796-7\\_10](https://doi.org/10.1007/978-3-319-72796-7_10)
- [15] Waldman, B., Huang, M. L., & Simonen, K. (2020). Embodied Carbon in Construction Materials: A framework for quantifying data quality in EPDs. *Buildings and Cities*, 1(1), 625–636. <https://doi.org/10.5334/bc.31>
- [16] Christian, Chang, Y., & Hsieh, S. (2021). BIM-based assessment of building circularity and embodied carbon for a circular built environment. ResearchGate. [https://www.researchgate.net/publication/355771540\\_BIM-based\\_assessment\\_of\\_building\\_circularity\\_and\\_embodied\\_carbon\\_for\\_a\\_circular\\_built\\_environment](https://www.researchgate.net/publication/355771540_BIM-based_assessment_of_building_circularity_and_embodied_carbon_for_a_circular_built_environment)
- [17] Engineers, I. O. S. (2023). CIRCULAR ECONOMY AND REUSE: Guidance for Designers.
- [18] NEN-EN 1995-1-1:2023 Ontw. en. (n.d.). Retrieved from <https://www.nen.nl/en/nen-en-1995-1-1-2023-ontw-en-315434>
- [19] Khorsandnia, N., Valipour, H., & Crews, K. (2014). Structural response of Timber-Concrete composite beams predicted by finite element models and manual calculations. *Advances in Structural Engineering*, 17(11), 1601–1621. <https://doi.org/10.1260/1369-4332.17.11.1601>
- [20] NVN-CEN/TS 19103:2021 en. (n.d.). Retrieved from <https://www.nen.nl/en/nvn-cen-ts-19103-2021-en-289779>
- [21] Estévez-Cimadevila, J., Gutiérrez, E. M., Ruárez-Riestra, F., Otero-Chans, D., & Vázquez-Rodríguez, J. A. (2022). Timber-concrete composite structural flooring system. *Journal of Building Engineering*, 49, 104078. <https://doi.org/10.1016/j.jobbe.2022.104078>
- [22] Aspila, A., Heinisuo, M., Mela, K., Malaska, M., & Pajunen, S. (2022). Elastic design of steel-timber composite beams. *Wood Material Science and Engineering*, 17(4), 243–252. <https://doi.org/10.1080/17480272.2022.2093128>
- [23] The CLT Handbook - Swedish wood. (n.d.). Retrieved from [https://www.swedishwood.com/publications/list\\_of\\_swedish\\_woods\\_publications/the-clt-handbook/](https://www.swedishwood.com/publications/list_of_swedish_woods_publications/the-clt-handbook/)
- [24] Ling, Z., Xiang, Z., Liu, W., Yang, H., & Tang, J. (2019). Load-slip behaviour of glue laminated timber connections with glued-in steel rod parallel to grain. *Construction and Building Materials*, 227, 117028. <https://doi.org/10.1016/j.conbuildmat.2019.117028>

- [25] Tlustochowicz, G., Serrano, E., & Steiger, R. (2010). State-of-the-art review on timber connections with glued-in steel rods. *Materials and Structures*, 44(5), 997–1020. <https://doi.org/10.1617/s11527-010-9682-9>
- [26] Azinović, B., Danielsson, H., Serrano, E., & Kramar, M. (2019). Glued-in rods in cross laminated timber – numerical simulations and parametric studies. *Construction and Building Materials*, 212, 431–441. <https://doi.org/10.1016/j.conbuildmat.2019.03.331>
- [27] Ayansola, G. S., Tannert, T., & Vallée, T. (2021). Glued-in multiple steel rod connections in cross-laminated timber. *Journal of Adhesion*, 98(6), 810–826. <https://doi.org/10.1080/00218464.2021.1962715>
- [28] Dlubal Software. (2024, April 28). Dlubal Software | Structural Analysis and Design Software. Retrieved from <https://www.dlubal.com/en>
- [29] Design Procedure of Reinforced Concrete T-beam with Example. (2020, November 15). Retrieved from <https://theconstructor.org/structural-engg/design-procedure-reinforced-concrete-beam/225363/>
- [30] Promete, B. (n.d.). (ASCE)ST.1943-541X.0001979. Retrieved from <https://www.scribd.com/document/571816366/ASCE-ST-1943-541X-0001979>
- [31] NEN Connect - NEN-EN 1994-1-1:2005 en. (n.d.). Retrieved from <https://connect.nen.nl/Standard/Detail/64948>
- [32] Emilie, G., Michael, G., Mona, N., & Paduart, A. (2021). Reuse in Environmental Impact Assessment Tools: A prospective report. ResearchGate. Retrieved from. [https://www.researchgate.net/publication/356915302\\_Reuse\\_in\\_Environmental\\_Impact\\_Assessment\\_Tools\\_A\\_prospective\\_report](https://www.researchgate.net/publication/356915302_Reuse_in_Environmental_Impact_Assessment_Tools_A_prospective_report)
- [33] Baker-Brown, D. (2021, October 1). The environmental impact of reuse in the construction sector: FutuREuse. Retrieved from <https://research.brighton.ac.uk/en/publications/the-environmental-impact-of-reuse-in-the-construction-sector-futu>
- [34] Van Gulck, L., Wastiels, L., & Steeman, M. (2022). How to evaluate circularity through an LCA study based on the standards EN 15804 and EN 15978. *The International Journal of Life Cycle Assessment*, 27(12), 1249–1266. <https://doi.org/10.1007/s11367-022-02099-w>
- [35] CLTDesigner - CLTDesigner. (n.d.). Retrieved from <https://www.cltdesigner.at/en/>
- [36] Loqman, N., Safiee, N. A., Bakar, N. A., & Nasir, N. a. M. (2018). Structural Behavior of Steel-Concrete Composite Beam using Bolted Shear Connectors: A Review. *MATEC Web of Conferences*, 203, 06010. <https://doi.org/10.1051/matecconf/201820306010>

- [37] Metsä Wood. (n.d.). Kerto LVL. Retrieved from [https://www.metsagroup.com/contentassets/e39dfa793cc343918376a4166feda0c4/kerto\\_lvl\\_for\\_load-bearing\\_applications3.pdf](https://www.metsagroup.com/contentassets/e39dfa793cc343918376a4166feda0c4/kerto_lvl_for_load-bearing_applications3.pdf)
- [38] Stora Enso. (2022, September). CLT Rib panels. Structural Design Manual (pp. 1–132). Retrieved from <https://www.storaenso.com/-/media/documents/download-center/documents/product-specifications/wood-products/rib-panel-technical/structural-design-manualclt-rib-panelsv021-sep-2022.pdf>
- [39] NEN Connect - EN 1990. (n.d.). Retrieved from <https://connect.nen.nl/Family/Detail/31942?compId=10037&collectionId=0>
- [40] NEN Connect - EN 1991-1-1. (n.d.). Retrieved from <https://connect.nen.nl/Family/Detail/28205?compId=10037&collectionId=0>
- [41] NEN Connect - NEN-EN 1993-1-1+C2+A1:2016 nl. (n.d.). Retrieved from <https://connect.nen.nl/Standard/Detail/3331940?compId=10037&collectionId=0>
- [42] Life Cycle Assessment (LCA) explained - PRé Sustainability. (2024, May 14). Retrieved from <https://pre-sustainability.com/articles/life-cycle-assessment-lca-basics/>
- [43] Federation, B. P. (n.d.). Life Cycle Analysis (LCA) - a complete guide to LCAs. Retrieved from [https://www.bpf.co.uk/sustainable\\_manufacturing/life-cycle-analysis-lca.aspx](https://www.bpf.co.uk/sustainable_manufacturing/life-cycle-analysis-lca.aspx)
- [44] The Structural carbon tool - version 2 - The Institution of Structural Engineers. (2023, September 20). Retrieved from <https://www.istructe.org/resources/guidance/the-structural-carbon-tool/>
- [45] Cross-laminated timber: Status and research needs in Europe :: BioResources. (n.d.). Retrieved from [https://bioresources.cnr.ncsu.edu/resources/cross-laminated-timber-status-and-research-needs-in-europe/#:~:text=Cross%2Dlaminated%20timber%20\(CLT\)%20is%20a%20construction%20technology%20developed,such%20as%20multi%2Dfamily%20buildings](https://bioresources.cnr.ncsu.edu/resources/cross-laminated-timber-status-and-research-needs-in-europe/#:~:text=Cross%2Dlaminated%20timber%20(CLT)%20is%20a%20construction%20technology%20developed,such%20as%20multi%2Dfamily%20buildings)

## Appendix A The Correction Factor for The Slip Modulus

The correction factor is determined with the help of EC5. To calculate the slip modulus for different types of mechanical fasteners, EC5 provides several equations that are related to the type of mechanical fasteners. However, all the equations are related to the same two parameters: the timber material's density and the mechanical fastener's diameter. The following equation is for bolts type of fasteners, so the  $k_{ser}$  is equal to:

$$k_{ser} = 2 \frac{\rho_m^{1.5} * d}{23} \quad (4.1)$$

Therefore, in this study, the pre-loaded shear connectors wanted to be utilized in the design of steel-CLT composition without applying any changes to the diameter ( $d$ ) of the connector's bolt. However, the push-out test is applied to steel-LVL composition, which means there will be a difference in the value of  $k_{initial}$  due to the difference in the density ( $\rho$ ) between the LVL and CLT. Therefore, the correction factor is going to be multiplied by  $k_{initial}$ , and it is determined as follows:

$$r = \frac{k_{ser,CLT}}{k_{ser,LVL}} = \frac{\rho_{m,CLT}^{1.5}}{\rho_{m,LVL}^{1.5}} = 0.75 \quad (4.2)$$

$\rho_{m,LVL}$ : 510 kg/m<sup>3</sup> (density of LVL used in the push-out test [37]).

$\rho_{m,CLT}$ : 420 kg/m<sup>3</sup> (density of CLT) [23].

Thus, the slip modulus for one shear connector in a steel-CLT composite connection is:

$$k_{initial,CLT} = k_{initial,LVL} * r = 66750 \text{ N/mm (per shear connector)} \quad (4.3)$$

A conservative perspective on this approach of obtaining the slip modulus may regard it as lenient and perhaps inaccurate, as the link between timber density and stiffness could be more complex. Thus, further analysis and validation using push-out tests are required to overcome these challenges. While it is understood that the previously estimated reduction factor may not reflect the exact correct slip modulus value, this disparity can be resolved by modifying the percentage of bolt pre-loading or increasing bolt diameter while maintaining the pre-loading percentage constant. As a result, while this method seeks to provide an acceptable estimate of the slip modulus, it does not eliminate the need to conduct push-out experiments on steel-CLT compositions to validate the accuracy of this value.



## Appendix B The Structural Analysis

### B.1 Baseline Design Structural Analysis

The structural design rules presented in Chapter 3 are applied here to perform the structural analysis on the floor system and design it accordingly with the Eurocode.

The Python script used for this purpose is to be found in Appendix D.1.

#### Permanent dead load

##### For the composite beam:

The permanent dead load includes the weight of the structure itself. This consists of:

- The weight of the steel beam.
- The weight of the CLT floor, multiplied by the distance between the beams.
- The weight of the ceiling and services, taken from the existing design ( $G_{serv} = 1.3 \text{ kN/m}^2$ ), also multiplied by the distance between the beams.
- • The weight of the steel bars and grout is not considered for simplicity.

The total dead load acting on the composite beam, considered as a distributed line load, is calculated as follows:

$$g_{k,j} = g_{Steel} + G_{CLT} * b + G_{serv} * b = 0.6 + 0.672 * 3 + 1.3 * 3 = 6.52 \text{ kN/m}$$

##### For the CLT Floor:

The total dead load acting on the floor, considered as a distributed surface load, is:

$$G_{k,j} = G_{CLT} + G_{serv} = 0.672 + 1.3 = 1.97 \approx 2.0 \text{ kN/m}^2$$

#### Results ULS

##### Composite Beam Design

##### Critical Load Combination

Determining the critical load combinations for ULS acting on the composite beam as distributed line load:

From Formula 6.10a:

$$\text{LC1: } q_{design,beam} = 1.1 * 1.35 * 6.52 = 9.7 \text{ kN/m}$$

$$\text{LC2: } q_{design,beam} = 1.1 * 1.35 * 6.52 + 1.1 * 1.5 * 0.4 * 6 = 13.6 \text{ kN/m}$$

From Formula 6.10b:

$$\text{LC3: } q_{design,beam} = 0.89 * 1.1 * 1.35 * 6.52 = 8.6 \text{ kN/m}$$

$$\text{LC4: } q_{design,beam} = 0.89 * 1.1 * 1.35 * 6.52 + 1.1 * 1.5 * 0.4 * 6 = 18.5 \text{ kN/m}$$

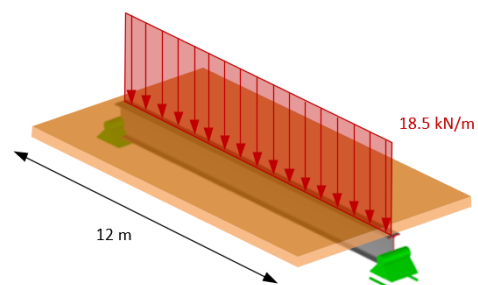


Figure 43: A 3D representation of the load

From the previous load combinations, the critical distributed line load that is acting on the composite beam is determined from LC4:  $q_{d,ULS,max,beam} = 18.5 \text{ kN/m}$

### Analysis Results

Performing the Gamma method on the composite beam provides the following results by applying the previous input from the material properties, geometry, and critical line load:

$$\gamma_1 = 0.82$$

$$(EI)_{ef} = 9.59 * 10^{13} \text{ Nmm}^2$$

$$\sigma_{Ed,steel} = \sigma_{i,t(c),steel} + \sigma_{i,m,steel} = 227.15 \text{ Mpa}$$

$$\sigma_{m,y,d} = \sigma_{i,t(c),timber} + \sigma_{i,m,timber} = 2.82 \text{ Mpa}$$

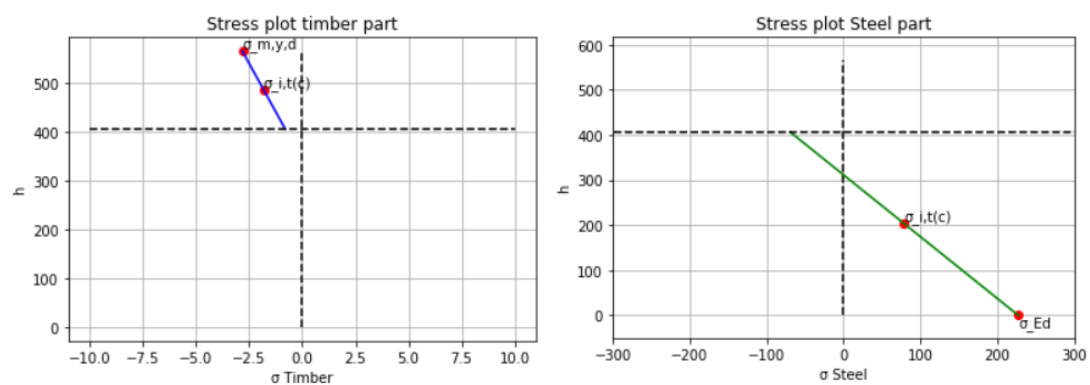


Figure 44: Normal stress distribution along the composite cross-section.

### Steel Design

Cross-section check:

$$\sigma_{Ed} \leq \frac{f_y}{\gamma_{M0}}$$

$$\sigma_{Ed,steel} = 227.15 \text{ Mpa}$$

$$f_y = 355 \text{ N/mm}^2$$

$$\gamma_{M0} = 1$$

$$UC = 0.6$$

### Timber Design

Cross-section check:

$$\sigma_{m,y,d} \leq f_{m,d} = k_{sys} * k_{mod} * \frac{f_{m,k}}{\gamma_M}$$

$$\sigma_{m,y,d} = 2.82 \text{ Mpa}$$

$$f_{m,k} = 24 \text{ N/mm}^2$$

$$k_{sys} = 1$$

$$k_{mod} = 0.5$$

$$\gamma_M = 1.3$$

$$UC = 0.3$$

### CLT Floor Design

#### Critical Load Combination

Determining the critical load combinations for ULS acting on the CLT floor as distributed surface load:

From Formula 6.10a:

$$LC1: Q_{design, floor} = 1.1 * 1.35 * 2.0 = 3.0 \text{ kN/m}^2$$

$$LC2: Q_{design, floor} = 1.1 * 1.35 * 2.0 + 1.1 * 1.5 * 0.4 * 2.0 = 4.3 \text{ kN/m}^2$$

From Formula 6.10b:

$$LC3: Q_{design, floor} = 0.89 * 1.1 * 1.35 * 2.0 = 2.6 \text{ kN/m}^2$$

$$LC4: Q_{design, floor} = 0.89 * 1.1 * 1.35 * 2.0 + 1.1 * 1.5 * 2.0 = 5.9 \text{ kN/m}^2$$

From the previous load combinations, the critical distributed surface load that is acting on the composite beam is determined from LC4:  $Q_{d, ULS, max, floor} = 5.9 \text{ kN/m}^2$

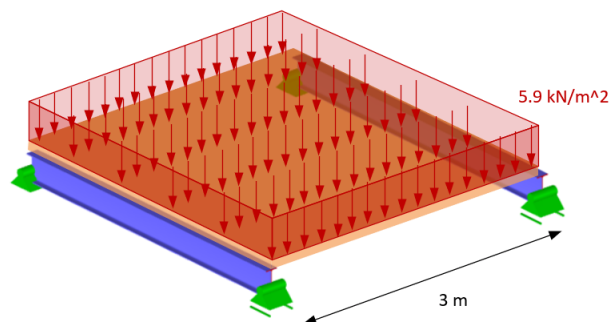


Figure 45: A 3D representation of the load application on the floor.

### Timber Design

Cross-section check:

$$\sigma_{m,y,d} \leq f_{m,d} = k_{sys} * k_{mod} * \frac{f_{m,k}}{\gamma_M}$$

$$\sigma_{m,y,d} = \frac{M_{y,d}}{W_{x,net}} = \frac{6637.5 * 10^3}{38 * 10^5} = 1.75 \text{ Mpa}$$

$$f_{m,k} = 24 \text{ N/mm}^2$$

$$k_{sys} = 1$$

$$k_{mod} = 0.5$$

$$\gamma_M = 1.3$$

$$UC = 0.2$$

### Results SLS

## Composite Beam Design

### Critical Load Combination

Determining the critical load combinations for SLS acting on the composite beam as a distributed line load involves two primary load cases:

$$\begin{aligned}\text{LC1: } q_{design,beam} &= g_{k,j} \\ q_{design,beam} &= 6,52 \text{ kN/m} \\ \text{LC2: } q_{design,beam} &= g_{k,j} + q_{k,1} \\ q_{design,beam} &= 6.52 + 6 = 12.52 \text{ kN/m}\end{aligned}$$

From these load combinations, the critical distributed line load acting on the composite beam is identified from LC2:

$$q_{d,SLS,max,beam} = 12.52 \text{ kN/m}$$

### Creep and Stiffness Reduction

$$E_{fin,timber} = \frac{E_{eff,timber}}{1+k_{def}} = \frac{3628.3}{1+0.6} = 2267.7 \text{ N/mm}^2$$

$$k_{ser,fin} = \frac{k_{test}}{1+k_{def}} = \frac{149600}{1+0.6} = 93500 \text{ N/mm}$$

$$k_{def} = 0.6.$$

### Analysis Results

Performing the Gamma method on the composite beam provides the following results by applying the previous input from the material properties, geometry, and critical line load:

$$\gamma_1 = 0.82$$

$$(EI)_{ef} = 8.17 * 10^{13} \text{ Nmm}^2$$

### Deflection Check

$$w \leq w_{max} = \frac{L}{250} = 48 \text{ mm}$$

$$w = \frac{5}{384} * \frac{q_{d,SLS,max,beam} * l^4}{(EI)_{ef}} = 41.4 \text{ mm}$$

$$UC = 0.9$$

### Vibration

Assessing the fundamental frequency of the steel beam (f) using the equation  $f = 18/\sqrt{w}$  gives a fundamental frequency of 2.8Hz. As this is below the typically accepted limit of 3Hz, in practice additional dynamic analysis should be undertaken to evaluate the vibrational response of the floor system. This analysis is outside the scope of this study.

## CLT Floor Design

### Critical Load Combination

Determining the critical load combinations for SLS acting on the CLT floor as a distributed surface load involves the following load cases:

$$\text{LC1: } Q_{design, floor} = 2.0 = 2.0 \text{ kN/m}^2$$

$$\text{LC2: } Q_{design, floor} = 2.0 + 2.0 = 4 \text{ kN/m}^2$$

From these load combinations, the critical distributed surface load acting on the CLT floor is identified from LC2:

$$Q_{d, SLS, max, floor} = 4 \text{ kN/m}^2$$

#### *Creep and Stiffness Reduction*

$$EI_{fin} = \frac{EI_{eff}}{1+k_{def}} = \frac{2.09 * 10^{12}}{1+0.6} = 2.09 * 10^{12} \text{ Nmm}^2$$

$$k_{def} = 0.6.$$

#### *Deflection Check*

$$w \leq w_{max} = \frac{b}{250} = 12 \text{ mm}$$

$$w = \frac{5}{384} * \frac{Q_{d, SLS, max, floor} * b^4}{(EI)_{ef}} = 2 \text{ mm}$$

$$UC = 0.2$$

#### *Vibration*

This analysis is outside the scope of this study, as previously stated.

## B.2 Optimized Design Structural Analysis

The structural design rules presented in Chapter 3 are applied here to perform the structural analysis on the floor system and design it accordingly with the Eurocode.

The python script used for this purpose is to be found in Appendix D.2.

### Permanent dead load

#### For the composite beam:

The permanent dead load includes the weight of the structure itself. This consists of:

- The weight of the steel beam.
- The weight of the CLT floor, multiplied by the distance between the beams.
- The weight of the ceiling and services, taken from the existing design ( $G_{serv} = 1.3 \text{ kN/m}^2$ ), also multiplied by the distance between the beams.
- The weight of the shear connectors is not considered for simplicity.

The total dead load acting on the composite beam, considered as a distributed line load, is calculated as follows:

$$g_{k,j} = g_{Steel} + G_{CLT} * b + G_{serv} * b = 0.6 + 0.5 * 3 + 1.3 * 3 = 6 \text{ kN/m}$$

#### For the CLT Floor:

The total dead load acting on the floor, considered as a distributed surface load, is:

$$G_{k,j} = G_{CLT} + G_{serv} = 0.5 + 1.3 = 1.8 \text{ kN/m}^2$$

### Results ULS

#### Composite Beam Design

##### Critical Load Combination

Determining the critical load combinations for ULS acting on the composite beam as distributed line load:

From Formula 6.10a:

$$\text{LC1: } q_{design,beam} = 1.1 * 1.35 * 6 = 8.91 \text{ kN/m}$$

$$\text{LC2: } q_{design,beam} = 1.1 * 1.35 * 6 + 1.1 * 1.5 * 0.4 * 6 = 12.9 \text{ kN/m}$$

From Formula 6.10b:

$$\text{LC3: } q_{design,beam} = 0.89 * 1.1 * 1.35 * 6 = 7.9 \text{ kN/m}$$

$$\text{LC4: } q_{design,beam} = 0.89 * 1.1 * 1.35 * 6 + 1.1 * 1.5 * 6 = 17.8 \text{ kN/m}$$

From the previous load combinations, the critical distributed line load that is acting on the composite beam is determined from LC4:  $q_{d,ULS,max,beam} = 17.8 \text{ kN/m}$

#### Analysis Results

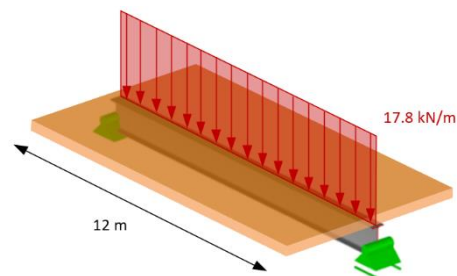


Figure 46: A 3D representation of the load

Performing the Gamma method on the composite beam provides the following results by applying the previous input from the material properties, geometry, and critical line load:

$$\gamma_1 = 0.85$$

$$(EI)_{ef} = 9.04 * 10^{13} \text{ Nmm}^2$$

$$\sigma_{Ed,steel} = \sigma_{i,t(c),steel} + \sigma_{i,m,steel} = 229.95 \text{ Mpa}$$

$$\sigma_{m,y,d} = \sigma_{i,t(c),timber} + \sigma_{i,m,timber} = 5.03 \text{ Mpa}$$

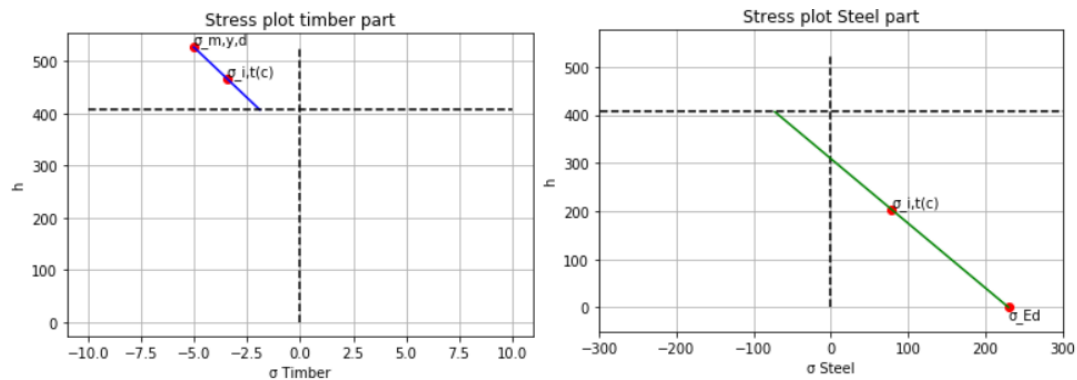


Figure 47: Normal stress distribution along the composite cross-section.

### Steel Design

Cross-section check:

$$\sigma_{Ed} \leq \frac{f_y}{\gamma_{M0}}$$

$$\sigma_{Ed,steel} = 229.95 \text{ Mpa}$$

$$f_y = 355 \text{ N/mm}^2$$

$$\gamma_{M0} = 1$$

$$UC = 0.6$$

### Timber Design

Cross-section check:

$$\sigma_{m,y,d} \leq f_{m,d} = k_{sys} * k_{mod} * \frac{f_{m,k}}{\gamma_M}$$

$$\sigma_{m,y,d} = 5 \text{ Mpa}$$

$$f_{m,k} = 24 \text{ N/mm}^2$$

$$k_{sys} = 1$$

$$k_{mod} = 0.5$$

$$\gamma_M = 1.3$$

$$UC = 0.5$$

### Shear Connection Design

In Chapter 4, a critical requirement for the pre-loaded shear connectors was introduced. This requirement specifies that the shear force acting on each connector must not exceed 30 kN to prevent initial slip and avoid any reduction in the slip modulus  $k_{initial,CLT,2}$ . Therefore, the fundamental condition is:

$$F_{joint} \leq 30 \text{ kN per shear connector}$$

Since the shear connectors are applied in pairs, the governing force is  $F_{Ed,max} \leq 60 \text{ kN}$ .

### Steel top flange checks:

The resistance of the steel flange is evaluated in this study because it differs from the original setup tested in the literature [10]. While components like the steel bolts and tubes were tested in the push-out experiment, where the bolt failure occurred around 96 kN—significantly higher than the 30 kN requirement—these components are not governing and need no further checks.

In the original experiment, a HEB 260 (S355) profile was used, featuring a flange thickness ( $t_f$ ) of 17.5 mm. In this study, the UB 406x178x60 profile is used for the composite beam in the floor system, with a flange thickness ( $t_f$ ) of 12.8 mm, which is less than the original. Therefore, the following check ensures that the steel top flange can withstand a 60 kN shear force across the entire cross-section (30 kN per shear connector). These checks are according to EN 1993-1-8 [41]

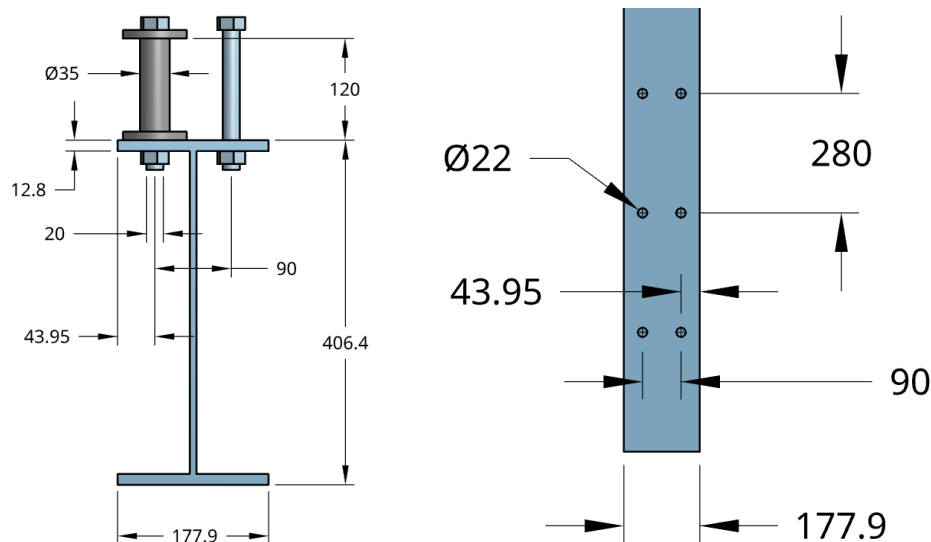


Figure 48: Front view of the shear connector and the steel beam left drawing. Top view steel beam right drawing.

### Indication of end-edge distances and pitches:



$$e_1 = p_1 = 280 \text{ mm.}$$

$$e_2 = 43.95 \text{ mm.}$$

$$p_2 = 90 \text{ mm.}$$

$$d_0 = 22 \text{ mm}$$

$$e_1 \geq 1.2 d_0 = 26.4 \text{ mm}$$

$$e_2 \geq 1.2 d_0 = 26.4 \text{ mm}$$

$$p_1 \geq 2.2 d_0 = 48.4 \text{ mm}$$

$$p_1 \geq 2.4 d_0 = 52.8 \text{ mm}$$

All distances meet the required specifications.

### Bearing resistance:

$$F_{b,Rd} = \frac{k_1 \cdot a_b \cdot f_u \cdot d \cdot t_f}{\gamma_{M2}} = 251 \text{ kN per bolt (not governing)}$$

$$a_b = \min \left[ 1; \frac{f_{ub}}{f_u}; \frac{e_1}{3d_0} \right] = 1$$

$$k_1 = \min \left[ 2.8 \frac{e_2}{d_0} - 1.7; 2.5 \right] = 2.5$$

$$f_u = 490 \text{ N/mm}^2$$

$$d = 20 \text{ mm}$$

$$t_f = 12.8 \text{ mm}$$

$$\gamma_{M2} = 1.25$$

### Design resistance of net section of steel plates loaded in tension:

For simplicity, only the top flange area is considered active for the calculation of the net area.

$$N_{t,Rd} = \frac{0.9 \cdot A_{net} \cdot f_u}{\gamma_{M2}} = 605 \text{ kN (not governing)}$$

$$A_{net} = 1713.92 \text{ mm}^2$$

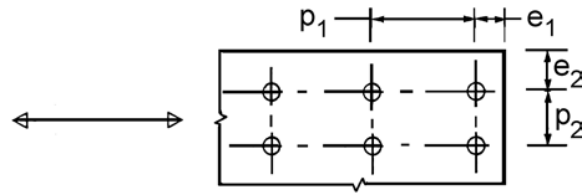


Figure 49: Symbols for spacing of fasteners [41].

### Timber checks:

This check is not expected to be critical since the previous requirement of a maximum 30 kN load on each shear connector must be fulfilled. To simplify the Johansen model calculation, the shear force acting on the joint

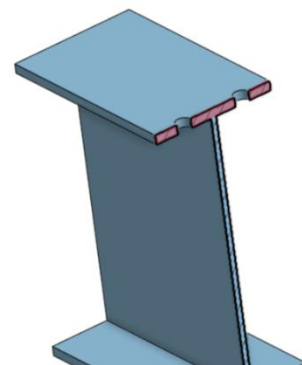


Figure 50: Net area of the top flange in red.

is assumed to be perpendicular to the grain of all the CLT panels. This means that during this check, all CLT panels' direction is considered uniform, with the shear force acting in the weaker direction of these panels (perpendicular to the grain). Additionally, the rope effect is neglected to streamline the calculation process. It's important to note that these assumptions reduce the characteristic load-carrying capacity of a steel-to-timber connection, but they do not compromise the reliability of the check.

The relationship between the steel plate thickness (the top flange thickness,  $t_f = 12.8 \text{ mm}$ ) and the tube diameter ( $d = 35 \text{ mm}$ ) is considered a thin plate according to the Johansen model ( $t \leq 0.5 * d$ ). However, the Johansen model does not account for the pre-loading of the steel bolts within the steel tube. Pre-stressing increases the load-bearing capacity of the bolt, preventing plastic hinge formation when the load is below 30 kN. In experiments documented in the literature [10], plastic hinges formed in this shear connection at around 96 kN. Therefore, preloading the bolts enhances the connection's resistance capacity, as evidenced by the results of the push-out test. Consequently, it is assumed that the steel part will not form a plastic hinge at a 30 kN load, which is significantly lower than the 96 kN load where plastic hinges began forming in the experiment.

Since the Johansen model does not consider the pre-loading effect in its equations, design equations for both thin and thick steel plates have been used to determine the load-carrying capacity for the shear connection according to EN 1995-1-1 [18]. However, failure mechanisms involving plastic hinge formation are not expected to occur under the specified load conditions. Further investigation and additional experiments are required to determine the impact of preloading on the Johansen model design equations and to accurately identify the failure mechanisms.

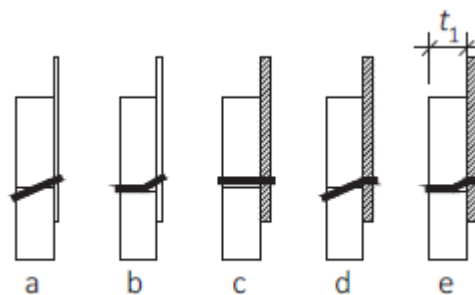


Figure 51: Failure mechanisms for a steel-to-timber connection [18].

In summary, while the timber checks in this context are simplified, they still provide a conservative and reliable assessment of the load-carrying capacity of the shear connection. However, the failure mechanism involving the formation of a plastic hinge in the steel parts at loads below 30 kN is not expected to occur, based on evidence from pushout tests documented in the literature. Therefore, further research and experimental validation are necessary to refine these assumptions and fully integrate the effects of preloading into the Johansen model.

**For a thin steel plate in single shear ( $t \leq 0.5 d$ ):**

$$F_{v,Rk,thin} = \min \begin{cases} 0.4 * f_{h,90,k} * t_1 * d & (a) \\ 1.15 * \sqrt{2 * M_{y,Rk} * f_{h,90,k} * d} & (b) \end{cases}$$

**For a thick steel plate in single shear ( $t \geq d$ ):**

$$F_{v,Rk,thick} = \min \begin{cases} f_{h,90,k} * t_1 * d & (c) \\ f_{h,90,k} * t_1 * d * \left( \sqrt{2 + \frac{4 * M_{y,Rk}}{f_{h,90,k} * d * t_1^2}} - 1 \right) & (d) \\ 2.3 * \sqrt{M_{y,Rk} * f_{h,90,k} * d} & (e) \end{cases}$$

$F_{v,Rk}$  The characteristic load-carrying capacity per shear plane per fastener.

$f_{h,90,k}$  The characteristic embedment strength perpendicular to grain.

$t_1$  The thickness of the timber.

$d$  The fastener diameter.

$M_{y,Rk}$  The characteristic fastener yield moment.

$$f_{h,90,k} = \frac{f_{h,0,k}}{k_{90} * \sin^2 90 + \cos^2 90} = \frac{f_{h,0,k}}{k_{90}} = 9.97 \text{ N/mm}^2$$

$$f_{h,0,k} = 0.082 * (1 - 0.01 * d) * \rho_k = 18.65 \text{ N/mm}^2$$

$$k_{90} = 1.35 + 0.015 * d = 1.87 \quad (\text{for softwood})$$

$$M_{y,Rk} = 0.3 * f_{u,k} * d^{2.6} = 1737345.51 \text{ Nmm}$$

$$f_{u,k} = 560 \text{ N/mm}^2 \quad (\text{steel tube class S460})$$

$$\rho_k = 350 \text{ kg/m}^3$$

$$t_1 = 120 \text{ mm}$$

$$d = 35 \text{ mm}$$

$f_{h,0,k}$  The characteristic embedment strength parallel to grain.

$f_{u,k}$  The characteristic tensile strength.

$\rho_k$  The characteristic timber density.

Results:

$$F_{v,Rk,thin} = \min \begin{cases} 16.7 \text{ kN} & (a) \\ 40.0 \text{ kN} & (b) \end{cases}$$

(a): Plastic hinge is not occurring according to push-out results.

(b): Plastic hinge is not occurring according to push-out results.

$$F_{v,Rk,thick} = \min \begin{cases} 41.9 \text{ kN} & (c) \\ 35.1 \text{ kN} & (d) \\ 56.6 \text{ kN} & (e) \end{cases}$$

(c): Not governing.

(d): Plastic hinge is not occurring according to push-out results.

(e): Plastic hinge is not occurring according to push-out results.

### CLT Floor Design

#### Critical Load Combination

Determining the critical load combinations for ULS acting on the CLT floor as distributed surface load:

From Formula 6.10a:

$$\text{LC1: } Q_{design, floor} = 1.1 * 1.35 * 1.8 = 2.7 \text{ kN/m}^2$$

$$\text{LC2: } Q_{design, floor} = 1.1 * 1.35 * 1.8 + 1.1 * 1.5 * 0.4 * 2.0 = 4 \text{ kN/m}^2$$

From Formula 6.10b:

$$\text{LC3: } Q_{design, floor} = 0.89 * 1.1 * 1.35 * 1.8 = 2.4 \text{ kN/m}^2$$

$$\text{LC4: } Q_{design, floor} = 0.89 * 1.1 * 1.35 * 1.8 + 1.1 * 1.5 * 2.0 = 5.7 \text{ kN/m}^2$$

From the previous load combinations, the critical distributed surface load that is acting on the composite beam is determined from LC4:  $Q_{d,ULS,max,floor} = 5.7 \text{ kN/m}^2$

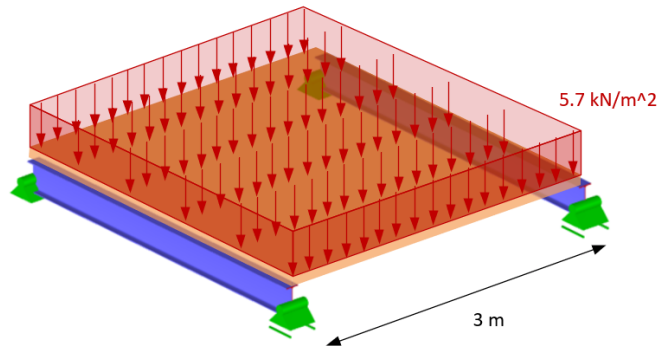


Figure 52: A 3D representation of the load application on the floor.

### Timber Design

Cross-section check:

$$\sigma_{m,y,d} \leq f_{m,d} = k_{sys} * k_{mod} * \frac{f_{m,k}}{\gamma_M}$$

$$\sigma_{m,y,d} = \frac{M_{y,d}}{W_{x,net}} = \frac{6412.5 * 10^3}{10.2 * 10^5} = 6.3 \text{ Mpa}$$

$$f_{m,k} = 24 \text{ N/mm}^2$$

$$k_{sys} = 1$$

$$k_{mod} = 0.5$$

$$\gamma_M = 1.3$$

$$UC = 0.7$$

## Results SLS

### Composite Beam Design

#### Critical Load Combination

Determining the critical load combinations for SLS acting on the composite beam as a distributed line load involves two primary load cases:

$$\text{LC1: } q_{design,beam} = 6 \text{ kN/m}$$

$$\text{LC2: } q_{design,beam} = 6 + 6 = 12 \text{ kN/m}$$

From these load combinations, the critical distributed line load acting on the composite beam is identified from LC2:

$$q_{d,SLS,max,beam} = 12 \text{ kN/m}$$

#### Creep and Stiffness Reduction

$$E_{fin,timber} = \frac{E_{eff,timber}}{1+k_{def}} = \frac{3628.3}{1+0.6} = 2267.7 \text{ N/mm}^2$$

$$k_{ser,fin} = \frac{k_{test}}{1+k_{def}} = \frac{149600}{1+0.6} = 93500 \text{ N/mm}$$

$$k_{def} = 0.6$$

#### Analysis Results

Performing the Gamma method on the composite beam provides the following results by applying the previous input from the material properties, geometry, and critical line load:

$$\gamma_1 = 0.85$$

$$(EI)_{ef} = 7.82 * 10^{13} \text{ Nmm}^2$$

#### Deflection Check

$$w \leq w_{max} = \frac{L}{250} = 48 \text{ mm}$$

$$w = \frac{5}{384} * \frac{q_{d,SLS,max,beam} * l^4}{(EI)_{ef}} = 41.5 \text{ mm}$$

$$UC = 0.9$$

#### Vibration

Assessing the fundamental frequency of the steel beam (f) using the equation  $f = 18/\sqrt{w}$  gives a fundamental frequency of 2.8Hz. As this is below the typically accepted limit of 3Hz, in practice additional dynamic analysis should be undertaken to evaluate the vibrational response of the floor system. This analysis is outside the scope of this study.

### CLT Floor Design

### *Critical Load Combination*

Determining the critical load combinations for SLS acting on the CLT floor as a distributed surface load involves the following load cases:

$$\text{LC1: } Q_{design, floor} = 1.8 \text{ kN/m}^2$$

$$\text{LC2: } Q_{design, floor} = 1.8 + 2.0 = 3.8 \text{ kN/m}^2$$

From these load combinations, the critical distributed surface load acting on the CLT floor is identified from LC2:

$$Q_{d, SLS, max, floor} = 3.8 \text{ kN/m}^2$$

### *Creep and Stiffness Reduction*

$$EI_{fin} = \frac{EI_{eff}}{1+k_{def}} = \frac{6.71 * 10^{11}}{1+0.6} = 4.19 * 10^{11} \text{ Nmm}^2$$

$$k_{def} = 0.6.$$

### *Deflection Check*

$$w \leq w_{max} = \frac{b}{250} = 12 \text{ mm}$$

$$w = \frac{5}{384} * \frac{Q_{d, SLS, max, floor} * b^4}{(EI)_{ef}} = 9.6 \text{ mm}$$

$$UC = 0.8$$

### *Vibration*

This analysis is outside the scope of this study, as previously stated.

# Appendix C Cumulative Carbon Emissions Over Time and Biogenic Carbon

## C.1 Baseline Design Graph

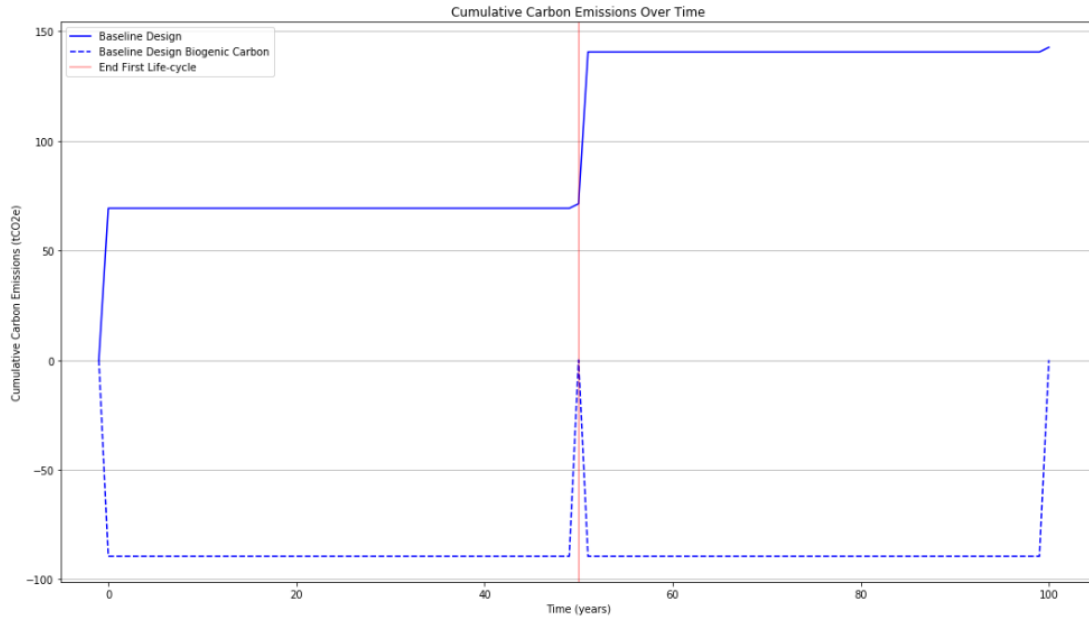


Figure 53: Cumulative carbon emissions over time and biogenic carbon for the baseline design.

## C.2 Optimized Design 50% Reused Graph

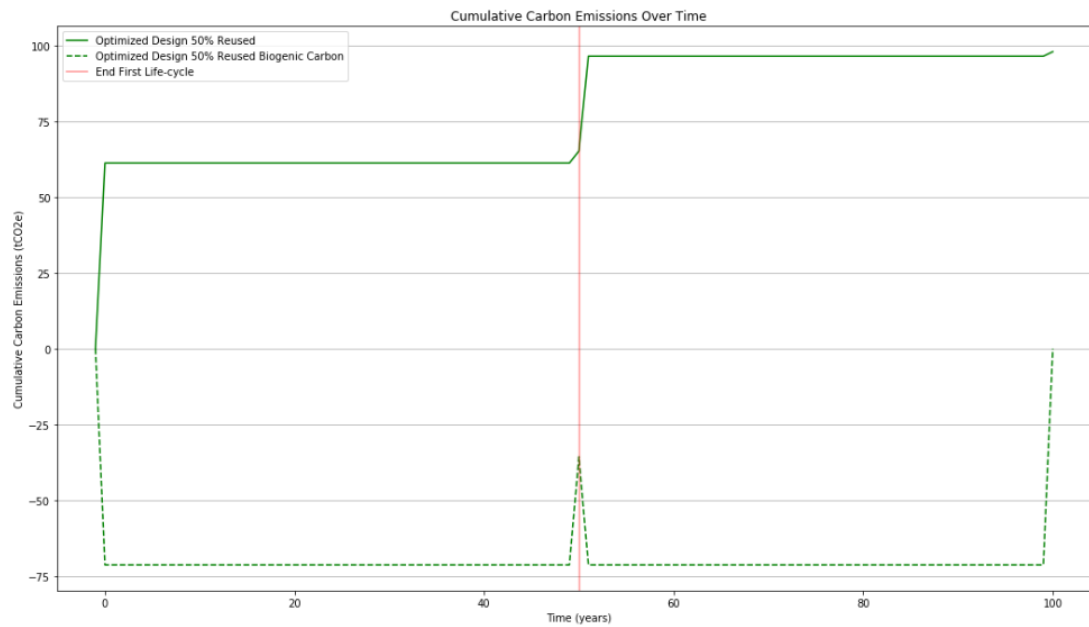


Figure 54: Cumulative carbon emissions over time and biogenic carbon for the optimized design 50% reused.

### C.3 Optimized Design 70% Reused Graph

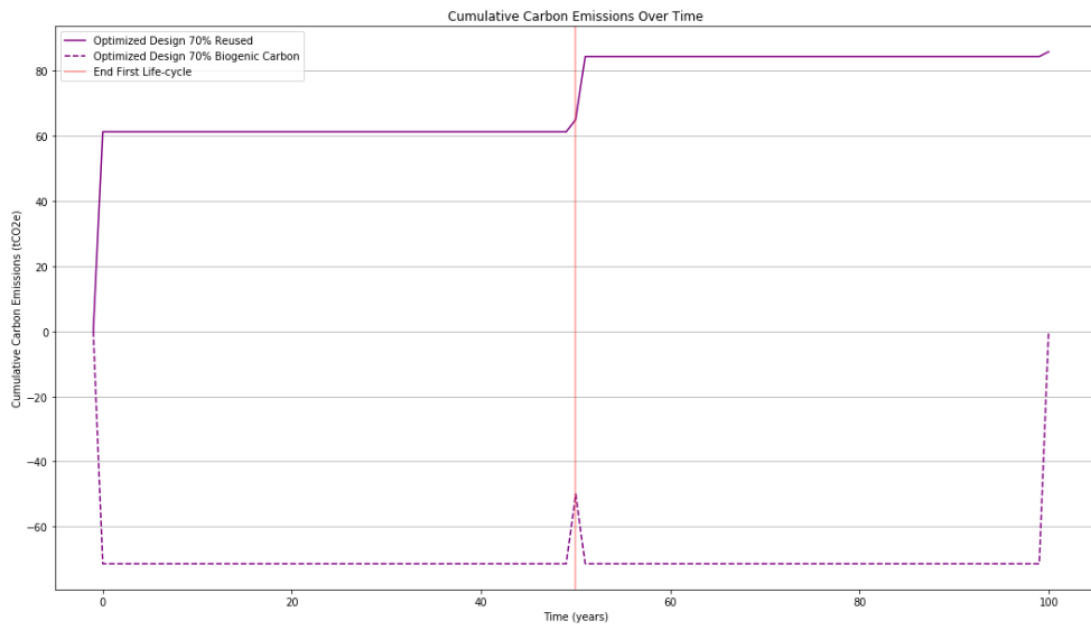


Figure 55: Cumulative carbon emissions over time and biogenic carbon for the optimized design 70% reused.

### C.4 Optimized Design 90% Reused Graph

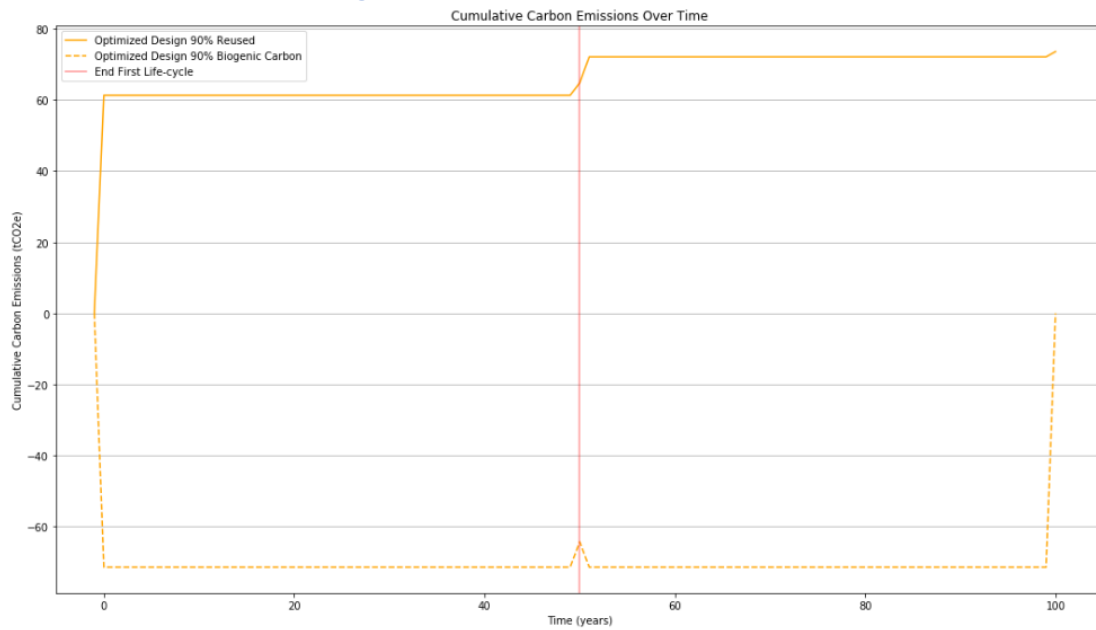


Figure 56: Cumulative carbon emissions over time and biogenic carbon for the optimized design 90% reused.



## Appendix D Python Script for Structural Analysis

### D.1 Baseline Composite Floor System

```
%matplotlib inline
import numpy as np
import matplotlib.pyplot as plt
import math
from scipy.interpolate import CubicSpline
pi = math.pi

# Function to format a large number
def format_large_number(number):
    order = math.floor(math.log10(number))
    rounded = round(number / 10**order, 2)
    return f"{rounded}e{order}"

#input box

# Beam/Floor input
l = 12000 # Length in mm
s = 400 # Spacing in mm

# Headed shear studs and groud shear connector
K = 149600 # (N/mm)

#CLT floor C24:
E_mean = 11000
b = 3000 #floor span in mm
I_floor = 3.04 * 10**8 # second moment of area mm^4
EI_floor = I_floor * E_mean # floor's bending stiffness
perpendicular to the composite beam

# Steel input s355
E2 = 210000 # Young's modulus in MPa (N/mm^2)
bf = 177.9 # Width of steel flange in mm
hf = 12.8 # Height of steel flange in mm
bw = 7.9 # Width of steel web in mm
hw = 380.8 # Height of steel web in mm
Af = bf * hf # Cross-sectional area of steel flange in mm^2
Aw = bw * hw # Cross-sectional area of steel web in mm^2
hs = hf * 2 + hw # the steel profile height

# Timber composite component input C24
E_eff = 3641.2 # Equivalent Young's modulus for the CLT in
composite beam in MPa (N/mm^2)
h1 = 160 # Height in mm

# Determining effective width
b1_EC4 = 1/4
EA_i = E_mean * 2 * 20 # E_mean * number of active layers *
thickness N/mm
GA_xy = 690 * 160 # N/mm
```

```

b1_EC5 = bf + 2* b * (0.5 - 0.35 * (b/l)**0.9 * (EA_i/GA_xy)**0.45
)
b1 = min(b1_EC4, b1_EC5)    # the effective Width in mm

A1 = h1 * b1    # Cross-sectional area of CLT in mm^2

h = h1 + hs # the totale height of composite beam

print(f"the totale height of composite beam {h} mm")
print(f"the effective Width of composite beam {b1} mm")

# Create figure and axes
fig, ax = plt.subplots()

# Draw timber profile
timber_x = [-b1/2, b1/2, b1/2, -b1/2, -b1/2]
timber_y = [h, h, h-h1, h-h1, h]
ax.plot(timber_x, timber_y, 'b-', label='Timber')

# Draw steel profile
steel_x = [-bf/2, bf/2, bf/2, bw/2, bw/2, -bw/2, -bw/2, -bf/2, -
bf/2]
steel_y = [h-h1, h-h1, h-h1-hf, h-h1-hf, h-h1-hf-hw, h-h1-hf-hw, h-
h1-hf, h-h1-hf, h-h1]
ax.plot(steel_x, steel_y, 'r-', label='Steel')

# Add bottom steel flange
bottom_flange_x = [-bf/2, bf/2, bf/2, -bf/2, -bf/2]
bottom_flange_y = [0, 0, hf, hf, 0]
ax.plot(bottom_flange_x, bottom_flange_y, 'r-')

# Set labels and title
ax.set_xlabel('Width (mm)')
ax.set_ylabel('Height (mm)')
ax.set_title('Cross-section of Composite Beam')

# Set aspect ratio
ax.set_aspect('equal', adjustable='box')

# Add legend
ax.legend()

# Show plot
plt.grid(True)
plt.show()

#ULS
print("\nULS:")

#Gamma method in ULS

p1 = (pi**2 * E_eff * A1 * s) / (K * l**2)
gamma1 = 1 / (1 + p1)

```

```

zy = ((gamma1 * E_eff * A1 * (h1 / 2 + hf * 2 + hw) +
      E2 * Af * (hf / 2 + hw + hf) +
      E2 * Aw * (hw / 2 + hf) +
      E2 * Af * (hf/2)) /
      (gamma1 * E_eff * A1 + E2 * (Af * 2 + Aw))) # Neutral
axis position from the bottom of the whole cross-section
a1 = h1 / 2 + hf * 2 + hw - zy # Distance from the center of
gravity of CLT to the the neutral axis
a2tf = hf / 2 + hw + hf - zy # Distance from the center of gravity
of steel top flange to the the neutral axis
a2w = zy - hf - hw / 2 # Distance from the center of gravity of
steel web to the the neutral axis
a2bf = zy - hf / 2 # Distance from the center of gravity of steel
bottom flange to the the neutral axis

EIeff = (E_eff * (b1 * h1**3 / 12 + gamma1 * A1 * a1**2) +
        E2 * (bf * hf**3 / 12 + Af * a2tf**2 + bw * hw**3 / 12
+ Aw * a2w**2 + bf * hf**3 / 12 + Af * a2bf**2))

#Composite Beam Design:
print("\nResults Composite beam:")
print(f"gamma1: {gamma1:.2f}")
print(f"EI_eff = {format_large_number(EIeff)} N*mm^2")

q_ULS_beam = 18.5 # kN/m
M1 = 1/8 * q_ULS_beam * l**2 # Moment at mid span in N*mm
Vmax = q_ULS_beam * l / 2 # Shear force at support point in N

# Stress in Steel
sigma2 = M1 * E2 * a2w / EIeff # Stress at the center of gravity
sigma_m2 = M1 * E2 * (hf+hw+hf) / 2 / EIeff
sigma_sb = sigma2 + sigma_m2 # Stress at the outer bottom fibers

print("Stress in Steel:")
print(f"sigma outer bottom fiber of steel profile at the mid span
position: sigma_Ed = {sigma_sb:.2f} MPa")
print(f"sigma_Rd = {355} MPa")
print(f"UC = {sigma_sb/355:.1f}")

# Stress in Timber
sigma1 = M1 * gamma1 * E_eff * a1 / EIeff # Stress at the center of
gravity
sigma_m1 = M1 * E_eff * h1 / 2 / EIeff
sigma_tt = sigma1 + sigma_m1 # Stress at the outer fibers of the timber
sigma_max_timber = 1 * 0.5 * 24 / 1.3 # k(sys) * k(mod) * fm / gamma(m)
F = Vmax * gamma1 * E_eff * A1 * a1 * s / EIeff # Force on the one
fastener

print("\nStress in Timber:")
print(f"sigma outer top fibers of CLT at the mid span position:
{sigma_tt:.2f} MPa")
print(f"sigma_max_timber = {sigma_max_timber:.1f} MPa")
print(f"UC = {sigma_tt/sigma_max_timber:.1f}")

```

```

#Floor Design:
Q_ULS = 5.9 # kN/m^2
M2 = 1/8 * Q_ULS * b**2 # Moment at mid span in N*mm
# Stress in Timber
σ_floor = M2 / I_floor * (h1 / 2) # N/mm^2

print("\nResults CLT floor:")
print(f"Stress CLT floor: {σ_floor:.1f} MPa")
print(f"σ_max_timber = {σ_max_timber:.1f} MPa")
print(f"UC = {σ_floor/σ_max_timber:.1f}")

#SLS
print("\nSLS:")

#Gamma method in SLS
# Creep impact
k_def = 0.6
E_fin = E_eff / (1+k_def)
K_fin = K / (1+k_def)

p1 = (pi**2 * E_fin * A1 * s) / (K_fin * l**2)
gamma1 = 1 / (1 + p1)

zy = ((gamma1 * E_fin * A1 * (h1 / 2 + hf * 2 + hw) +
      E2 * Af * (hf / 2 + hw + hf) +
      E2 * Aw * (hw / 2 + hf) +
      E2 * Af * (hf/2)) /
      (gamma1 * E_fin * A1 + E2 * (Af * 2 + Aw))) # Neutral
axis position from the bottom of the whole cross-section
a1 = h1 / 2 + hf * 2 + hw - zy # Distance from the center of
gravity of CLT to the the neutral axis
a2tf = hf / 2 + hw + hf - zy # Distance from the center of gravity
of steel top flange to the the neutral axis
a2w = zy - hf - hw / 2 # Distance from the center of gravity of
steel web to the the neutral axis
a2bf = zy - hf / 2 # Distance from the center of gravity of steel
bottom flange to the the neutral axis

EIeff = (E_fin * (b1 * h1**3 / 12 + gamma1 * A1 * a1**2) +
        E2 * (bf * hf**3 / 12 + Af * a2tf**2 + bw * hw**3 / 12
+ Aw * a2w**2 + bf * hf**3 / 12 + Af * a2bf**2))

#Composite Beam Design:
print("\nResults Composite beam:")
print(f"gamma1: {gamma1:.2f}")
print(f"EI_eff_fin = {format_large_number(EIeff)} N*mm^2")
q_SLS_beam = 12.52 # kN/m
#Deflection check
w_max = 1/250
w1 = (5/384 * q_SLS_beam * (l)**4) / EIeff # Deflection in mm
print(f"w_beam = {w1:.1f} mm")
print(f"w_max = {w_max:.1f} mm")

```

```

print(f"UC = {w1/w_max:.1f}")

#Floor Design:
print("\nResults CLT floor:")
EI_floor_fin = EI_floor / (1+k_def)
print(f"EI_floor_fin: {format_large_number(EI_floor_fin)} N*mm^2")

#Deflection check
Q_SLS = 4 # kN/m^2
w_floor_max = b/250
w_floor = 5/384 * Q_SLS * (b)**4 / EI_floor_fin
print(f"w_floor = {w_floor:.1f} mm")
print(f"w_max_floor = {w_floor_max} mm")
print(f"UC = {w_floor/w_floor_max:.1f}")

print("\nULS loads:")
print(f"Q_ULS = {Q_ULS:.2f} kN/mm^2" )
print(f"q_ULS_beam = {q_ULS_beam} kN/m")

print("\nSLS loads:")
print(f"Q_SLS = {Q_SLS:.2f} kN/mm^2" )
print(f"q_SLS_beam = {q_SLS_beam} kN/m")

# Calculate the slope of the line connecting points 3 and 4
slope_34 = (hs/2 - 0) / ( $\sigma_2$  - ( $\sigma_2$  +  $\sigma_{m2}$ ))

# Calculate the x-coordinate of the intersection point with the
horizontal line at hs
x_intersect_34 =  $\sigma_2$  +  $\sigma_{m2}$  + (hs - 0) / slope_34

# Plotting
# Plotting the vertical line
plt.plot([0, 0], [0, h], 'k--')

# Marking point 3
plt.plot( $\sigma_2$  +  $\sigma_{m2}$ , 0, 'ro')
plt.text( $\sigma_2$  +  $\sigma_{m2}$ , 0, ' $\sigma_{Ed}$ ', verticalalignment='top')

# Marking point 4
plt.plot( $\sigma_2$ , hs/2, 'ro')
plt.text( $\sigma_2$ , hs/2, ' $\sigma_{i,t(c)}$ ', verticalalignment='bottom')

# Drawing the line connecting points 3 and 4
plt.plot([ $\sigma_2$  +  $\sigma_{m2}$ , x_intersect_34], [0, hs], 'g-')

# Drawing the horizontal line
plt.plot([-355, 355], [hs, hs], 'k--')

# Setting plot limits and labels
plt.xlim(-300, 300) # Set the same limits for both axes
plt.ylim(-50, h+50) # Set the same limits for both axes
plt.xlabel(' $\sigma$  Steel')
plt.ylabel('h')
plt.title('Stress plot Steel part')

```

```

# Displaying the plot
plt.grid(True)
plt.show()

# Calculate the slope of the line passing through points 1 and 2
slope = (a1 + zy - h) / (σ1 - σtt)

# Calculate the x-coordinate of the intersection point with the
horizontal line at hs
x_intersect = (hs - (a1+zy)) / slope + σ1

# Plotting
# Plotting the vertical line
plt.plot([0, 0], [0, h], 'k--')

# Marking point 1
plt.plot(-σtt, h, 'ro')
plt.text(-σtt, h, 'σm,y,d', verticalalignment='bottom')

# Marking point 2
plt.plot(-σ1, a1+zy, 'ro')
plt.text(-σ1, a1+zy, 'σi,t(c)', verticalalignment='bottom')

# Drawing the line connecting points 1 and 2
plt.plot([-σtt, -x_intersect], [h, hs], 'b-')

# Drawing the horizontal line
plt.plot([-10, 10], [hs, hs], 'k--')

# Setting plot limits and labels
plt.xlabel('σ Timber')
plt.ylabel('h')
plt.title('Stress plot timber part')

# Displaying the plot
plt.grid(True)
plt.show()

```

## D.2 Optimized Composite Floor System

```
%matplotlib inline
import numpy as np
import matplotlib.pyplot as plt
import math
from scipy.interpolate import CubicSpline
pi = math.pi

# Function to format a large number
def format_large_number(number):
    order = math.floor(math.log10(number))
    rounded = round(number / 10**order, 2)
    return f"{rounded}e{order}"

#input box

# Beam/Floor input
l = 12000 # Length in mm
s = 280 # Spacing in mm

# pre-loaded demountable shear connectors (pair)
K = 133500 # (N/mm)

#CLT floor C24:
E_mean = 11000
b = 3000 #floor span in mm
I_floor = 6.1 * 10**7 # second moment of area mm^4
EI_floor = I_floor * E_mean # floor's bending stiffness
perpendicular to the composite beam

# Steel input s355
E2 = 210000 # Young's modulus in MPa (N/mm^2)
bf = 177.9 # Width of steel flange in mm
hf = 12.8 # Height of steel flange in mm
bw = 7.9 # Width of steel web in mm
hw = 380.8 # Height of steel web in mm
Af = bf * hf # Cross-sectional area of steel flange in mm^2
Aw = bw * hw # Cross-sectional area of steel web in mm^2
hs = hf * 2 + hw # the steel profile height
A_steel = Af * 2 + Aw

# Timber composite component input C24
E_eff = 7333 # Equivalent Young's modulus for the CLT in composite
beam in MPa (N/mm^2)
h1 = 120 # Height in mm

# Determining effective width
b1_EC4 = 1/4
EA_i = E_mean * 2 * 40 # E_mean * number of active layers *
thickness N/mm
GA_xy = 690 * 120 # N/mm
b1_EC5 = bf + 2* b * (0.5 - 0.35 * (b/l)**0.9 * (EA_i/GA_xy)**0.45
)
b1 = min(b1_EC4, b1_EC5) # the effective Width in mm
```

```

A1 = h1 * b1 # Cross-sectional area of CLT in mm^2

h = h1 + hs # the totale height of composite beam

print(f"the totale height of composite beam {h} mm")
print(f"the effective Width of composite beam {b1} mm")

# Create figure and axes
fig, ax = plt.subplots()

# Draw timber profile
timber_x = [-b1/2, b1/2, b1/2, -b1/2, -b1/2]
timber_y = [h, h, h-h1, h-h1, h]
ax.plot(timber_x, timber_y, 'b-', label='Timber')

# Draw steel profile
steel_x = [-bf/2, bf/2, bf/2, bw/2, bw/2, -bw/2, -bw/2, -bf/2, -
bf/2]
steel_y = [h-h1, h-h1, h-h1-hf, h-h1-hf, h-h1-hf-hw, h-h1-hf-hw, h-
h1-hf, h-h1-hf, h-h1]
ax.plot(steel_x, steel_y, 'r-', label='Steel')

# Add bottom steel flange
bottom_flange_x = [-bf/2, bf/2, bf/2, -bf/2, -bf/2]
bottom_flange_y = [0, 0, hf, hf, 0]
ax.plot(bottom_flange_x, bottom_flange_y, 'r-')

# Set labels and title
ax.set_xlabel('Width (mm)')
ax.set_ylabel('Height (mm)')
ax.set_title('Cross-section of Composite Beam')

# Set aspect ratio
ax.set_aspect('equal', adjustable='box')

# Add legend
ax.legend()

# Show plot
plt.grid(True)
plt.show()

#ULS
print("\nULS:")

#Gamma method in ULS

p1 = (pi**2 * E_eff * A1 * s) / (K * l**2)
gamma1 = 1 / (1 + p1)

zy = ((gamma1 * E_eff * A1 * (h1 / 2 + hf * 2 + hw) +
E2 * Af * (hf / 2 + hw + hf) +

```



```

        E2 * Aw * (hw / 2 + hf) +
        E2 * Af * (hf/2)) /
        (gamma1 * E_eff * A1 + E2 * (Af * 2 + Aw))) # Neutral
axis position from the bottom of the whole cross-section
a1 = h1 / 2 + hf * 2 + hw - zy # Distance from the center of
gravity of CLT to the the neutral axis
a2tf = hf / 2 + hw + hf - zy # Distance from the center of gravity
of steel top flange to the the neutral axis
a2w = zy - hf - hw / 2 # Distance from the center of gravity of
steel web to the the neutral axis
a2bf = zy - hf / 2 # Distance from the center of gravity of steel
bottom flange to the the neutral axis

EIeff = (E_eff * (b1 * h1**3 / 12 + gamma1 * A1 * a1**2) +
        E2 * (bf * hf**3 / 12 + Af * a2tf**2 + bw * hw**3 / 12
+ Aw * a2w**2 + bf * hf**3 / 12 + Af * a2bf**2))

#Composite Beam Design:
print("\nResults Composite beam:")
print(f"gamma1: {gamma1:.2f}")
print(f"EI_eff = {format_large_number(EIeff)} N*mm^2")

q_ULS_beam = 17.8 # kN/m
M1 = 1/8 * q_ULS_beam * l**2 # Moment at mid span in N*mm
Vmax = q_ULS_beam * l / 2 # Shear force at support point in N

# Stress in Steel
sigma2 = M1 * E2 * a2w / EIeff # Stress at the center of gravity
sigma_m2 = M1 * E2 * (hf+hw+hf) / 2 / EIeff
sigma_sb = sigma2 + sigma_m2 # Stress at the outer bottom fibers

print("Stress in Steel:")
print(f"sigma outer bottom fiber of steel profile at the mid span
position: {sigma_sb:.2f} MPa")
print(f"sigma_max_steel = {355} MPa")
print(f"UC = {sigma_sb/355:.1f}")

# Stress in Timber
sigma1 = M1 * gamma1 * E_eff * a1 / EIeff # Stress at the center of
gravity
sigma_m1 = M1 * E_eff * h1 / 2 / EIeff
sigma_tt = sigma1 + sigma_m1 # Stress at the outer fibers of the timber
sigma_max_timber = 1 * 0.5 * 24 / 1.3 # k(sys) * k(mod) * fm / gamma(m)
F = Vmax * gamma1 * E_eff * A1 * a1 * s / EIeff / 2 # Force per
fastener

print("\nStress in Timber:")
print(f"sigma outer top fibers of CLT at the mid span position:
{sigma_tt:.2f} MPa")
print(f"sigma_max_timber = {sigma_max_timber:.1f} MPa")
print(f"UC = {sigma_tt/sigma_max_timber:.1f}")

#Joint load
print("\nJoint load check:")
print(f"F joint: {F/1000:.2f} kN < 30")

```

```

#Floor Design:
Q_ULS = 5.7 # kN/m^2
M2 = 1/8 * Q_ULS * b**2 # Moment at mid span in N*mm
# Stress in Timber
σ_floor = M2 / I_floor * (h1 / 2) # N/mm^2

print("\nResults CLT floor:")
print(f"Stress CLT floor: {σ_floor:.1f} MPa")
print(f"σ_max_timber = {σ_max_timber:.1f} MPa")
print(f"UC = {σ_floor/σ_max_timber:.1f}")

#SLS
print("\nSLS:")

#Gamma method in SLS
# Creep impact
k_def = 0.6
E_fin = E_eff / (1+k_def)
K_fin = K / (1+k_def)

p1 = (pi**2 * E_fin * A1 * s) / (K_fin * l**2)
gamma1 = 1 / (1 + p1)

zy = ((gamma1 * E_fin * A1 * (h1 / 2 + hf * 2 + hw) +
      E2 * Af * (hf / 2 + hw + hf) +
      E2 * Aw * (hw / 2 + hf) +
      E2 * Af * (hf/2)) /
      (gamma1 * E_fin * A1 + E2 * (Af * 2 + Aw))) # Neutral
axis position from the bottom of the whole cross-section
a1 = h1 / 2 + hf * 2 + hw - zy # Distance from the center of
gravity of CLT to the the neutral axis
a2tf = hf / 2 + hw + hf - zy # Distance from the center of gravity
of steel top flange to the the neutral axis
a2w = zy - hf - hw / 2 # Distance from the center of gravity of
steel web to the the neutral axis
a2bf = zy - hf / 2 # Distance from the center of gravity of steel
bottom flange to the the neutral axis

EIeff = (E_fin * (b1 * h1**3 / 12 + gamma1 * A1 * a1**2) +
        E2 * (bf * hf**3 / 12 + Af * a2tf**2 + bw * hw**3 / 12
+ Aw * a2w**2 + bf * hf**3 / 12 + Af * a2bf**2))

#Composite Beam Design:
print("\nResults Composite beam:")
print(f"gamma1: {gamma1:.2f}")
print(f"EI_eff_fin = {format_large_number(EIeff)} N*mm^2")
q_SLS_beam = 12 # kN/m

#Deflection check
w_max = 1/250
w1 = (5/384 * q_SLS_beam * (l)**4) / EIeff # Deflection in mm
print(f"w_beam = {w1:.1f} mm")

```

```

print(f"w_max = {w_max:.1f} mm")
print(f"UC = {w1/w_max:.1f}")

#Floor Design:
print("\nResults CLT floor:")
EI_floor_fin = EI_floor / (1+k_def)
print(f"EI_floor_fin: {format_large_number(EI_floor_fin)} N*mm^2")

#Deflection check
Q_SLS = 3.8 # kN/m^2
w_floor_max = b/250
w_floor = 5/384 * Q_SLS * (b)**4 / EI_floor_fin
print(f"w_floor = {w_floor:.1f} mm")
print(f"w_max_floor = {w_floor_max} mm")
print(f"UC = {w_floor/w_floor_max:.1f}")

print("\nULS loads:")
print(f"Q_ULS = {Q_ULS:.2f} kN/mm^2" )
print(f"q_ULS_beam = {q_ULS_beam} kN/m")

print("\nSLS loads:")
print(f"Q_SLS = {Q_SLS:.2f} kN/mm^2" )
print(f"q_SLS_beam = {q_SLS_beam} kN/m")

# Calculate the slope of the line connecting points 3 and 4
slope_34 = (hs/2 - 0) / (σ2 - (σ2 + σm2))

# Calculate the x-coordinate of the intersection point with the
horizontal line at hs
x_intersect_34 = σ2 + σm2 + (hs - 0) / slope_34

# Plotting
# Plotting the vertical line
plt.plot([0, 0], [0, h], 'k--')

# Marking point 3
plt.plot(σ2 + σm2, 0, 'ro')
plt.text(σ2 + σm2, 0, 'σ_Ed', verticalalignment='top')

# Marking point 4
plt.plot(σ2, hs/2, 'ro')
plt.text(σ2, hs/2, 'σ_i,t(c)', verticalalignment='bottom')

# Drawing the line connecting points 3 and 4
plt.plot([σ2 + σm2, x_intersect_34], [0, hs], 'g-')

# Drawing the horizontal line
plt.plot([-355, 355], [hs, hs], 'k--')

# Setting plot limits and labels
plt.xlim(-300, 300) # Set the same limits for both axes
plt.ylim(-50, h+50) # Set the same limits for both axes
plt.xlabel('σ Steel')
plt.ylabel('h')

```

```

plt.title('Stress plot Steel part')

# Displaying the plot
plt.grid(True)
plt.show()

# Calculate the slope of the line passing through points 1 and 2
slope = (a1 + zy - h) / ( $\sigma_1$  -  $\sigma_{tt}$ )

# Calculate the x-coordinate of the intersection point with the
horizontal line at hs
x_intersect = (hs - (a1+zy)) / slope +  $\sigma_1$ 

# Plotting
# Plotting the vertical line
plt.plot([0, 0], [0, h], 'k--')

# Marking point 1
plt.plot(- $\sigma_{tt}$ , h, 'ro')
plt.text(- $\sigma_{tt}$ , h, ' $\sigma_{m,y,d}$ ', verticalalignment='bottom')

# Marking point 2
plt.plot(- $\sigma_1$ , a1+zy, 'ro')
plt.text(- $\sigma_1$ , a1+zy, ' $\sigma_{i,t(c)}$ ', verticalalignment='bottom')

# Drawing the line connecting points 1 and 2
plt.plot([- $\sigma_{tt}$ , -x_intersect], [h, hs], 'b-')

# Drawing the horizontal line
plt.plot([-10, 10], [hs, hs], 'k--')

# Setting plot limits and labels
plt.xlabel('σ Timber')
plt.ylabel('h')
plt.title('Stress plot timber part')

# Displaying the plot
plt.grid(True)
plt.show()

# Calculate the slope of the line connecting points 3 and 4
slope_34 = (hs/2 - 0) / ( $\sigma_2$  - ( $\sigma_2$  +  $\sigma_{m2}$ ))

# Calculate the x-coordinate of the intersection point with the
horizontal line at hs
x_intersect_34 =  $\sigma_2$  +  $\sigma_{m2}$  + (hs - 0) / slope_34

# Plotting
plt.figure(figsize=(18, 10))
# Plotting the vertical line
plt.plot([0, 0], [0, h], 'k--')

# Marking point 1
plt.plot(- $\sigma_{tt}$ , h, 'ro')
plt.text(- $\sigma_{tt}$ , h, ' $\sigma_{m,y,d}$ ', verticalalignment='bottom')

```

```

# Marking point 2
plt.plot(- $\sigma_1$ , a1+zy, 'ro')
plt.text(- $\sigma_1$ , a1+zy, ' $\sigma_{i,t(c)}$ ', verticalalignment='bottom')

# Drawing the line connecting points 1 and 2
plt.plot([- $\sigma_{tt}$ , -x_intersect], [h, hs], 'b-')

# Marking point 3
plt.plot( $\sigma_2 + \sigma_m2$ , 0, 'ro')
plt.text( $\sigma_2 + \sigma_m2$ , 0, ' $\sigma_{Ed}$ ', verticalalignment='top')

# Marking point 4
plt.plot( $\sigma_2$ , hs/2, 'ro')
plt.text( $\sigma_2$ , hs/2, ' $\sigma_{i,t(c)}$ ', verticalalignment='bottom')

# Drawing the line connecting points 3 and 4
plt.plot([ $\sigma_2 + \sigma_m2$ , x_intersect_34], [0, hs], 'g-')

# Drawing the horizontal line
plt.plot([-355, 355], [hs, hs], 'k--')

# Setting plot limits and labels
plt.xlim(-320, 320) # Set the same limits for both axes
plt.ylim(-20, h+20) # Set the same limits for both axes
plt.xlabel('σ [Mpa]')
plt.ylabel('h [mm]')
plt.title('Stress plot along the composite cross-section')

# Displaying the plot
plt.grid(True)
plt.show()

#ULS
# Determining the spacing between shear connectors

# Initialize lists to store w, Q2, s, and Fjoint
Q2_values = []
s_values = []
Fjoint_values = []

# Iterate over increasing values of Q2 and s
for s in range(100, 601, 10): # Iterate over Q2
    for Q2_int in range(1, 10000): # Iterate over s
        Q2 = Q2_int / 100
        # Calculations
        p1 = (np.pi**2 * E_eff * A1 * s) / (K * 1**2)
        gamma1 = 1 / (1 + p1)

        zy = ((gamma1 * E_eff * A1 * (h1 / 2 + hf * 2 + hw) +
                E2 * Af * (hf / 2 + hw + hf) +
                E2 * Aw * (hw / 2 + hf) +
                E2 * Af * (hf/2)) /
                (gamma1 * E_eff * A1 + E2 * (Af * 2 + Aw)))
        a1 = h1 / 2 + hf * 2 + hw - zy

```

```

a2tf = hf / 2 + hw + hf - zy
a2w = zy - hf - hw / 2
a2bf = zy - hf / 2

EIeff = (E_eff * (b1 * h1**3 / 12 + gamma1 * A1 * a1**2) +
         E2 * (bf * hf**3 / 12 + Af * a2tf**2 + bw * hw**3
/ 12 + Aw * a2w**2 + bf * hf**3 / 12 + Af * a2bf**2))

w2 = (5/384 * Q2 * (l)**4) / EIeff # Deflection in mm

M = 1/8 * Q2 * l**2 # Moment at mid span in N*mm
Vmax = Q2 * l / 2 # Shear force at support point in N

sigma2 = M * E2 * a2w / EIeff
sigma_m2 = M * E2 * (hf+hw+hf) / 2 / EIeff
sigma_sb = sigma2 + sigma_m2 # Stress at the outer fibers
F = Vmax * gamma1 * E_eff * A1 * a1 * s / EIeff / 2 # Force
per fastener

# Break if Fjoint exceeds 30000
if F > 30000:
    #print(f"F joint: {F:.2f}")
    #print(f"Q2: {Q2}, s: {s}")
    Q2_values.append(Q2)
    s_values.append(s)
    Fjoint_values.append(F)
    break

# Plotting
plt.figure(figsize=(10, 6))
plt.plot(s_values, Q2_values, '-', label='Fjoint = 30 kN')
plt.axhline(y=q_ULS_beam, color='red', label='q_design_beam_ULS',
linestyle='--')
plt.xlabel('s (mm)')
plt.ylabel('q (kN/mm)')
plt.legend()
plt.grid(True)
plt.show()

#SLS
# Determining the spacing between shear connectors

# Initialize lists to store w, Q2, s, and Fjoint
Q2_values = []
s_values = []
Fjoint_values = []

# Iterate over increasing values of Q2 and s
for s in range(100, 601, 10): # Iterate over Q2
    for Q2_int in range(1, 10000): # Iterate over s
        Q2 = Q2_int / 100

```

```

# Calculations
k_def = 0.6
E_fin = E_eff / (1+k_def)
K_fin = K / (1+k_def)

p1 = (pi**2 * E_fin * A1 * s) / (K_fin * l**2)
gamma1 = 1 / (1 + p1)

zy = ((gamma1 * E_fin * A1 * (h1 / 2 + hf * 2 + hw) +
      E2 * Af * (hf / 2 + hw + hf) +
      E2 * Aw * (hw / 2 + hf) +
      E2 * Af * (hf/2)) /
      (gamma1 * E_fin * A1 + E2 * (Af * 2 + Aw))) #
Neutral axis position from the bottom of the whole cross-section

a1 = h1 / 2 + hf * 2 + hw - zy # Distance from the center
of gravity of CLT to the the neutral axis
a2tf = hf / 2 + hw + hf - zy # Distance from the center of
gravity of steel top flange to the the neutral axis
a2w = zy - hf - hw / 2 # Distance from the center of
gravity of steel web to the the neutral axis
a2bf = zy - hf / 2 # Distance from the center of gravity of
steel bottom flange to the the neutral axis

EIeff = (E_fin * (b1 * h1**3 / 12 + gamma1 * A1 * a1**2) +
        E2 * (bf * hf**3 / 12 + Af * a2tf**2 + bw *
hw**3 / 12 + Aw * a2w**2 + bf * hf**3 / 12 + Af * a2bf**2))

w2 = (5/384 * Q2 * (l)**4) / EIeff # Deflection in mm

M = 1/8 * Q2 * l**2 # Moment at mid span in N*mm
Vmax = Q2 * l / 2 # Shear force at support point in N

sigma2 = M * E2 * a2w / EIeff
sigma_m2 = M * E2 * (hf+hw+hf) / 2 / EIeff
sigma_sb = sigma2 + sigma_m2 # Stress at the outer fibers
F = Vmax * gamma1 * E_eff * A1 * a1 * s / EIeff / 2 # Force
per fastener

# Break if Fjoint exceeds 30000
if F > 30000:
    #print(f"F joint: {F:.2f}")
    #print(f"Q2: {Q2}, s: {s}")
    Q2_values.append(Q2)
    s_values.append(s)
    Fjoint_values.append(F)
    break

# Plotting
plt.figure(figsize=(10, 6))
plt.plot(s_values, Q2_values, '-', label='Fjoint = 30 kN')

```

```
plt.axhline(y=q_SLS_beam, color='green',  
label='q_design_beam_SLS', linestyle='--')  
plt.xlabel('s (mm)')  
plt.ylabel('q (kN/mm)')  
plt.legend()  
plt.grid(True)  
plt.show()
```